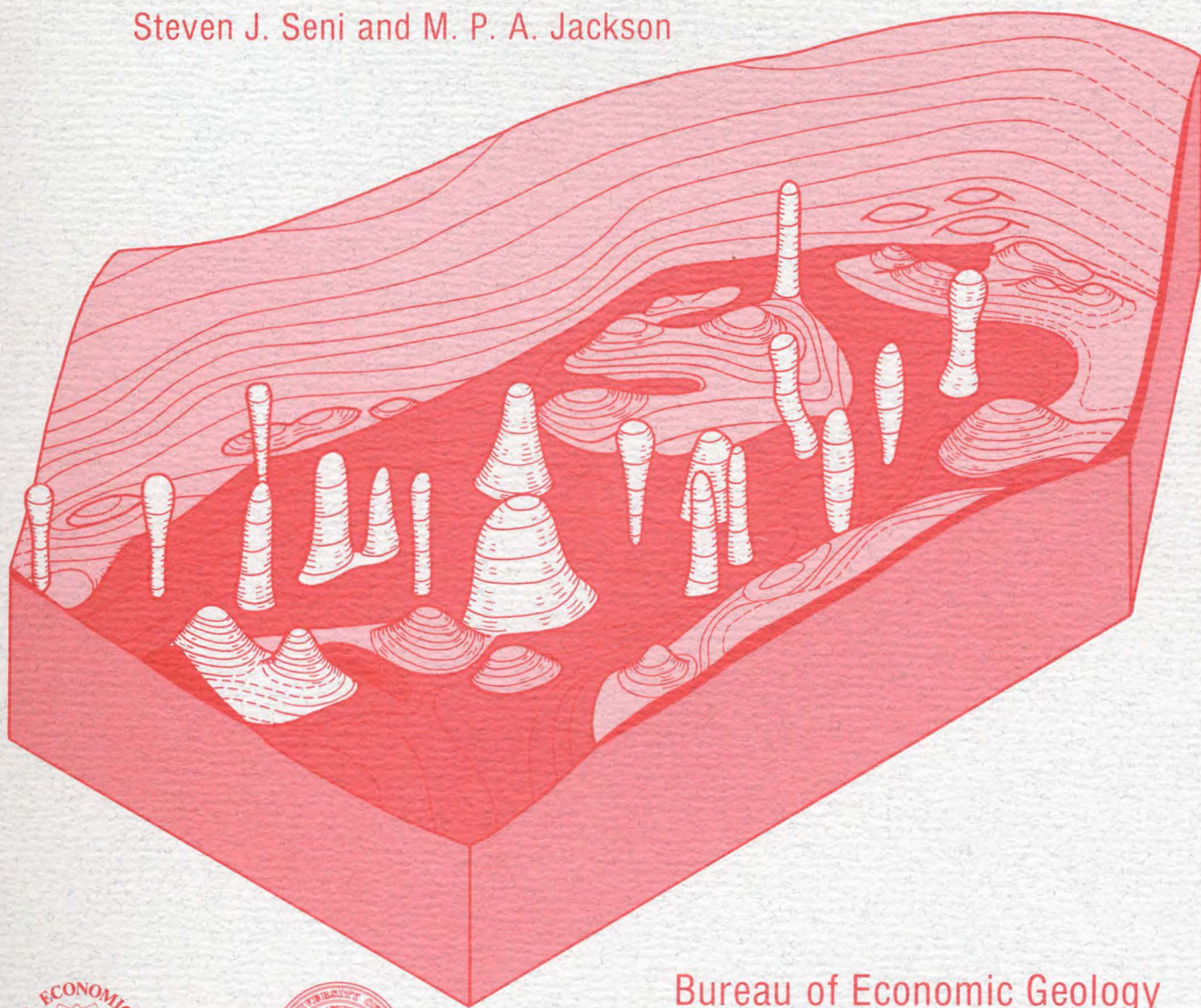


# SEDIMENTARY RECORD OF CRETACEOUS AND TERTIARY SALT MOVEMENT, EAST TEXAS BASIN:

Times, Rates, and Volumes of Salt Flow and  
Their Implications for Nuclear Waste Isolation  
and Petroleum Exploration

Steven J. Seni and M. P. A. Jackson



1984



Bureau of Economic Geology

W. L. Fisher, Director  
The University of Texas at Austin  
Austin, Texas 78712

# SEDIMENTARY RECORD OF CRETACEOUS AND TERTIARY SALT MOVEMENT, EAST TEXAS BASIN:

Times, Rates, and Volumes of Salt Flow and  
Their Implications for Nuclear Waste Isolation  
and Petroleum Exploration

Steven J. Seni and M. P. A. Jackson

assisted by

E. Bramson, R. J. Burks, R. D. Conti, S. A. Ghazi, S. E. Lovell,  
B. C. Richter, J. L. Smith, and D. H. Wood

Research supported by the U.S. Department of Energy,  
under Contract No. DE-AC97-80ET46617



1984



Bureau of Economic Geology

W. L. Fisher, Director

The University of Texas at Austin

Austin, Texas 78712

# CONTENTS

<b>ABSTRACT</b> .....	1
<b>INTRODUCTION</b> .....	1
Data base .....	3
Early history of basin formation and filling .....	3
Geometry of salt structures .....	5
<b>EVOLUTIONARY STAGES OF DOME GROWTH</b> .....	11
Pillow stage .....	11
Geometry of overlying strata .....	11
Geometry of surrounding strata .....	12
Depositional facies and lithostratigraphy .....	17
Diapir stage .....	19
Geometry of surrounding strata .....	20
Depositional facies and lithostratigraphy .....	20
Postdiapir stage .....	20
Geometry of surrounding strata .....	27
Depositional facies and lithostratigraphy .....	30
Holocene analogs .....	33
Summary .....	33
Formation of subtle petroleum traps .....	37
<b>PATTERNS OF SALT MOVEMENT IN TIME AND SPACE</b> .....	38
Group 1 diapirs: Pre-Glen Rose Subgroup (pre-112 Ma) .....	38
Group 2 diapirs: Glen Rose Subgroup to Washita Group (112 to 98 Ma) .....	43
Group 3 diapirs: Post-Austin Group (86 to 56 Ma) .....	43
Initiation and acceleration of salt flow .....	45
Overview of dome history .....	45
<b>RATES OF SALT MOVEMENT AND DOME GROWTH</b> .....	46
Propositions .....	46
Proven propositions .....	46
Unproven propositions .....	47
Simplified propositions .....	47
Distinguishing between syndepositional and postdepositional thickness variations .....	49
The problem .....	49
Structural evidence .....	49
Sedimentological evidence .....	55
Methodology .....	56
Distinguishing between regional and salt-related thickness variations .....	58
Calculating volumes of salt mobilized and of salt lost .....	61
Rates of dome growth .....	68
Net rates of pillow growth .....	68
Net rates of diapir growth .....	68
Gross rates of diapir growth .....	74
Growth rates and strain rates .....	75
<b>IMPLICATIONS FOR WASTE ISOLATION</b> .....	79
<b>CONCLUSIONS</b> .....	80
<b>ACKNOWLEDGMENTS</b> .....	80
<b>REFERENCES</b> .....	81
<b>APPENDICES</b>	
1. Calculation of diapiric strain rates from diapiric growth rates .....	85
2. List of wells by cross sections .....	86

## Figures

1. Location map showing the East Texas Basin and surrounding area .....	3
2. Index map of the East Texas Basin showing cross-section lines and logged wells .....	4
3. Stratigraphic column of the East Texas Basin .....	5
4. Schematic cross sections showing evolution of the East Texas Basin and the Gulf of Mexico .....	6
5. Schematic block diagrams of facies around salt structures during early evolution of the East Texas Basin .....	7
6. Isometric block diagrams of salt structures in the East Texas Basin .....	8
7. Structure map showing four salt provinces in the East Texas Basin .....	10
8. Schematic stages of dome growth and characteristics of strata, East Texas Basin .....	12
9. Mapped areas of stratal thinning over salt pillows in the East Texas Basin .....	14
10. Southwest-northeast cross section and map, Hainesville Dome .....	15
11. Map of primary peripheral sinks, East Texas Basin .....	16
12. Map of net sandstone, Paluxy Formation .....	17
13. Cross section D-D', Paluxy Formation, across Van, Hainesville, and Hawkins salt structures .....	18
14. Schematic cross sections showing inferred evolution of salt structures .....	19
15. Map of secondary peripheral sinks, East Texas Basin .....	21
16. Cross section U-U', Hainesville Dome area .....	22
17. Isopach map, Lower Taylor Formation - Austin Group, Hainesville Dome area .....	23
18. Isopach map of salt-withdrawal basins, Paluxy and Walnut Formations .....	24
19. Isopach map of salt-withdrawal basins, Washita Group .....	25
20. Isopach map of salt-withdrawal basins, Glen Rose Subgroup .....	26
21. Cross section Z-Z', Glen Rose Subgroup .....	27
22. Cross section X-X', and maps of isopach, net sandstone, and structure, Paluxy Formation .....	28
23. Map of tertiary peripheral sinks, Wilcox Group, southern part of the East Texas Basin .....	29
24. Sand-percent map, Wilcox Group .....	30
25. Cross section B-B', Wilcox Group, Bethel Dome area .....	31
26. Cross section A-A', Wilcox Group, Oakwood Dome area .....	32
27. Relation between above-dome topography and surficial sand distribution, Upper Texas Gulf Coast .....	34
28. Location map of Hormuz salt plugs and Yas Island salt dome, Persian Gulf .....	35
29. Schematic block diagrams of facies around salt structures during late evolution of the East Texas Basin .....	36
30. Schematic cross section through a mature diapir showing typical facies variations and potential petroleum traps .....	37
31. Three groupings of domes in the East Texas Basin based on the timing of stages of salt movement .....	39
32. Map of three age groups of salt diapirs in the East Texas Basin .....	40
33. Regional isopach map, Glen Rose Subgroup .....	41
34. Regional isopach map, Paluxy and Walnut Formations .....	42
35. Regional isopach map, Lower Taylor Formation and Austin Group .....	44

36. Technique for calculating the volume of a salt-withdrawal basin.....	46
37. Dome-growth-rate curves calculated on the basis of compacted and decompactd sediments, East Texas Basin.....	48
38. Percentage thickness change around selected diapirs and pillows in the East Texas Basin.....	50
39. Fold-shape analysis.....	51
40. Cross sections of model domes .....	52
41. Measurement of isochore thickness parameters in model domes .....	53
42. Histograms showing frequency distribution of thickness changes in model domes .....	54
43. Comparison of axial-trace positions for salt domes in the East Texas Basin and for model domes.....	55
44. Cross sections of Hainesville, Grand Saline, and Keechi Domes.....	57
45. Methods of calculating net and gross rates of dome growth.....	58
46. Histograms of thickness and rate of regional sediment accumulation of major stratigraphic units in the East Texas Basin .....	63
47. Cumulative-probability curves of sediment-accumulation rate in the East Texas Basin.....	64
48. Contour map showing sample grid spacing and standard deviation of sediment-accumulation rate, Lower Taylor Formation and Austin Group .....	65
49. Histogram of the volumes of salt-withdrawal basins and volumetric rates at which salt-withdrawal basins were filled in the East Texas Basin .....	67
50. Histogram of the volumes of salt-withdrawal basins for diapirs in the East Texas Basin.....	68
51. Net rates of salt-pillow growth, East Texas Basin.....	69
52. Maximum net rates of dome growth, Oakwood and Hainesville Domes .....	70
53. Maximum net rates of dome growth and mean rate of regional sediment accumulation in the East Texas Basin .....	72
54. Residual rates of dome growth for 16 East Texas salt domes.....	73
55. Gross rates of dome growth in the East Texas Basin .....	74
56. Hypothetical gross and actual heights of diapirs in the East Texas Basin .....	75
57. Comparison of published net and gross rates and methods of dome growth .....	76

## Tables

1. Net rate of pillow growth, East Texas Basin .....	60
2. Net rate of diapir growth, East Texas Basin .....	60
3. Gross rate of diapir growth, East Texas Basin .....	61
4. Statistical analysis of data on thickness and rate of regional sediment accumulation for major stratigraphic units, East Texas Basin.....	62
5. Volume of salt-withdrawal basins, East Texas Basin .....	66
6. Comparison of rates of salt-dome growth and methods used to calculate them .....	77
7. Overall and fastest bulk-strain rates in East Texas Basin salt diapirs .....	78

## ABSTRACT

Post-Aptian strata (younger than 112 Ma) in the East Texas Basin were strongly influenced by halokinesis and record the evolution of associated salt structures. Comparisons with model diapirs and dome-induced changes in patterns of sandstone distribution, depositional facies, and reef growth indicate that thickness variations in strata surrounding domes were caused by syndepositional processes rather than by tectonic distortion.

Salt domes in the East Texas Basin exhibit three stages of growth: pillow, diapir, and postdiapir. Each stage affected surrounding strata differently. Pillow growth caused broad uplifting of strata over the crest of the pillows. The resulting topographic swells influenced depositional trends and were susceptible to erosion. Fluvial-channel systems bypassed pillow crests and stacked vertically in primary peripheral sinks on the updip flanks of the pillows. Diapir growth was characterized by expanded sections of shelf and deltaic strata in secondary peripheral sinks around the diapirs. Lower Cretaceous (Aptian stage) reefs on topographic saddles between secondary peripheral sinks now host major oil production at Fairway Field. Postdiapir crestal uplifting and peripheral subsidence affected smaller areas than did equivalent processes that occurred during pillow or diapir stages.

Pre-Aptian domes grew in three areas around the margin of the diapir province, apparently in pre-Aptian depocenters. Maximum dome growth along the basin axis coincided with maximum regional sedimentation there during the Early and Late Cretaceous (Aptian, Albian, and Cenomanian stages). In the Late Cretaceous, the sites of maximum diapirism migrated to the margin of the diapir province. Diapirism began after pillows were erosionally breached, which led to salt extrusion and formation of peripheral sinks.

The duration of pillow and diapir stages of growth was subequal, ranging from 10 to 30 Ma. Postdiapiric growth continued for more than 112 Ma in some cases. Diapirs grew fastest in the Early Cretaceous, when peak growth rates ranged from 150 to 530 m/Ma, declining in the early Tertiary to 10 to 60 m/Ma. Assuming steady-state conditions over periods of 1 to 17 Ma, strain rates during growth of the East Texas diapirs averaged  $6.7 \times 10^{-16}/s$ ; peak gross rates of growth averaged  $2.3 \times 10^{-15}/s$ , similar to slow orogenic rates. The evolution of East Texas salt domes essentially ended in the early Tertiary, when uplift rates were less than 30 m/Ma.

Long-term and recent rates of dome growth in East Texas indicate a low probability that future dome uplift will breach an intradomal waste repository. During deposition of the Eocene Wilcox Group, fine-grained floodplain sediments accumulated over and around active diapirs in the East Texas Basin, including Oakwood salt dome. These fine-grained sediments now sheathing diapirs are aquitards favorable for waste isolation. However, sand-rich channel facies in rim synclines commonly surround the fine-grained sheath and constitute interconnected aquifers around diapirs. A potential pathway for radionuclides leaking from a dome could occur if interconnected aquifers intercept the dome. Dome-specific facies variability is difficult to detect because the variability commonly exceeds available well spacing. Site characterization of a potential waste repository must therefore be based on dense well control and on an understanding of dome growth history and diapiric processes in order to better predict facies distributions around domes.

Facies variations over and around domes at different stages of growth enable prediction of the location of subtle, facies-controlled hydrocarbon traps. These facies traps are likely to be the only undiscovered traps remaining in mature petroliferous basins such as the East Texas Basin.

**Keywords:** Cretaceous-Tertiary, depositional facies, East Texas Basin, petroleum exploration, petroleum traps, rates of dome growth, salt domes, salt tectonics, stress-strain, waste disposal.

## INTRODUCTION

Many studies of salt domes of the Texas-Louisiana Gulf Coast and Gulf Interior Basins have been published since the turn of the century. These range in scope from work on grain-scale deformation in domal rock to studies of the role of salt-related tectonics in the structural evolution of the Gulf of Mexico. Study of salt domes has historically been propelled by economic motives, initially in the search for salt in shallow diapirs and for sulfur and

gypsum in cap rocks, and later in exploration for structural traps of oil and gas.

By about 10 years ago the basic subsurface exploration of all major interior and coastal domes was completed, and interest in salt-dome studies had declined. Two developments in the mid-1970's, however, fueled a resurgence of interest in salt domes. First, as a result of the 1974 oil embargo and the subsequent quadrupling of oil prices, economic

incentives encouraged a program of active exploration in the United States to decrease dependence on imported oil. The abundance of structural and stratigraphic traps around salt structures made them renewed targets for both onshore and offshore petroleum exploration. Second, the search for a safe method of disposing of high-level nuclear wastes, which had been accumulating in temporary storage for decades, inspired the systematic evaluation of potential repositories, including salt domes. Thus was born the National Waste Terminal Storage (NWTS) program in 1976. One of the most important aspects of this investigation is the evaluation of the relative merits of different geologic media that could serve as long-term repositories of waste and that could safely isolate such wastes from the biosphere until radiation declines to acceptable levels.

A program coordinated by the Office of Nuclear Waste Isolation (ONWI) at Battelle Memorial Institute has examined the usefulness of salt domes and bedded salt as host media for such a repository. Salt has been considered the favored medium since 1957 because of its high thermal conductivity, high ductility, stability against radiation, opacity to gamma radiation, ease of mining, and abundance (National Academy of Science - National Research Council, 1957; ONWI, 1982). Against these advantages must be set the disadvantages of high solubility, low shear strength, and high potential for flow of salt.

This study, which was funded by the Department of Energy through the NWTS program, represents a new look at salt domes in the most highly explored interior salt-dome province in the world. There are several approaches to the problem of assessing salt-dome stability (Kreitler and others, 1980, 1981); these approaches must be integrated to arrive at reliable conclusions concerning future dome stability. Geologic processes that influence stability of salt domes include regional faulting, fracturing, and seismicity (Dix and Jackson, 1981; Jackson, 1982; Pennington and Carlson, in preparation), subsurface dissolution by ground water (Fogg, 1981a, 1981b; Fogg and Kreitler, 1981), and rates of erosion and stream incision (Collins, 1982). This paper describes the stages of Cretaceous and Tertiary dome growth in the East Texas Basin (fig. 1). Our approach has been to reconstruct, both qualitatively and quantitatively, the history of salt flow throughout the basin by studying the subsurface sedimentary record around the salt domes. Subsurface data down to the depth of the salt source layer are not necessary for reconstruction of the Cretaceous to Tertiary history of salt movement. Studies of pre-Cretaceous salt movement are handicapped by a paucity of data in much of the basin. Nevertheless, this early history is de-

scribed qualitatively in this report. In addition to studying depositional systems, we determined the volumes of salt and sediments by planimetry, compared gross versus net rates of dome growth, determined strain rates based on regional subsurface data, used cumulative-probability analysis on thickness patterns, and constructed standard-deviation maps of sediment-accumulation rates. Regional isopach maps show integrated thickness data and were used in a number of ways. Closed isopach contours around salt structures delineate the area influenced by local salt flow in different stratigraphic intervals. Our basinwide, depositional-systems approach emphasizes regional as well as local variations in salt-related thickness and facies.

Thickness variations in the East Texas Basin have been studied by means of facies maps, lithostratigraphic cross sections, and regional isopach maps (fig. 2). All thickness values refer to vertical thickness (isochores) rather than stratigraphic thickness (isopachs). However, with maximum regional dips of 9.7 degrees in the rim synclines and mean regional dips of approximately 1.6 degrees in the entire basin, the maximum difference between isochores and isopachs of 1.4 percent and 0.04 percent, respectively, is negligible. These techniques allow differentiation between regional thickness and local salt-related subsidence.

Results of this research have important implications both for nuclear waste isolation and for oil and gas exploration. Geologic stability of host rock is an important criterion in repository site evaluation (ONWI, 1981). One critical concern regarding the geologic stability of salt domes is whether or not such structures are still rising. The present study provides quantitative estimates of the growth rate of the diapirs from 112 Ma (millions of years) to 48 Ma ago, the age of the youngest strata exposed. Growth declined to negligible rates by the end of the sedimentary record. We consider the potential for halokinetic rise of the East Texas domes by more than 15 m (50 ft) in the next 250,000 yr to be small.

Dome growth creates a wide range of subtle traps for migrating petroleum, including stratigraphic, unconformity, and paleogeomorphic types (Halbouty, 1980). Their early formation enables oil to be trapped at the onset of migration. These subtle traps are especially significant for future exploration in highly mature areas such as the Gulf Interior and Gulf Coast Basins. Using logs from approximately 2,000 wells in the East Texas Basin, we recognize specific stages of salt-dome growth, each characterized by different combinations of subtle traps, as well as by more obvious structural ones. Understanding this domal evolution and its lithologic and structural effects allows prediction of subtle traps

both in mature basins and in other, less explored salt basins. On the basis of this information, it is possible to anticipate the occurrence of stratigraphic traps in different areas and at different stratigraphic levels. Knowing the geometry of individual salt structures at different evolutionary stages is also vital for reconstructing the history of petroleum migration and pooling in structural traps.

point (CDP) seismic data, a residual-gravity map (Exploration Techniques, 1979), and gravity models of specific salt domes (Exploration Techniques, 1979). Appendix 1 shows two methods of calculating diapiric strain rates. Appendix 2 lists wells included on major cross sections within this report.

## DATA BASE

The data base for this study consists of electric, density, and sonic logs from about 2,000 wells (fig. 2), core control for the shallow stratigraphic section, 740 km (444 mi) of sixfold common-depth-

## EARLY HISTORY OF BASIN FORMATION AND FILLING

The East Texas Basin is one of several inland Mesozoic salt basins in Texas, Louisiana, and Mississippi that flank the northern Gulf of Mexico (fig. 1). The general stratigraphy (fig. 3) and

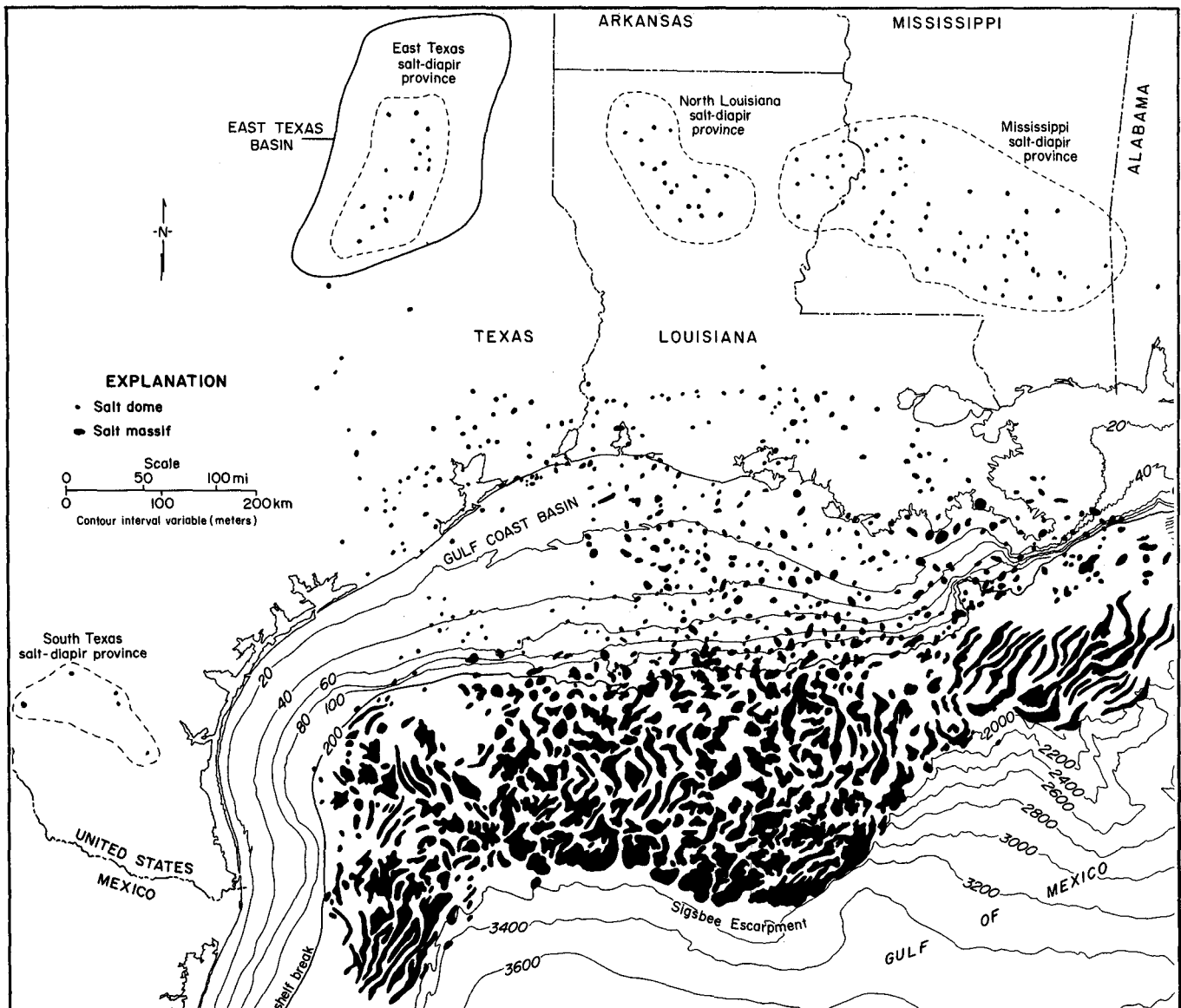


FIGURE 1. Location map showing the East Texas Basin, Gulf Coast Basin, inland salt-diapir provinces, and salt domes and massifs. (After Martin, 1978.)



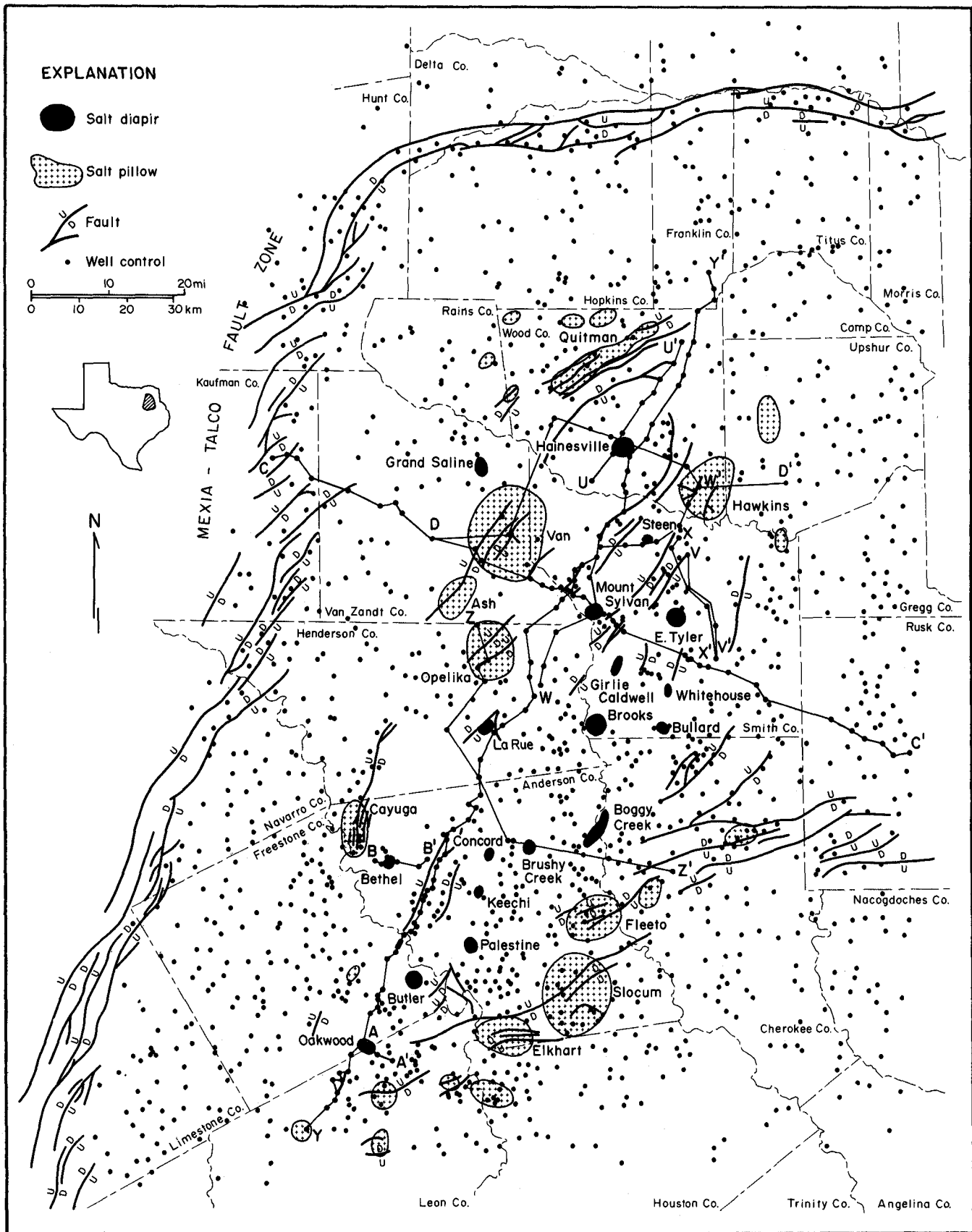
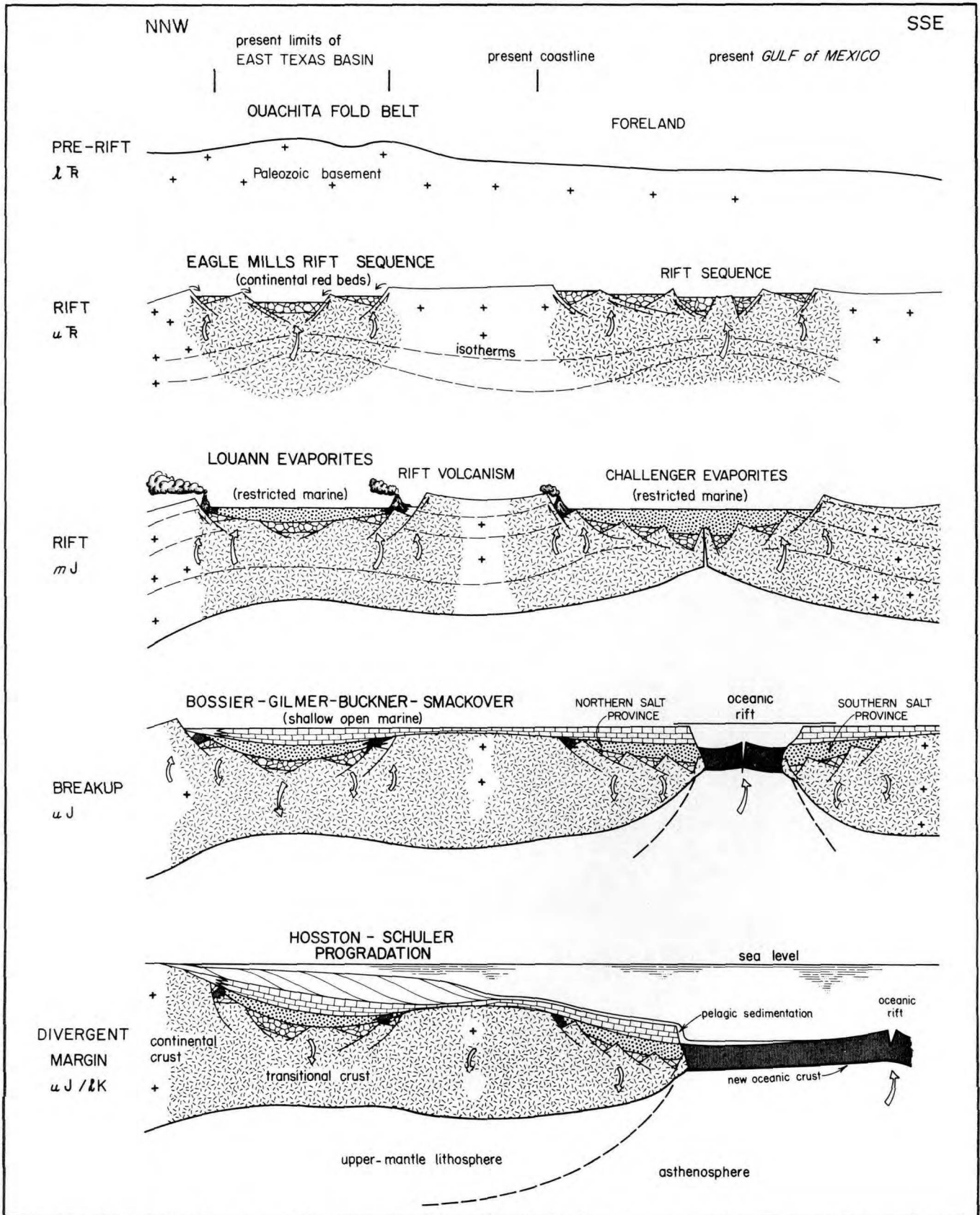


FIGURE 2. Index map of the East Texas Basin showing cross-section lines and locations of logged wells used in interval isopach mapping.





**FIGURE 4.** Schematic north-northwest - south-southeast cross sections showing evolutionary stages in formation of the East Texas Basin and adjoining Gulf of Mexico (not to scale). Intervening area lies just south of the present Sabine Arch. Arrows indicate inferred thermally induced isostatic movement of the crust. (From Jackson and Seni, 1983a.)

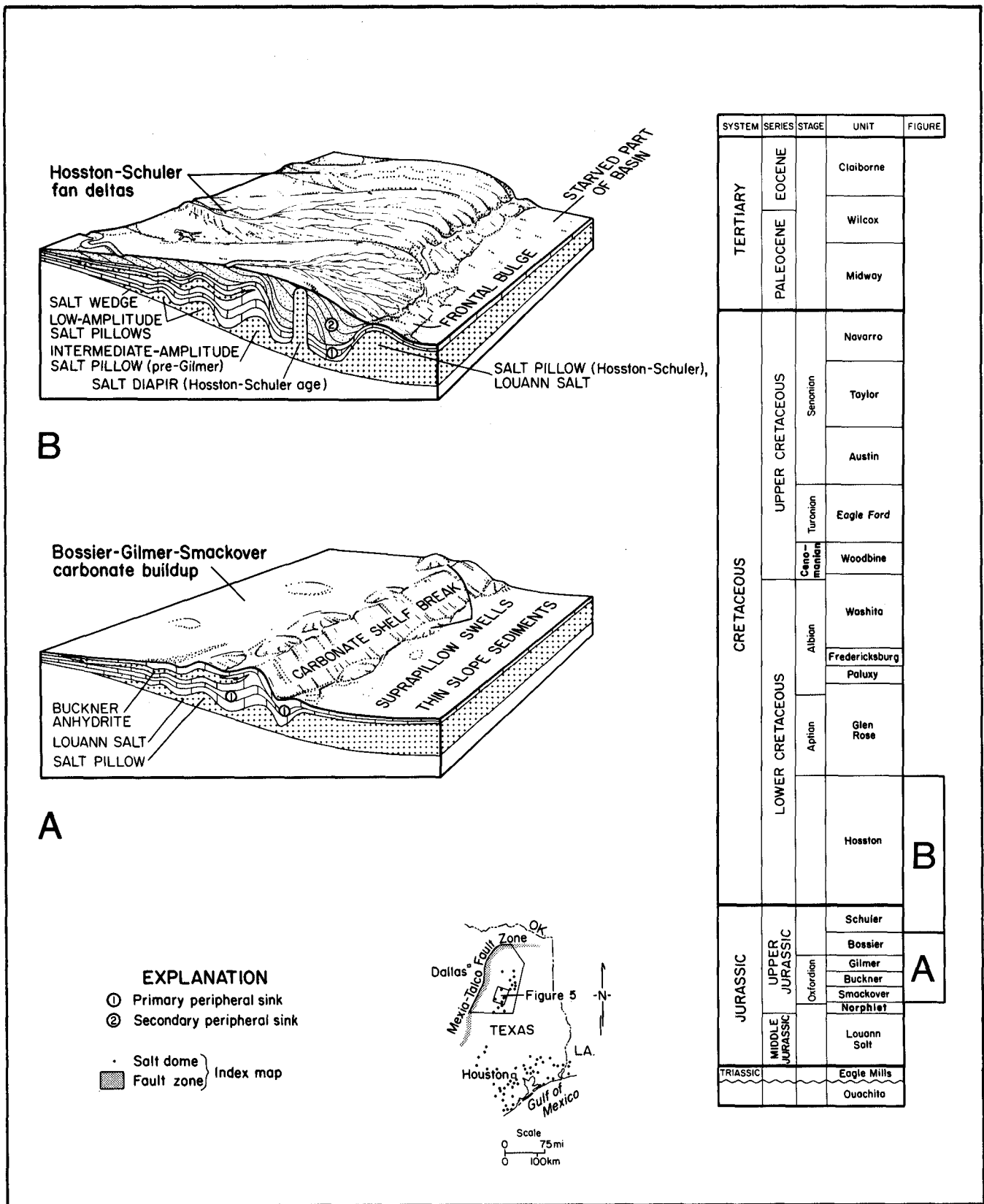
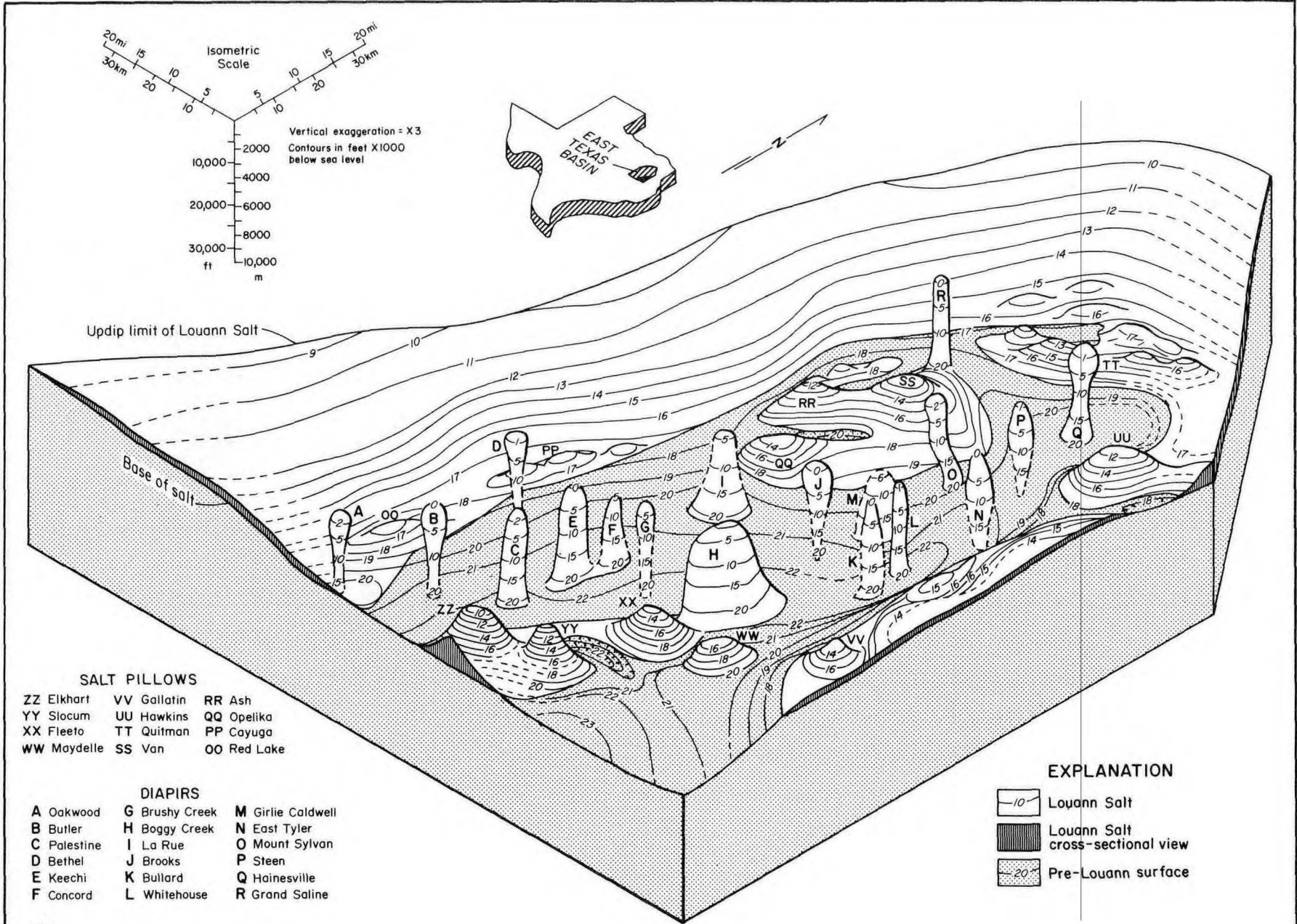


FIGURE 5. Schematic block diagrams of facies around salt structures, showing relation between salt flow and sediment accumulation during early evolution of the East Texas Basin. (A) Initiation of salt flow in Late Jurassic, 150 to 137 Ma ago. (B) Initiation of group 1 diapirs in Late Jurassic - Early Cretaceous time, 137 to 115 Ma ago. (After Jackson and Seni, 1983a.) See fig. 29 for later evolution, labeled (C) and (D).



20mi 15 10 5  
30km 20 10 5

Isometric Scale

Vertical exaggeration = X3  
Contours in feet X1000  
below sea level

10,000  
20,000  
30,000  
ft  
10,000  
m

Updip limit of Louann Salt

Base of salt

**SALT PILLOWS**

- |             |             |             |
|-------------|-------------|-------------|
| ZZ Elkhart  | VV Gallatin | RR Ash      |
| YY Slocum   | UU Hawkins  | QQ Opelika  |
| XX Fleeto   | TT Quitman  | PP Cayuga   |
| WW Maydelle | SS Van      | OO Red Lake |

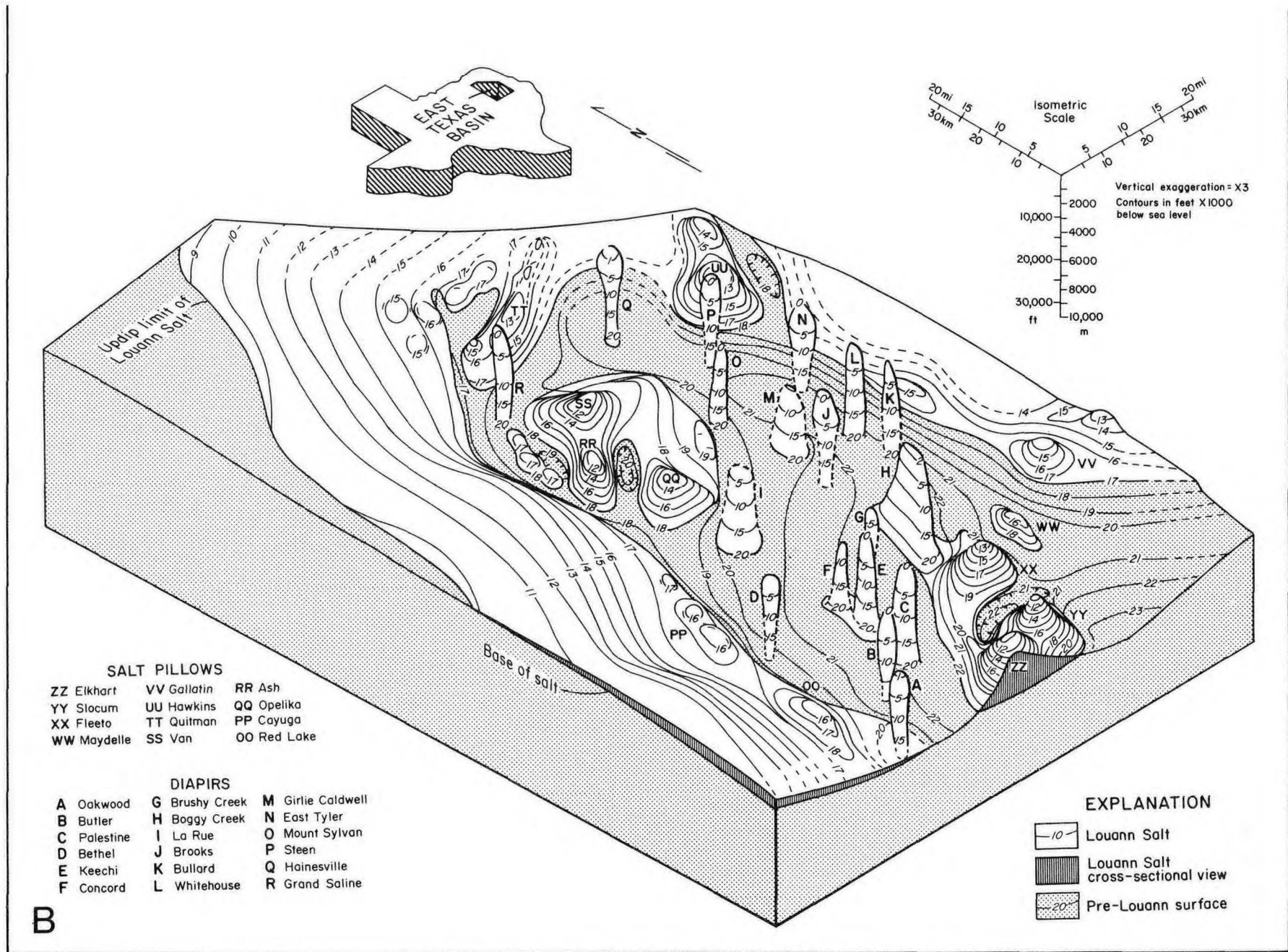
**DIAPIRS**

- |             |                |                   |
|-------------|----------------|-------------------|
| A Oakwood   | G Brushy Creek | M Girlie Caldwell |
| B Butler    | H Boggy Creek  | N East Tyler      |
| C Palestine | I La Rue       | O Mount Sylvan    |
| D Bethel    | J Brooks       | P Steen           |
| E Keechi    | K Bullard      | Q Hainesville     |
| F Concord   | L Whitehouse   | R Grand Saline    |

**EXPLANATION**

- 10 Louann Salt
- Louann Salt cross-sectional view
- 20 Pre-Louann surface

A



**FIGURE 6. Isometric block diagrams of salt structures in the East Texas Basin showing three-dimensional configuration of structure contours on top of Louann Salt or, where salt is absent, on top of pre-Louann basement. (A) Northwest view (Jackson and Seni, 1983a). (B) Northeast view. Constructed by isometric projection and incremental translation of contours, following Lobeck (1924, p. 138-142).**



center is largely a function of increasing thickness of the original salt layer toward the basin center (Jackson and Seni, 1982). However, lithofacies and thickness variations of postsalt strata controlled when and where salt was gravitationally mobilized, rather than controlling the form of the salt structures.

## EVOLUTIONARY STAGES OF DOME GROWTH

The evolution of salt from planar beds to near-vertical subcylindrical stocks involves pillow, diapir, and postdiapir stages in the Zechstein Salt Basin of North Germany (Trusheim, 1960). Data presented here indicate that the three-stage model of dome growth for that salt basin is also appropriate for the East Texas Basin. Each stage had distinctive effects on depositional facies, lithostratigraphy, and thickness of surrounding sediments (fig. 8).

Salt structural evolution has received much attention in the literature (for example, Bornhauser, 1958; Atwater and Forman, 1959; Trusheim, 1960; Bishop, 1978; Halbouty, 1979) because such structures form obvious structural traps for petroleum. Controversy surrounds the hypotheses of diapir emplacement and hinges on whether the dominant process was intrusion (favored by DeGolyer, 1925; Barton, 1933; Nettleton, 1934; Trusheim, 1960; Sannemann, 1968; Smith and Reeve, 1970; Kupfer, 1970, 1976; O'Neill, 1973; Stude, 1978; Kent, 1979; Woodbury and others, 1980) or extrusion (favored by Loocke, 1978; Turk, Kehle and Associates, 1978; Jaritz, 1980; R. O. Kehle, personal communication, 1982). Bishop (1978) theorized that diapirism typically either occurs by extrusion or alternates between intrusion and extrusion. Barton (1933), Bornhauser (1958, 1969), and Johnson and Bredeson (1971) emphasized the role of sediment "downbuilding" around salt structures whose crests remain more or less stationary and relatively close to the depositional surface. Bishop (1978) emphasized the importance of understanding the depositional history of surrounding sediments in interpreting dome growth history, an approach followed here.

Irrespective of the mechanism responsible for salt movement and diapirism, flow of salt into a growing structure creates a withdrawal basin that is a structural low and isopachous thick. "Withdrawal basin" is a general term that includes the rim syncline (a geometric term) and primary, secondary, and tertiary peripheral sinks (genetic terms) (fig. 8). Trusheim (1960) defined primary peripheral sinks as forming during pillow growth, secondary peripheral sinks as forming during diapir growth, and tertiary peripheral sinks as forming during postdiapir

growth. We retain Trusheim's definition of primary peripheral sinks and distinguish quantitatively between secondary and tertiary peripheral sinks. We define secondary peripheral sinks as containing units at least 50 percent thicker than adjacent units unaffected by salt withdrawal. We define tertiary peripheral sinks as containing units that are less than 50 percent thicker than adjacent unaffected strata because of much slower rates of salt movement at this later stage. The term "sink" is used in a structural sense. Ramberg (1981, p. 286) pointed out that in terms of fluid dynamics, the rim syncline is actually the source of the flow, whereas the dome is the true sink.

The following sections present effects of the three stages of dome growth on the lithology of surrounding strata in the East Texas Basin (fig. 8).

### PILLOW STAGE

Salt pillows are defined here as concordant anticlinal or laccolith-shaped salt structures characterized by any amplitude/wavelength ratio. The growth of salt pillows is influenced by uneven sediment loading, salt buoyancy, downdip creep of salt, subsalt discontinuities, and depositional rate and erosional rate of postsalt deposits on the pillow crest. Although the relative importance of these processes is poorly understood, evidence of early (pre-Gilmer) salt movement under thin sedimentary cover of less than 600 m (2,000 ft) (Hughes, 1968; Jackson, 1982) suggests that uneven sediment loading and rate of deposition were the principal mechanisms that controlled the early history of salt movement (Bishop, 1978; R. O. Kehle, personal communication, 1982).

Deposition during pillow growth is characterized by (1) thinning toward the axis of salt uplifts, (2) only minor thickening in relatively distant primary peripheral sinks, and (3) lithostratigraphic variations over the crests of pillows and in primary peripheral sinks.

### Geometry of Overlying Strata

Syn depositional thinning of sediments over the crest and flanks of growing salt pillows is the most diagnostic feature of salt movement during the pillow stage. Quitman, Van, and Hawkins salt pillows (fig. 2) are at similar elevations, about -3,650 m (-12,000 ft), but show differing patterns of sediment thinning over the pillow crests. Accordingly, drape and differential compaction of sediments over the salt structures had less effect on thinning than did rate of salt movement.



Four salt pillows—Van, Hawkins, Hainesville, and Bethel—influenced local thickness (fig. 9) and facies variations in sediments deposited from the Early to Late Cretaceous (112 to 86 Ma ago). Two of these pillows (Hainesville and Bethel) subsequently evolved into diapirs. The remaining pillows in the East Texas Basin exerted little concurrent effect on thickness or facies in surrounding strata, remaining quiescent the past 112 Ma.

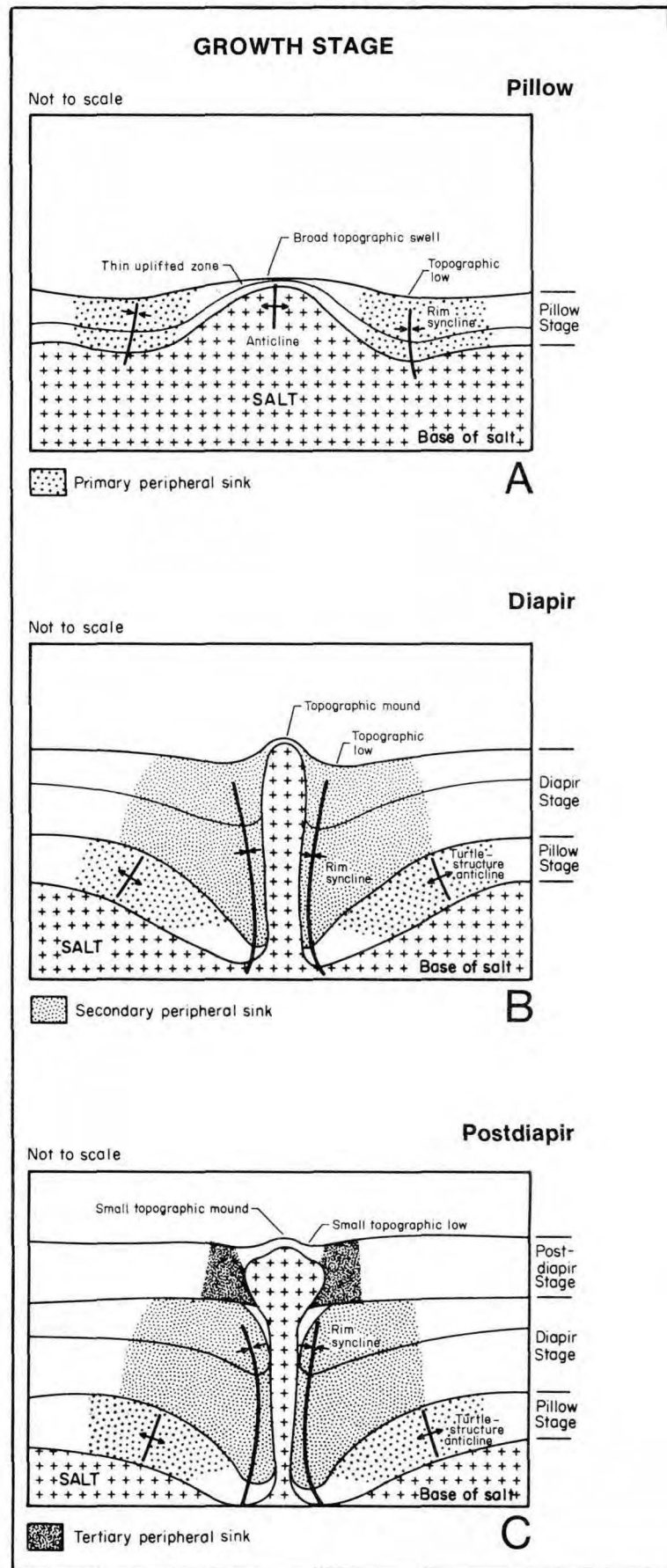
An area of 100 to 400 km<sup>2</sup> (40 to 155 mi<sup>2</sup>) over each of the four active Paluxy Formation salt pillows mentioned in the preceding paragraph contains stratigraphic intervals thinned from 10 to 100 percent; thinning is typically about 25 percent. Strata that have been thinned by salt uplift are stacked vertically over the crest of each pillow (fig. 9). The thin areas over the crests of salt pillows did not migrate laterally.

Hainesville Dome provides the best example of the geometry of strata around a growing pillow (fig. 10). Lower Cretaceous strata onlap and pinch out toward the dome, indicating syndepositional sedimentation and erosion around a growing swell during pillow-stage growth (Loocke, 1978, p. 40-46).

### Geometry of Surrounding Strata

A second but less diagnostic characteristic of pillow growth is the presence of primary peripheral sinks (fig. 11). Primary peripheral sinks are typically broad, shallow basins that are 10 to 30 percent thicker than adjacent strata unaffected by salt flow. The axial traces of these basins are located 5 to 20 km (3 to 12 mi) from the crests of Van, Hawkins, Hainesville, and Bethel salt pillows (fig. 11). The axial traces are either subparallel to crest lines of pillows or partially concentric to them, as in a rim syncline. Sinks are equidimensional or elongate in plan and are concentrated on the updip side of the salt structures, as exemplified by Bethel, Van, and Hainesville salt pillows (fig. 11). In the Zechstein Salt Basin of North Germany, the primary peripheral sinks migrated toward the growing salt pillows as the flanks of the salt pillows continually steepened (Trusheim, 1960). This migration of primary peripheral sinks was not observed near East Texas pillows, but secondary and tertiary sinks in East Texas are nearer to the domes than are primary peripheral sinks (see section on "Distinguishing Between Syndepositional and Postdepositional Thickness Variations," this report, p. 49-55).

FIGURE 8. Schematic stages of dome growth in the East Texas Basin showing typical lithologic and thickness variations in strata above and around the salt structures during (A) pillow stage, (B) diapir stage, and (C) postdiapir stage.



## UPLIFTED AREA

### Geometry

Sediments above pillow are thin over broad, equidimensional to elongate area. Maximum thinning over crest. Area ranges from 100 to 400 km<sup>2</sup> (40 to 150 mi<sup>2</sup>), depending on size of pillow. Percent thinning, 10 to 100%.

### Facies

Thin, sand-poor, fluvial-deltaic deposits over crest of pillow include interchannel and interdeltic facies. Erosion common. Carbonate deposits on crest would include reef, reef-associated, and high-energy facies.

### Geometry

Strata are largely absent above dome. An area ranging from 8 to 50 km<sup>2</sup> (3 to 20 mi<sup>2</sup>) around diapir is thinned; area depends on size and dip on flanks of dome.

### Facies

Facies immediately over dome crest are not preserved because of piercing by diapir of all but the youngest strata. Sand bodies commonly pinch out against dome flanks.

### Geometry

Strata are thin or absent in an area ranging from 10 to 50 km<sup>2</sup> (4 to 20 mi<sup>2</sup>) over crest and adjacent to dome; area depends on size of dome and dip of flanks.

### Facies

Facies and strata over crest of dome are not preserved in cases of complete piercement. Modern analogs have interchannel and interdeltic facies in uplifted area. Mounds above dome include thin sands. Carbonate strata would include reef or high-energy deposits; erosion common.

## WITHDRAWAL BASIN

### Geometry

Sediments are thickened in broad to elongate primary peripheral sink, generally located on updip side of salt pillow. Axial trace of sink parallels axial trace of elongate uplift; axial traces are generally 5 to 20 km (3 to 12 mi) apart. Area of sink ranges up to 300 km<sup>2</sup> (120 mi<sup>2</sup>), depending on size of pillow. Percent thickening, 10 to 30%. Recognition of primary peripheral sink may be hindered by interference of nearby salt structures.

### Facies

Thick, sand-rich fluvial-deltaic deposits in primary peripheral sink include channel axes and deltaic depocenters. Aggradation common in topographically low area of sink. Carbonate deposits in sink would include low-energy facies caused by increase in water depth.

### Geometry

Sediments are thickened from 50 to 215% in secondary peripheral sink. Area of sink ranges up to 1,000 km<sup>2</sup> (390 mi<sup>2</sup>) in extent. Sink is equidimensional to elongate and preferentially surrounds single or multiple domes.

### Facies

Expanded section of marine facies, including limestones, chinks, and mudstones, dominates. Generally sink is filled with deeper-water, low-energy facies caused by increased water depth. Elevated saddles between withdrawal basins are favored sites of reef growth and accumulated high-energy carbonate deposits.

### Geometry

Area of tertiary peripheral sink ranges from 20 to 200 km<sup>2</sup> (8 to 80 mi<sup>2</sup>). Sediments are thickened up to 50%, commonly by > 30 m (100 ft). Axial trace of elongate to equidimensional sink surrounds or flanks a single dome, or connects a series of domes.

### Facies

Modern analogs have channel axes in sink. Aggradation of thick sands common in subsiding sink. Carbonate strata would include low-energy facies.

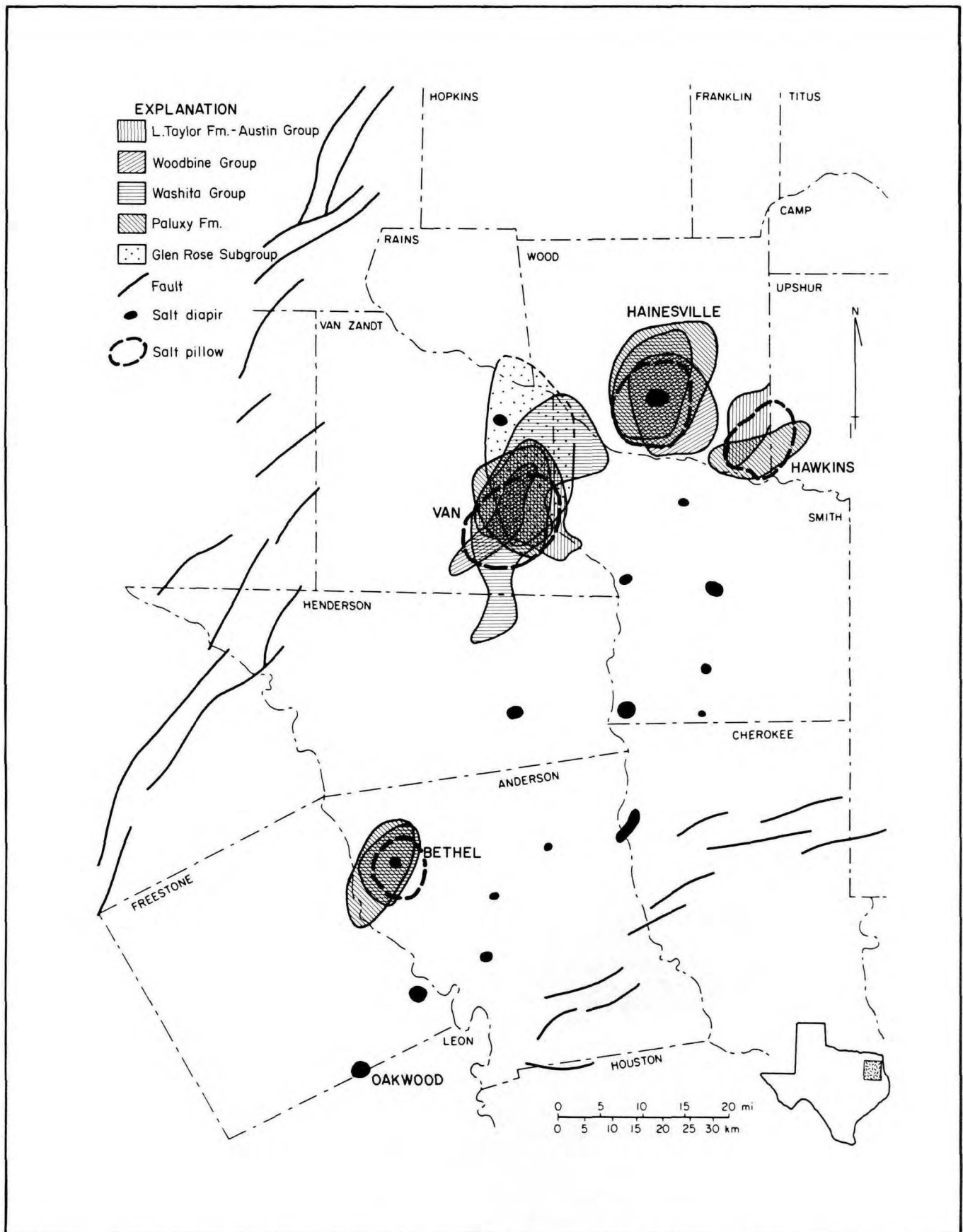
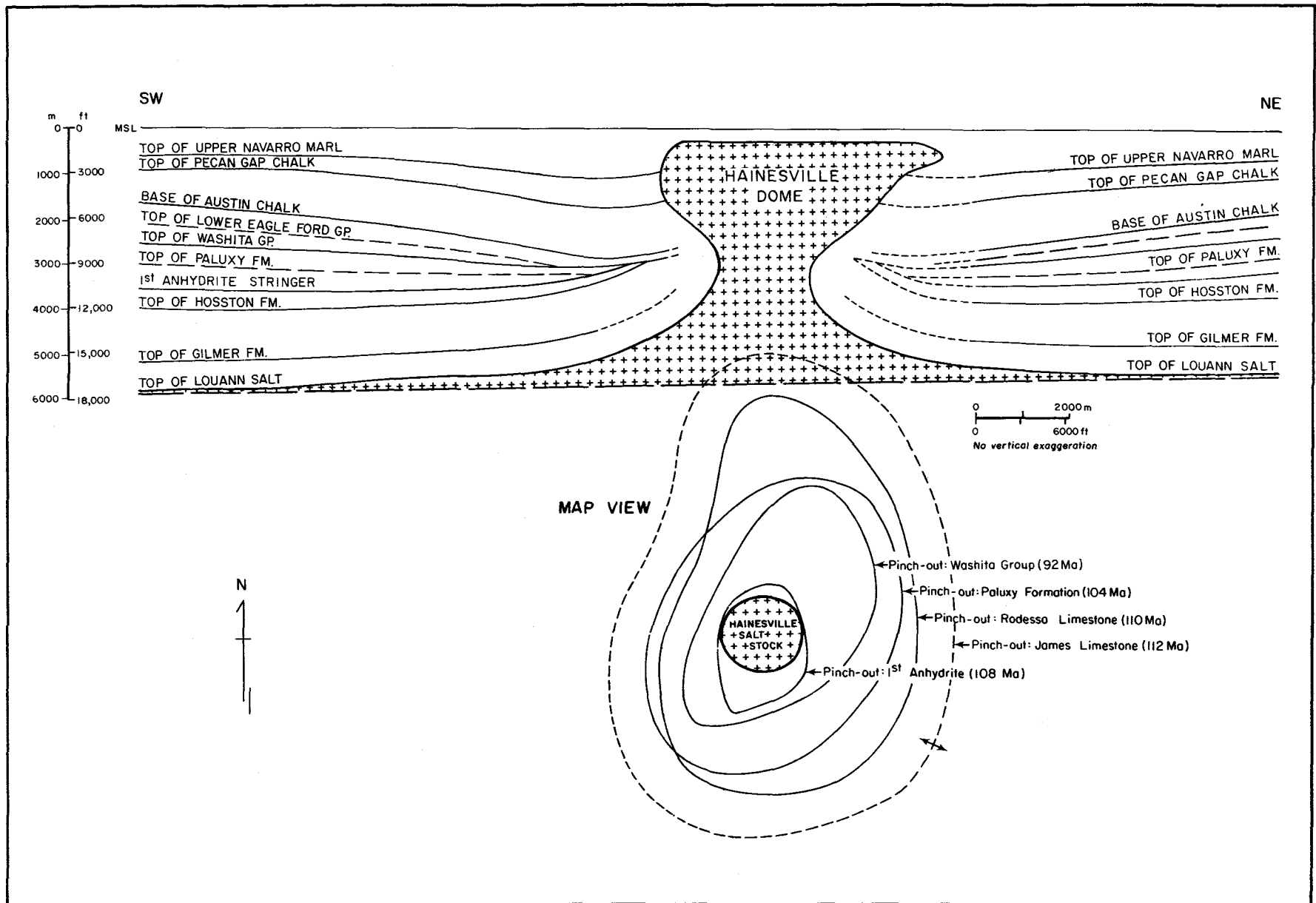


FIGURE 9. Mapped areas of stratal thinning in five isopach intervals over the crests of salt pillows in East Texas Basin.



**FIGURE 10.** Southwest-northeast cross section and map of Hainesville Dome, East Texas Basin, showing the structure of surrounding strata. Lower Cretaceous strata onlap, offlap, and pinch out around the dome. Both syndepositional and postdepositional erosion were active. Dome growth evolved from pillow stage to diapir stage between the end of Washita time and the end of Eagle Ford time. Cross section and map from interpretation of seismic data after Loocke (1978).

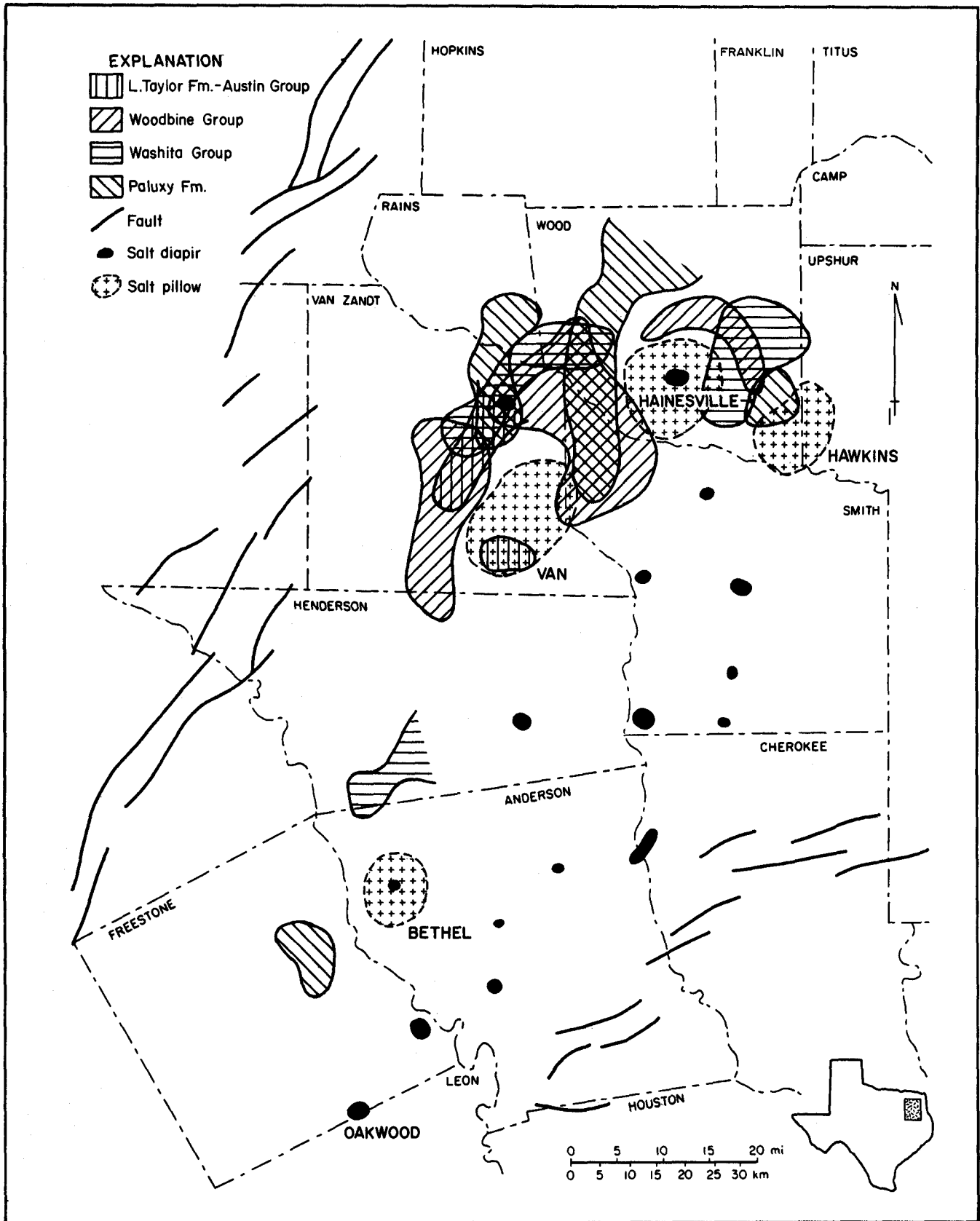


FIGURE 11. Map of primary peripheral sinks in East Texas Basin based on isopach maps of four stratigraphic units. Strata in primary peripheral sinks thickened mainly by salt flow from areas updip of the salt pillows; subordinate lateral flow was into the growing pillows.

## Depositional Facies and Lithostratigraphy

Depositional facies and sandstone distribution patterns in the Lower Cretaceous Paluxy Formation illustrate the influence of syndepositional salt movement on surrounding strata. The Paluxy Formation is typical of relatively thin (generally less than 150m, or 500 ft) Cretaceous siliciclastics around the margin of the basin that interfinger with basin-center carbonates (Walnut Formation) (Caughey, 1977; Seni, 1981).

A net-sandstone map of the Paluxy Formation (fig. 12) documents sandstone distribution in fluvial

and deltaic deposits around three salt pillows—Van, Hawkins, and Hainesville. Pillow growth is shown by decreased net and percent sandstone in strata deposited over these structures. Dip-oriented trends of net sandstone outline fluvial axes that bypassed the pillows.

Sediments in the primary peripheral sinks are significantly richer in sand than are deposits over the pillows (fig. 13); F- and t-tests at the 95-percent confidence level indicate that on the basis of boreholes shown in figure 13, the crestal areas contain between 5 and 20 percent less sand. The response of facies trends in other environments is summarized in figure 8.

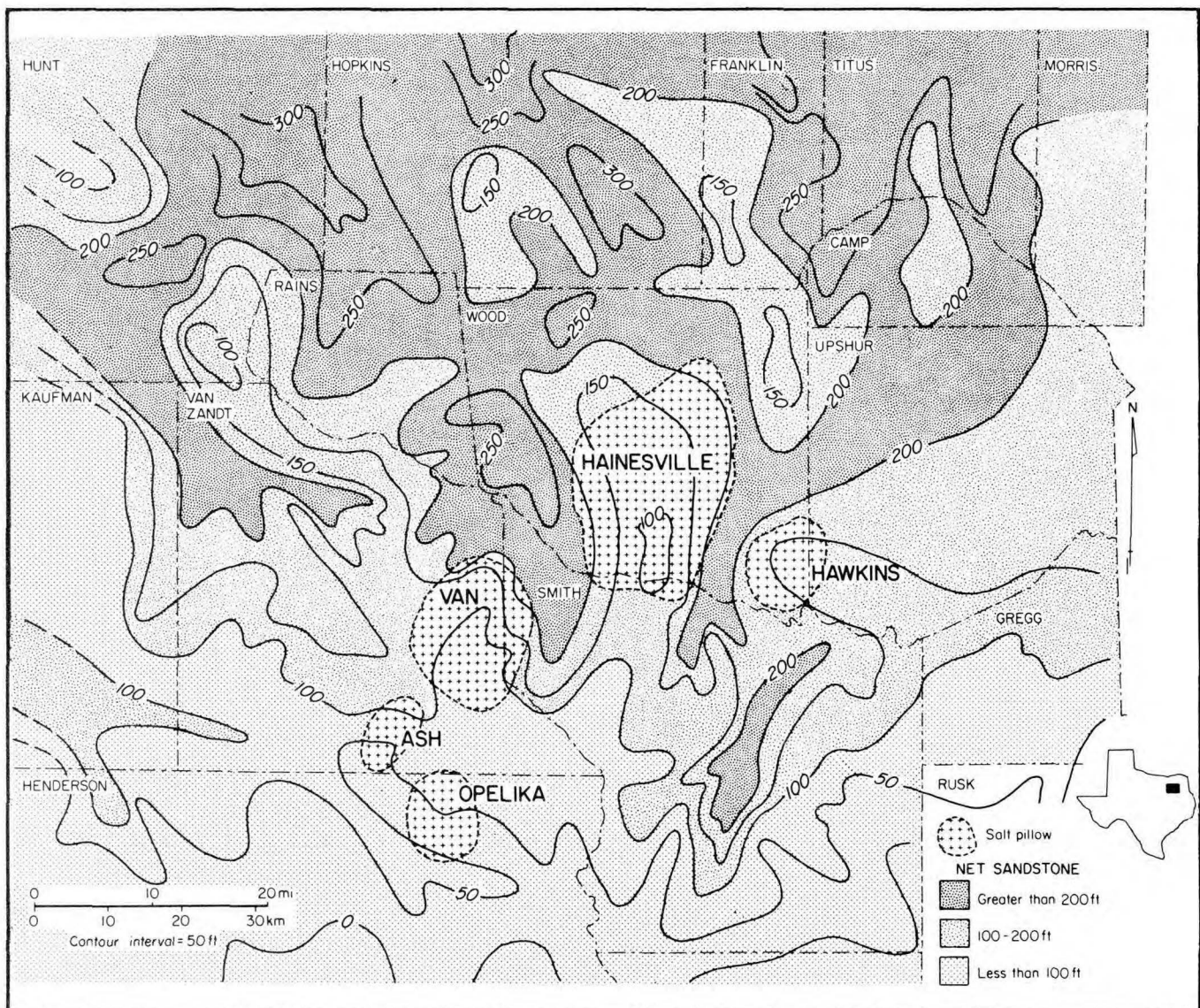
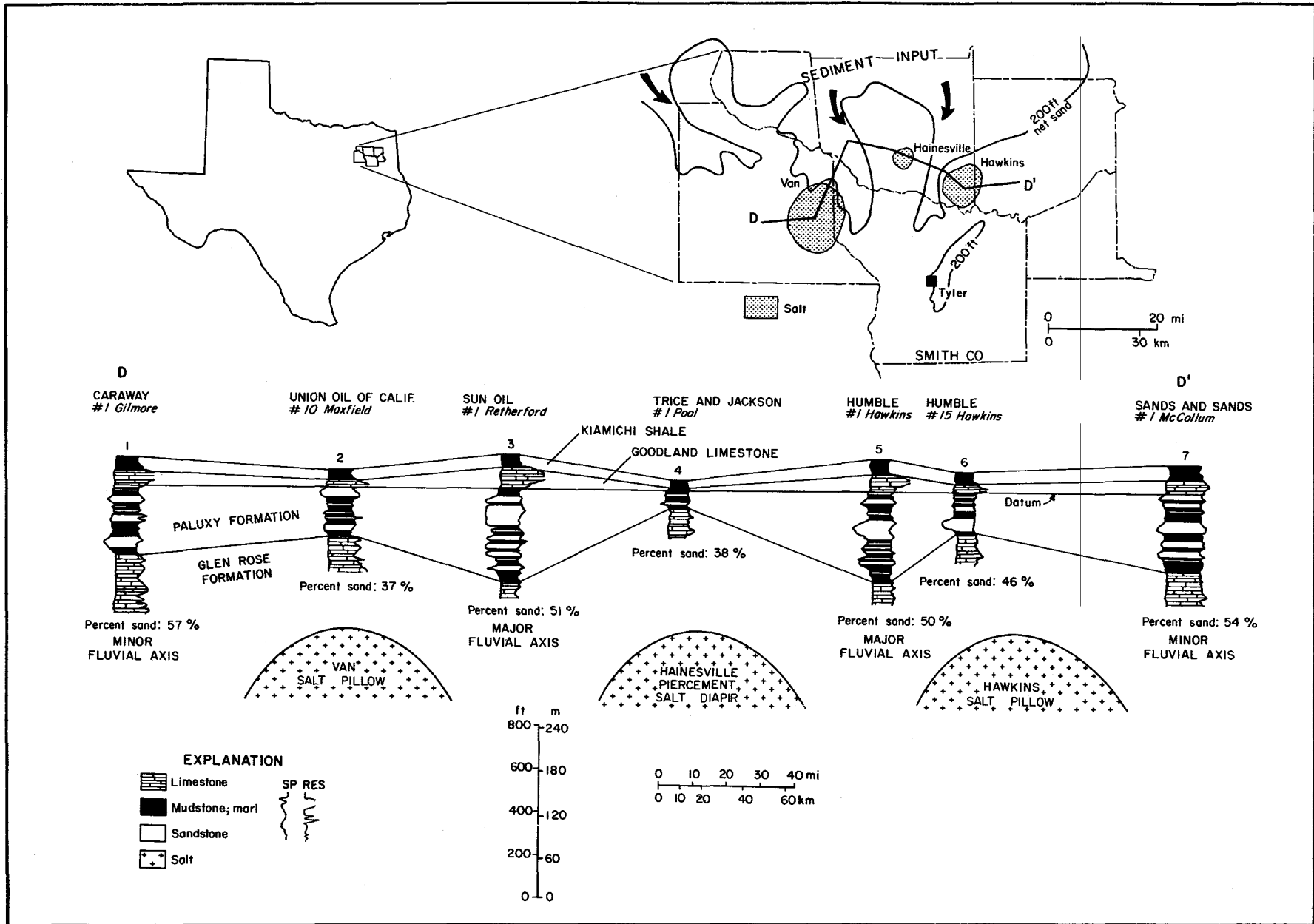


FIGURE 12. Map of net sandstone, Paluxy Formation, central and northern East Texas Basin. Dip-oriented trends of net sandstone bypass topographic highs over Van, Hainesville, and Hawkins pillows. Syndepositional erosion associated with major fluvial axes on the eastern and western flanks of the Hainesville pillow may have aided diapirism there at the expense of the Van and Hawkins pillows.



**FIGURE 13. Cross section D-D', Paluxy Formation, across Van, Hainesville, and Hawkins salt structures, northern part of the diapir province in the East Texas Basin. Decreased thickness and sand percent over each structure indicate that fluvial systems bypassed topographic swells over these salt structures in Paluxy time, as shown in the inset map.**

## DIAPIR STAGE

A primary peripheral sink is synclinal during the pillow stage (figs. 14B and 14C). During the subsequent diapir stage, the flanks of the pillow deflate because of salt withdrawal into the central, growing diapir. Pillow deflation results in a secondary peripheral sink into which the original uplifted and thinned strata collapse (fig. 14D). The thickened primary peripheral sink remains unaffected by collapse, thereby forming an anticlinal structure with a core of undeformed, thickened sediments, flanked by collapsed, thinned sediments (fig. 14E). Interdomal strata thereby undergo structural inversion from a syncline to an anticline, creating a turtle-structure anticline (Trusheim, 1960), whereas the reverse takes place for strata immediately adjacent

to diapirs. Turtle-structure anticlines are economically important because they have yielded 363 million bbl of oil, or 22 percent of the cumulative oil production from the central part of the East Texas Basin (Wood and Giles, 1982).

The diapir stage of salt movement is therefore characterized by deep, sediment-filled sinks that surround or flank the salt dome in the form of rim synclines. Secondary peripheral sinks contain thicker sediment accumulations and cover greater areas than do primary or tertiary peripheral sinks. Diapiric uplift exposes overlying strata to erosion, thereby destroying the sedimentary record over the diapir. We can only speculate on the nature of these sedimentary environments (fig. 8). Commonly, units thin abruptly near the diapir crests. This thinning may be either syndepositional or postdepositional.

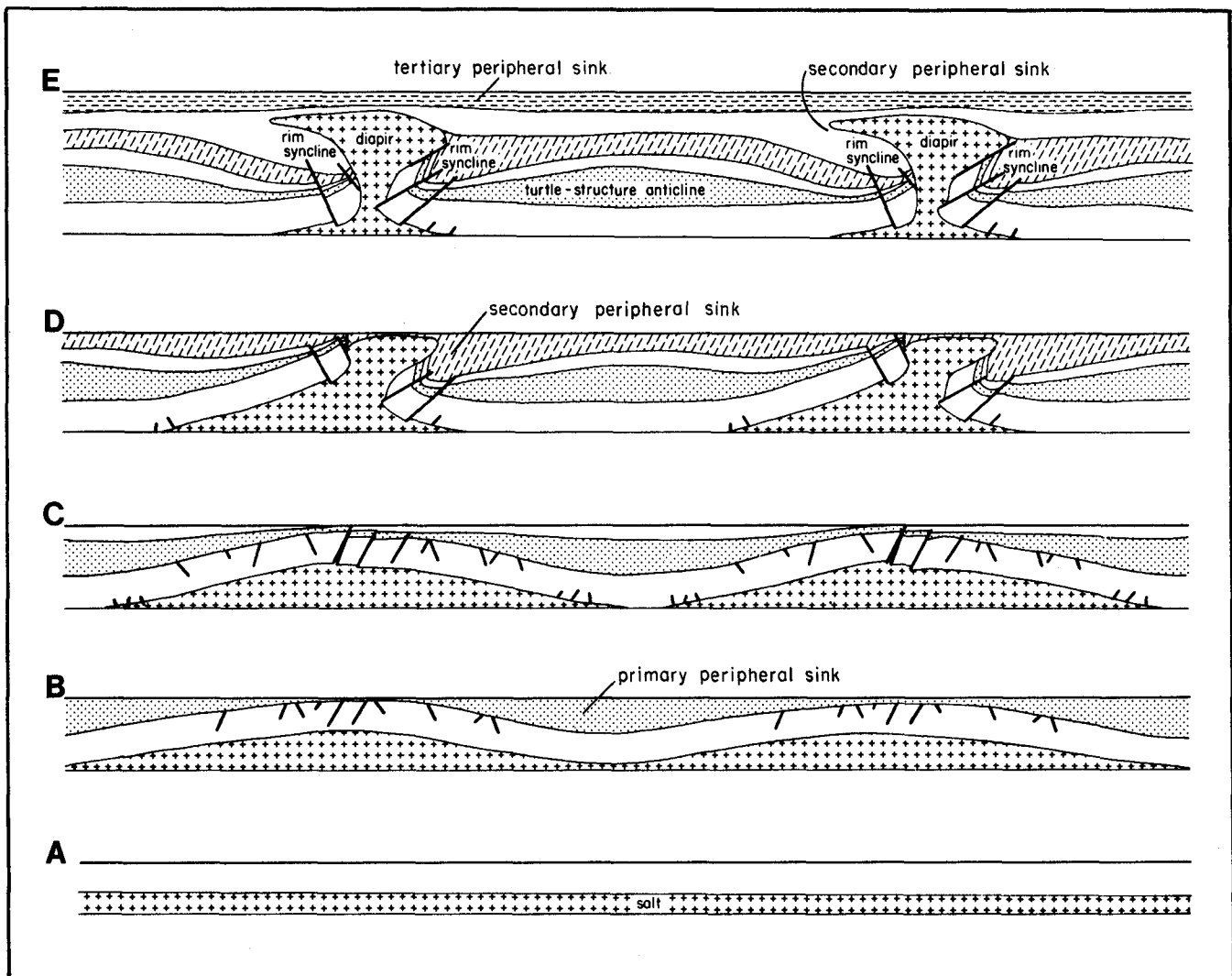


FIGURE 14. Schematic cross sections showing the inferred evolution of salt structures from (A) original salt layer, through (B and C) pillow stage, (D) diapir stage, and (E) postdiapir stage. (Modified from Trusheim, 1960.)



## Geometry of Surrounding Strata

Seven secondary peripheral sinks are recognized in the East Texas Basin; these encircle or flank Bethel, Brooks, Boggy Creek, East Tyler, Hainesville, La Rue, and Steen Domes (fig. 15). These basins vary from equidimensional to elongate in plan. All but two axial traces of the secondary peripheral sinks intercept the associated domes; the remaining two are within 6 km (3.6 mi) of the associated domes.

Axial traces of these secondary peripheral sinks are aligned in two dominant directions, northwest and northeast. Possible controls on this alignment are either orientation of early salt anticlines (northeast) and their crestal depressions (northwest), interference folding of salt, or regional faulting (Jackson, 1982). The orientation of salt-withdrawal basins may in turn partly control similar orientations of surface lineaments in the East Texas Basin (Dix and Jackson, 1981).

Secondary peripheral sinks are up to 215 percent thicker than adjacent strata unaffected by salt movement. The maximum increase in thickness that we measured was 1,347 m (4,420 ft) in the fine-grained terrigenous elastics and carbonates of the Austin through Midway Groups around Hainesville Dome. In figures 16 and 17 the effects of this thickening are shown for the Lower Taylor Formation and Austin Group.

The timing of maximum withdrawal-basin subsidence was different for different domes, even for adjacent domes. This variation in both timing and location of salt flow is evidenced by comparing isopach maps of salt-withdrawal basins in the Paluxy and Walnut Formations (fig. 18) and the overlying Washita Group (fig. 19). Sediments accumulated in withdrawal basins during Paluxy and Walnut time around East Tyler, Steen, and Brooks Domes (fig. 18). In contrast, during deposition of Washita strata (fig. 19), salt withdrawal continued around Steen and East Tyler Domes, ceased around Brooks Dome, and started around Mount Sylvan Dome.

## Depositional Facies and Lithostratigraphy

Marine and deltaic strata (mostly limestone and fine-grained terrigenous elastics) dominate the thickened stratigraphic section within secondary peripheral sinks in the East Texas Basin. Uplift and erosion over the diapir accompanied subsidence and deposition of deeper-water facies in the adjacent peripheral sinks.

La Rue, Boggy Creek, and Brushy Creek Domes are surrounded by prominent salt-withdrawal basins

containing 243 km<sup>3</sup> (59 mi<sup>3</sup>) of thickened strata. Most of the salt flow (194 km<sup>3</sup>, or 47 mi<sup>3</sup>) into these domes was during deposition of the Glen Rose Subgroup (fig. 20). The region between these large basins was an elevated saddle, which favored growth of reefs during deposition of the Lower Cretaceous James Limestone (fig. 21). Today these reefs and reef-associated facies host oil production of the Fairway Field (Terriere, 1976) (fig. 20).

Diapiric growth of Steen and East Tyler Domes affected distribution of sand and mud in nearshore deposits of the Paluxy Formation (fig. 22). A strike-oriented trend of thick, aggregate sandstone is isolated in the mudstone fill of a withdrawal basin around East Tyler Dome (fig. 22). Continued subsidence in this basin preserved what is interpreted to be a barrier bar or a shelf sand body produced by delta destruction.

## POSTDIAPIR STAGE

Postdiapir growth can be viewed as the waning phase of salt movement that follows rapid growth during the diapir stage. The postdiapir stage is generally the longest stage of salt flow. Over geologic time this movement is steady-state compared with the relatively brief surge of diapirism. During the postdiapir stage, domes stay at or near the sediment surface despite continued regional subsidence and deposition.

Postdiapir salt movement is characterized by tertiary peripheral sinks (Trusheim, 1960). These sinks surround or flank domes and in some cases are characterized by lithologic variations in fluvial deposits that encase the diapirs. Given the contour interval used in this study (30 m, or 100 ft), changes in thickness may be too subtle to define some tertiary peripheral sinks.

All diapirs examined here show some evidence of postdiapir growth. All but five of these domes are within 600 m (2,000 ft) of the surface. The exceptions are Boggy Creek, Brushy Creek, Concord, Girlie Caldwell, and La Rue Domes, which are in the center of the East Texas Basin. The postdiapir rise of these five deep domes did not keep pace with sedimentation and subsidence of the salt source layer in the basin center.

The Eocene Wilcox Group of the East Texas Basin was chosen for a study of the influence of postdiapir salt flow on thickness and geometry of surrounding strata, depositional systems, and lithostratigraphy for three reasons. (1) Postdiapir salt flow during deposition of the Wilcox Group was relatively minor and had little influence on surrounding strata. Its effects are thus best revealed in the youngest units, which have been less complicated

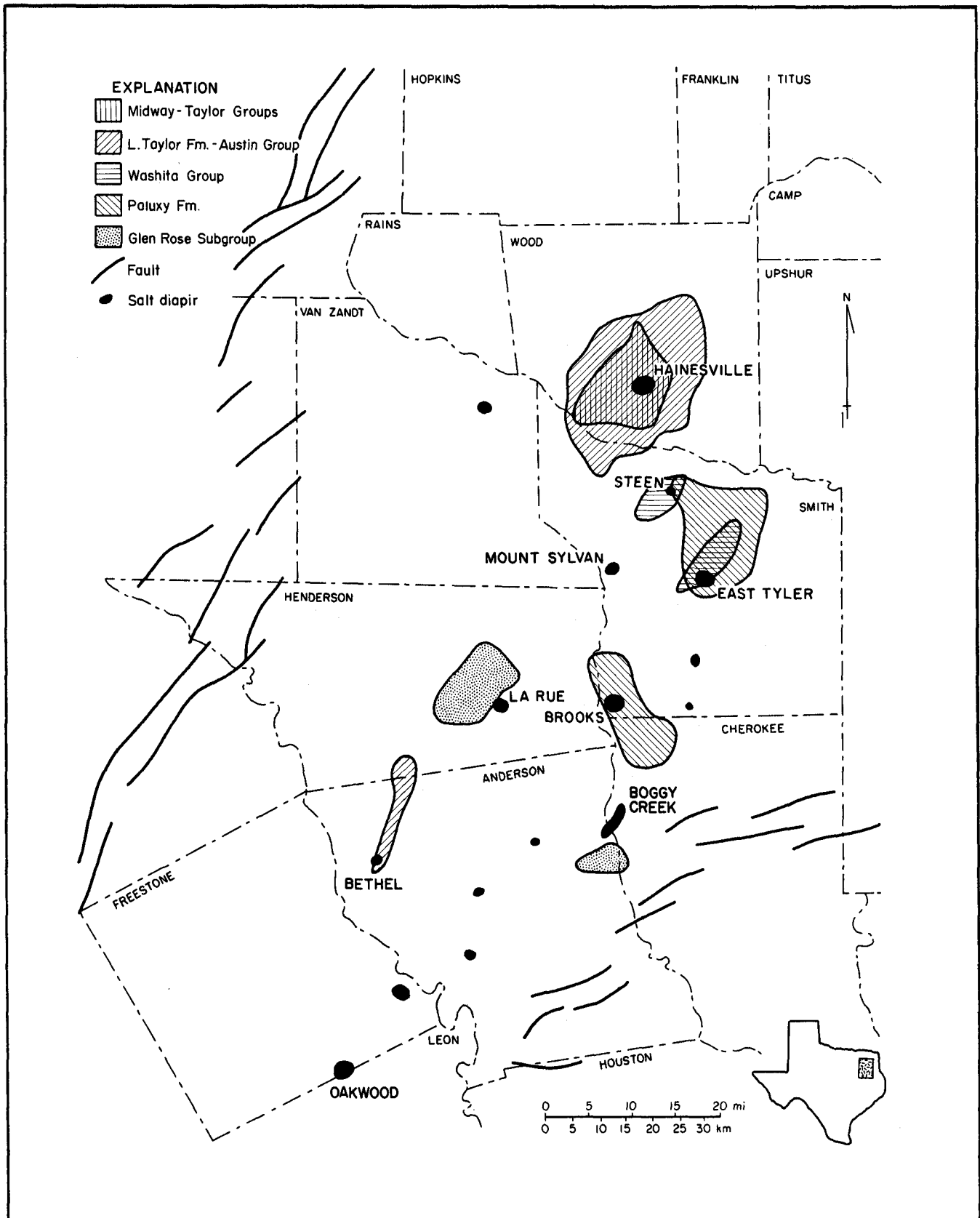
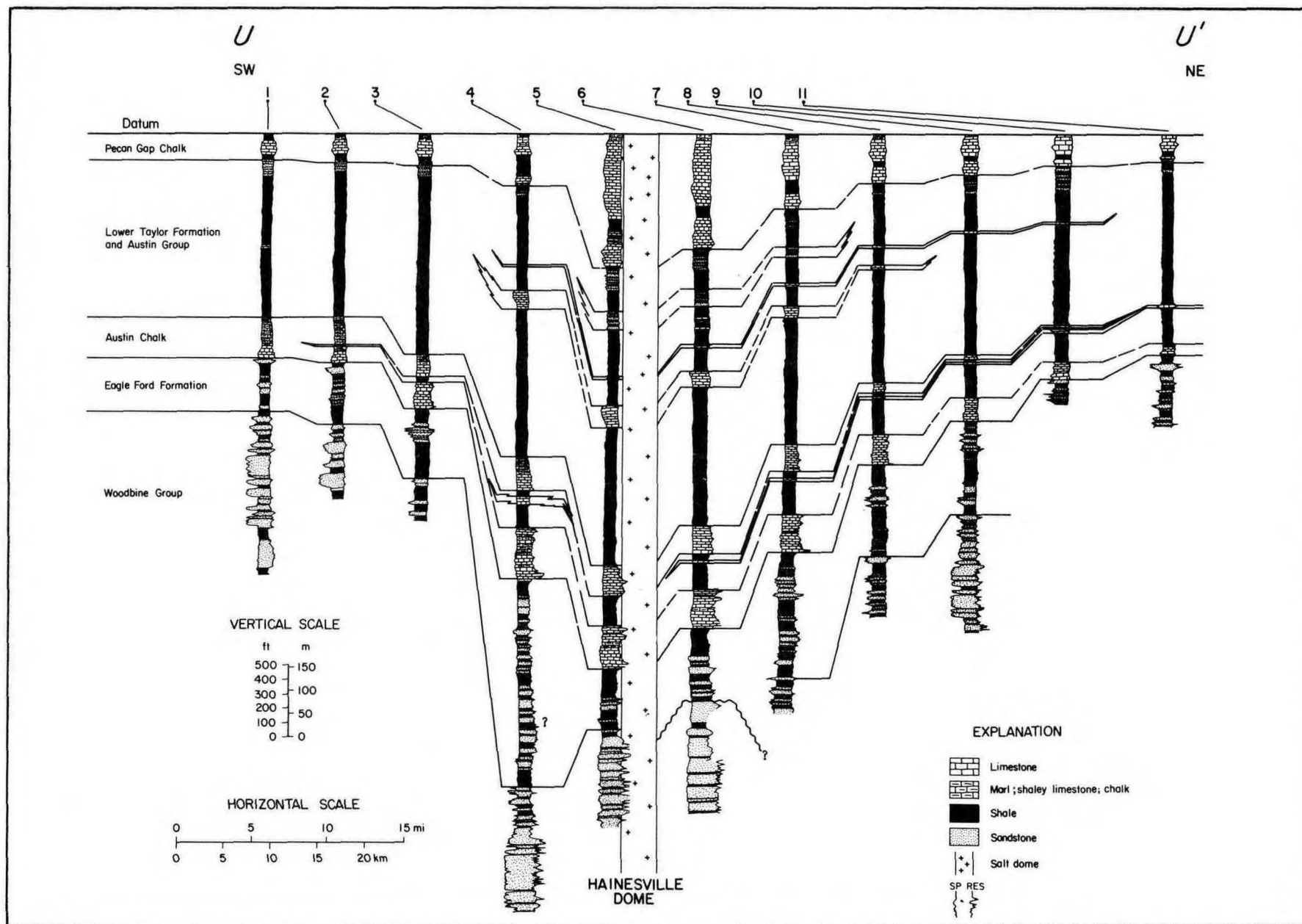


FIGURE 15. Map of secondary peripheral sinks, East Texas Basin, based on isopach maps of five stratigraphic units. Only sinks thickened greater than 50 percent with respect to regional thickness are shown. The actual area affected by salt withdrawal is much greater than the secondary peripheral sinks shown here (compare with figs. 17, 18, 19, and 20).



**FIGURE 16.** Cross section U-U', pre-Pecan Gap Chalk (Upper Cretaceous) strata, in a secondary peripheral sink, Hainesville Dome area. Stratigraphic section is up to 215 percent thicker than surrounding sediments, indicating massive flow of salt into the dome; however, lithic variations are minor. Location of cross section is given in figures 2 and 17.

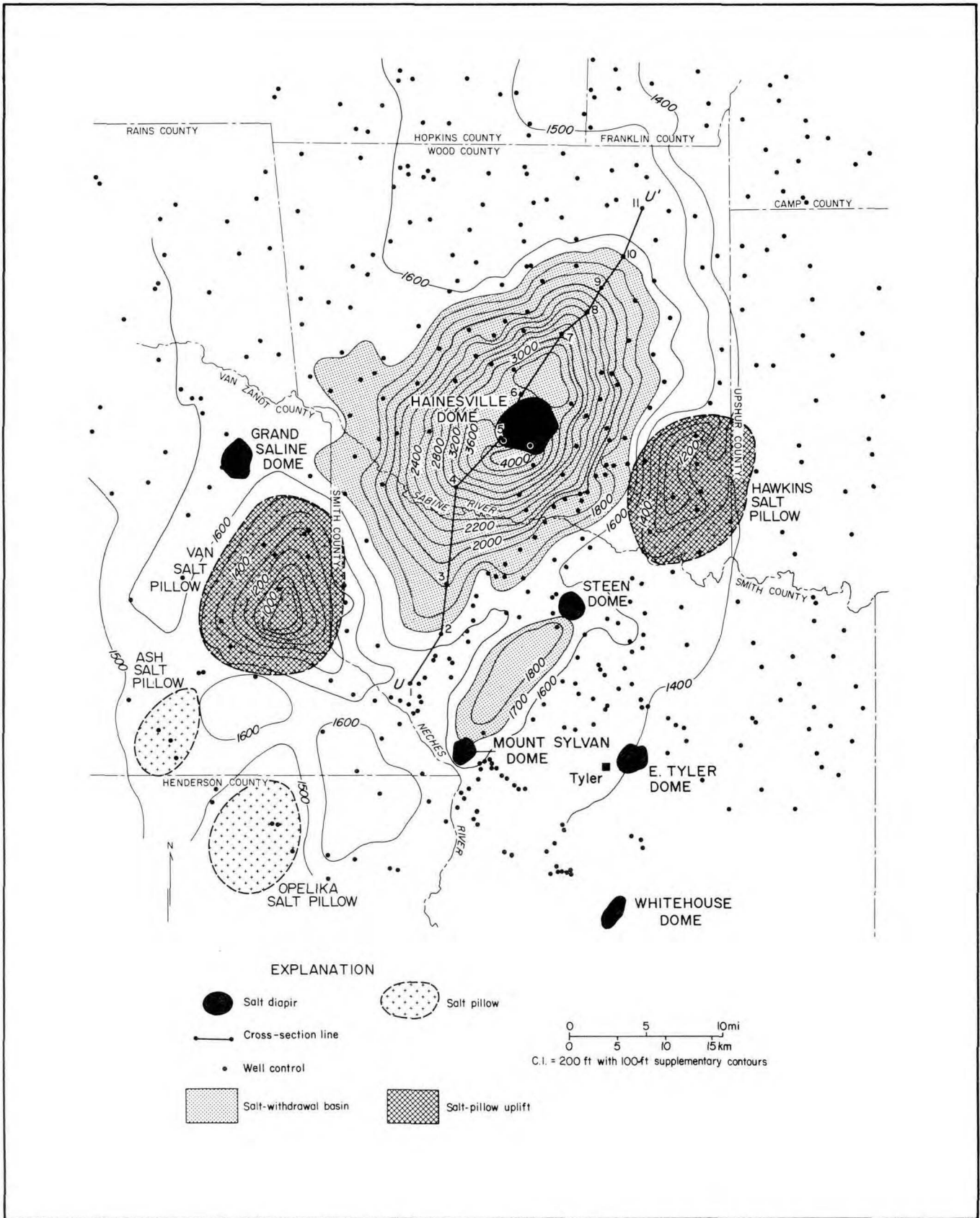


FIGURE 17. Isopach map of Lower Taylor Formation - Austin Group, Hainesville Dome area, northern part of the East Texas Basin. Axial trace (approximately along cross section U-U') of the secondary peripheral sink intercepts Hainesville Dome.

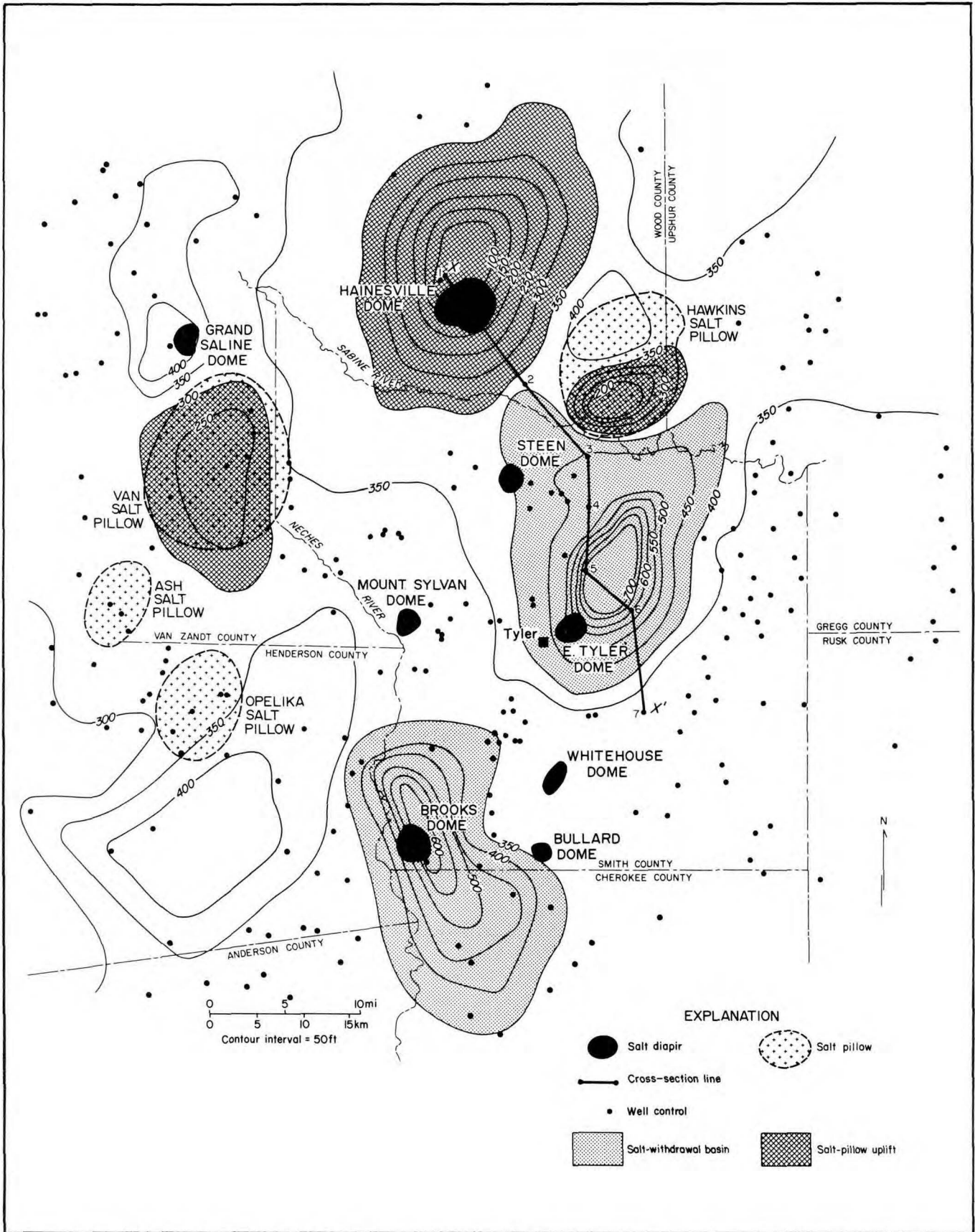


FIGURE 18. Isopach map of Paluxy and Walnut Formations, central East Texas Basin, showing thickened strata in salt-withdrawal basins around Brooks and East Tyler Domes. Thin areas overlie Van, Hainesville, and Hawkins salt pillows.

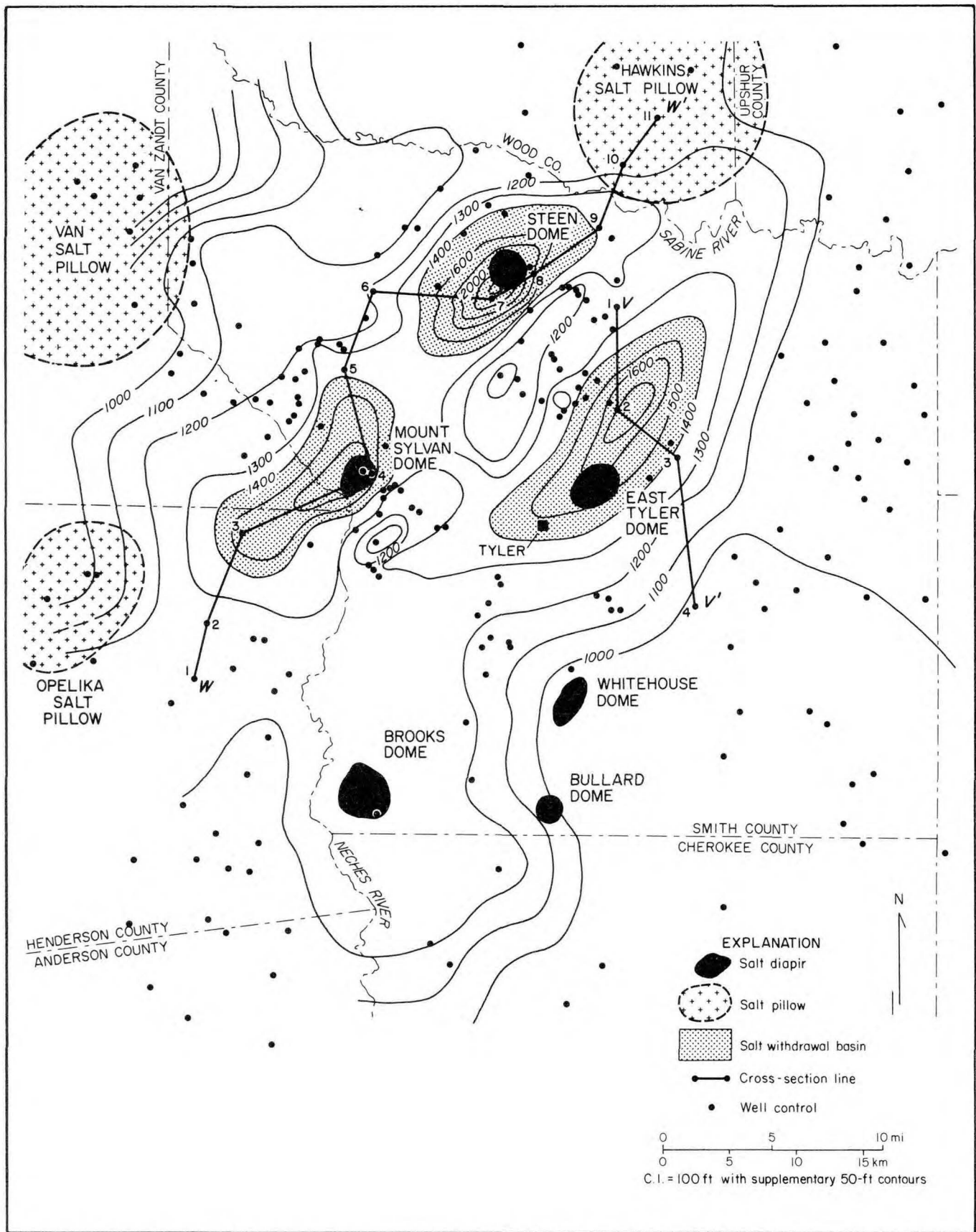


FIGURE 19. Isopach map of Washita Group, central East Texas Basin, showing thickened strata in salt-withdrawal basins around Mount Sylvan, Steen, and East Tyler Domes.

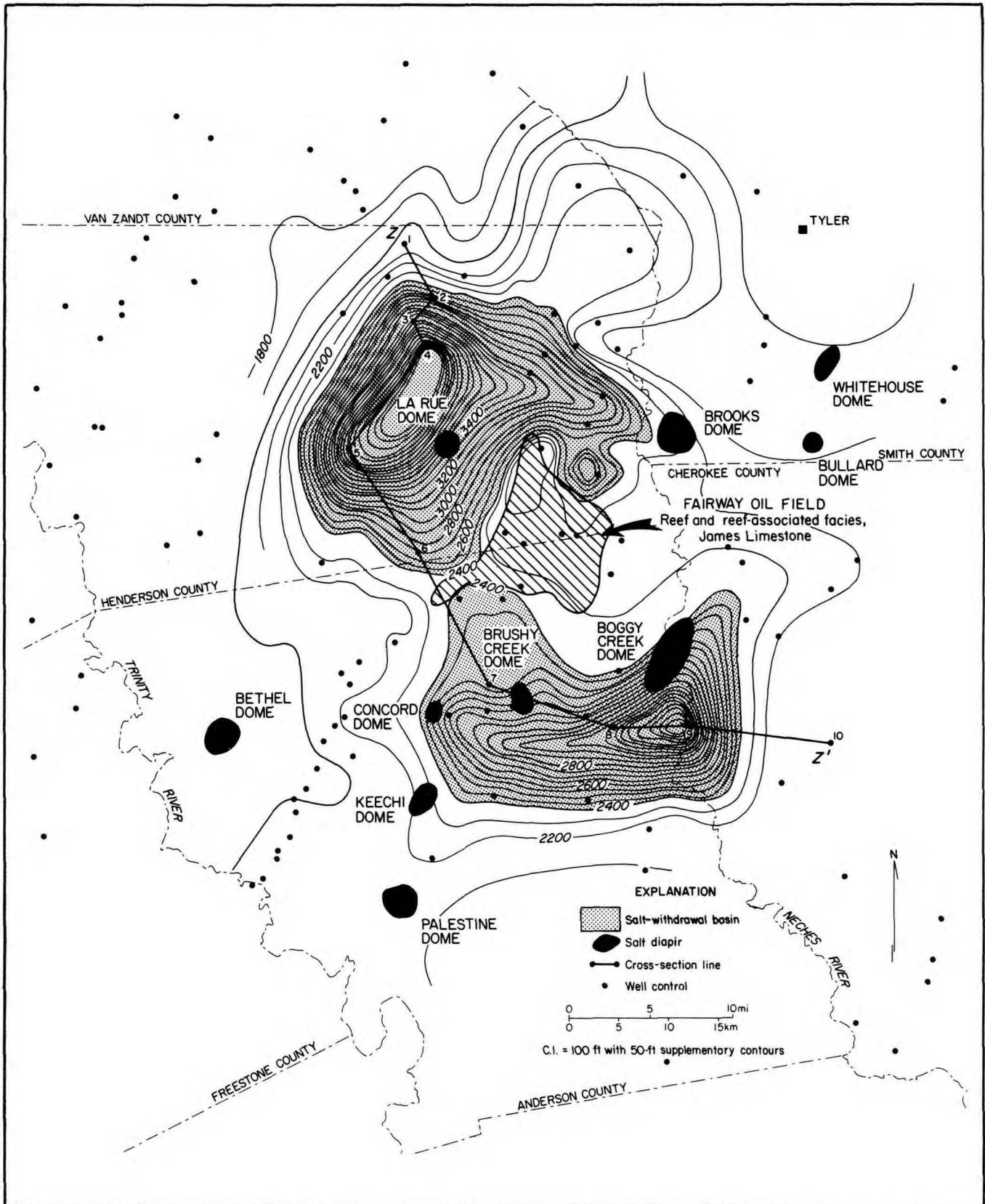


FIGURE 20. Isopach map of Glen Rose Subgroup, central East Texas Basin, showing thickened strata in salt-withdrawal basins near La Rue, Brushy Creek, and Boggy Creek Domes. These domes are flanked by a large secondary peripheral sink indicating rapid dome growth during Glen Rose deposition. The Fairway Field (diagonal pattern) is located in reef and reef-associated facies on an elevated saddle between the withdrawal basins.

than other units by differential subsidence and compaction. (2) Domes have not completely "pierced" the Wilcox Group in East Texas, so that strata over the domes can also be investigated. (3) Sand-body geometry and depositional systems of the Wilcox Group in Texas are well known (Fisher and McGowen, 1967; Kaiser, 1974; Kaiser and others, 1978, 1980).

## Geometry of Surrounding Strata

In the southern part of the East Texas Basin, eight diapirs were active in the early Tertiary and are flanked by tertiary peripheral sinks 8 to 40 percent thicker than surrounding areas unaffected by salt flow (fig. 23). The sink areas range from 20 to 100 km<sup>2</sup> (8 to 39 mi<sup>2</sup>). The tertiary peripheral sink

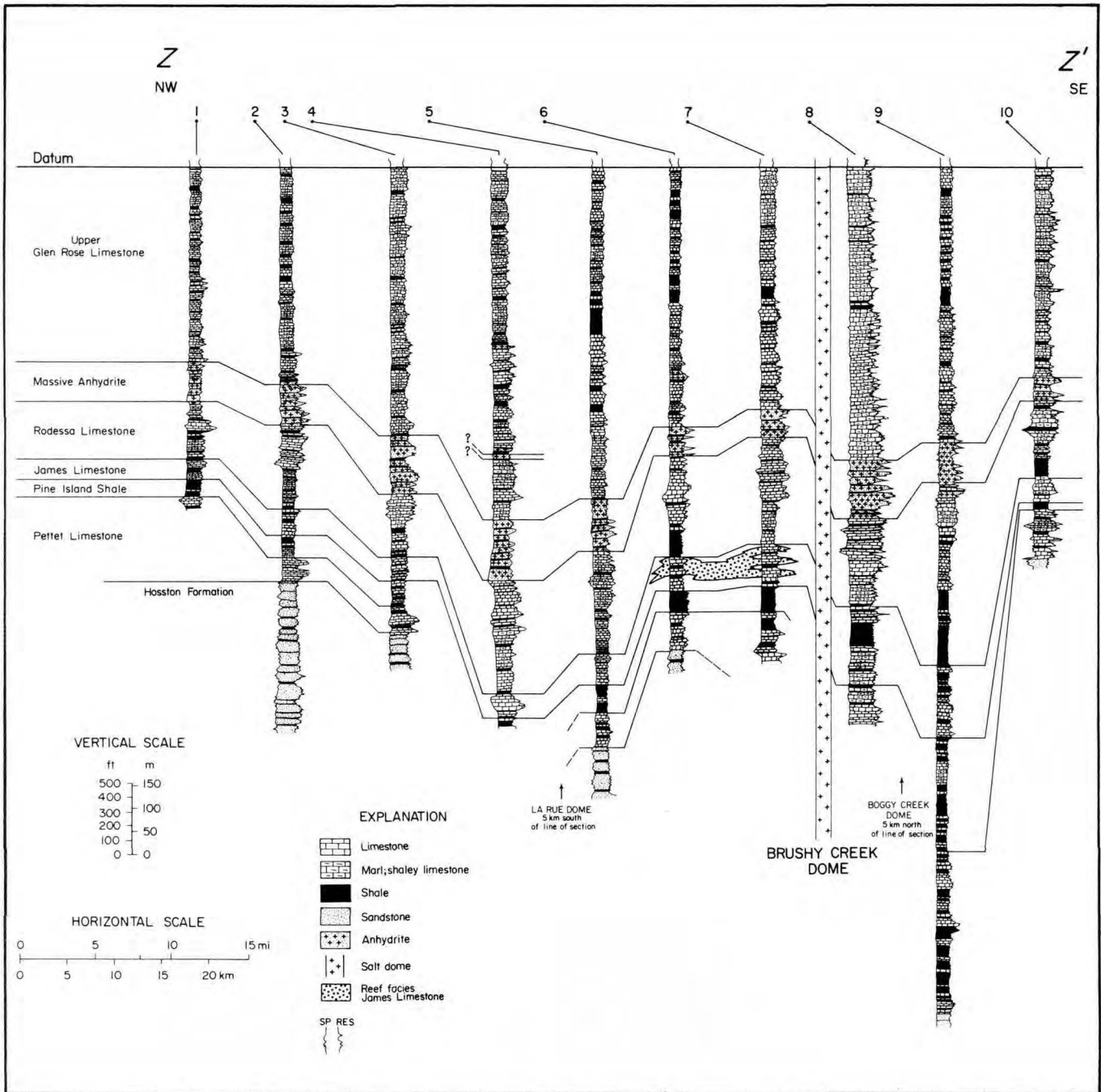
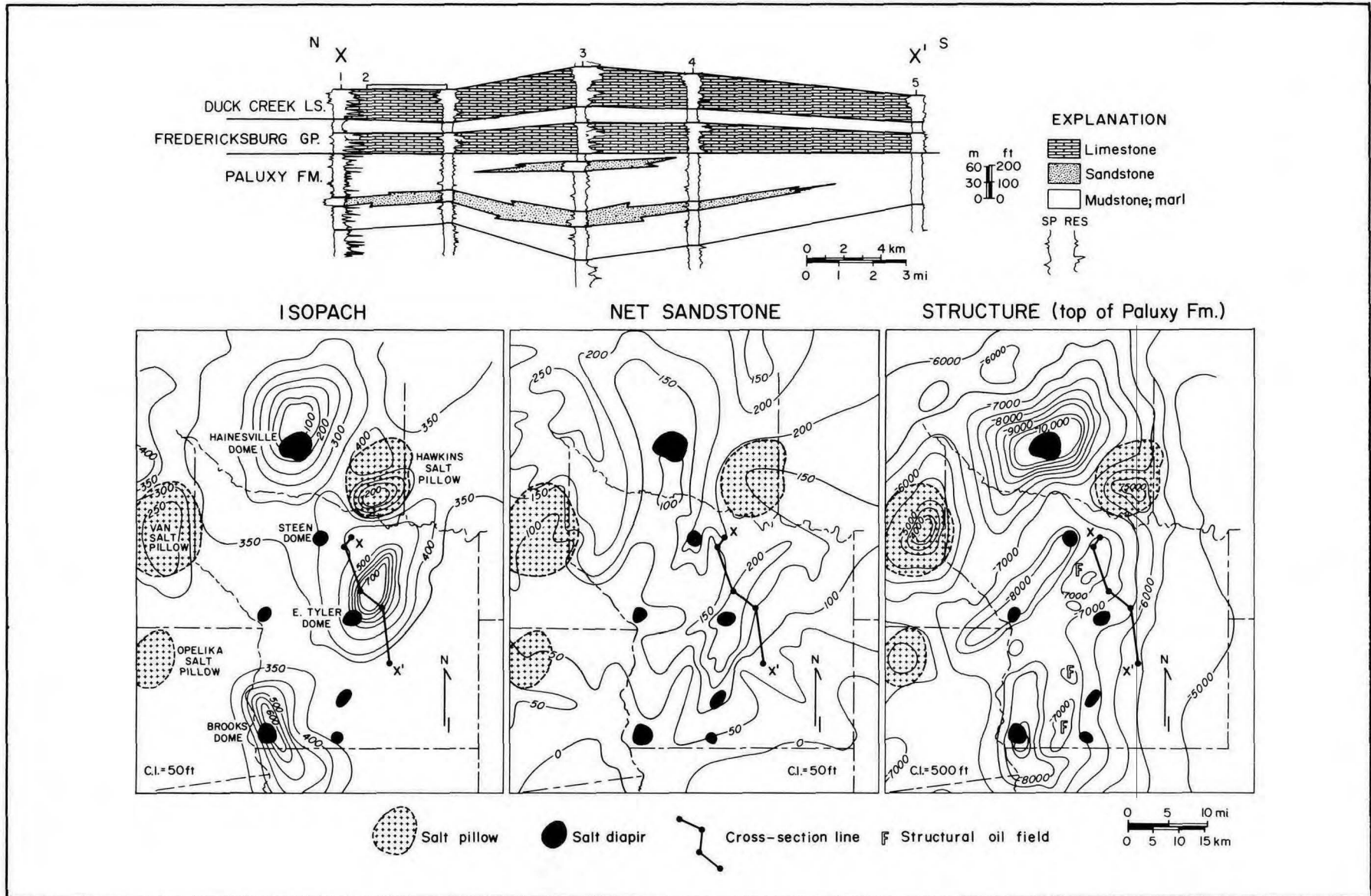


FIGURE 21. Cross section Z-Z' , Glen Rose Subgroup, through Brushy Creek Dome and near La Rue and Boggy Creek Domes, East Texas Basin. Glen Rose strata thicken in the secondary peripheral sinks, and reef facies occur in the James Limestone on an elevated saddle between sinks. Location of cross section is given on figures 2 and 20.





**FIGURE 22.** Cross section X-X' and maps of isopach, net sandstone, and structure, Paluxy Formation, northern part of the East Texas Basin. Effects of both salt pillow movement (represented by Van, Hainesville, and Hawkins pillows) and diapiric salt movement (represented by Brooks and East Tyler Domes) are shown. The sand body in the withdrawal basin around East Tyler Dome (on cross section and on net-sandstone map) was isolated from the sandstone feeder system between Hainesville and Hawkins pillows by a subtle structural saddle east of Steen Dome (structure map). This saddle was also a topographic high in Paluxy time (isopach map).

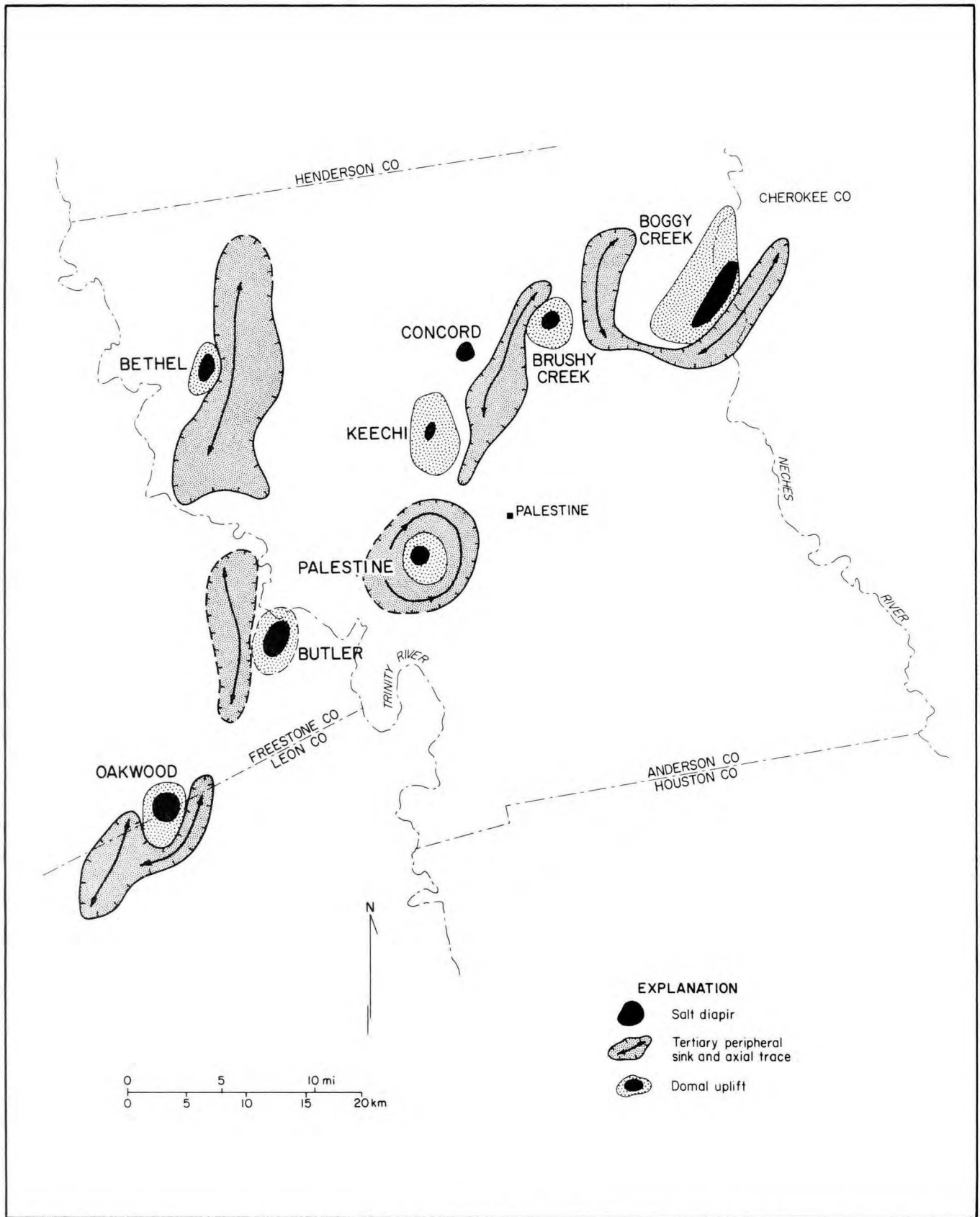


FIGURE 23. Map of tertiary peripheral sinks in the Wilcox Group around domes and uplifted areas over domes, southern part of the East Texas Basin. Subsidence in sinks affected greater areas than did uplift over domes. Strata are well preserved in withdrawal areas and are poorly preserved in uplifted areas.

with the largest volume is on the eastern flank of Bethel Dome. The uplifted and thinned areas over the crests of the diapirs cover 8 to 50 km<sup>2</sup> (3 to 20 mi<sup>2</sup>) (fig. 23), but rarely extend more than 3 km (2 mi) beyond the salt stocks.

### Depositional Facies and Lithostratigraphy

Postdiapir growth produced mounds over the domes that locally influenced distribution of sand and mud in Wilcox fluvial deposits. Aggrading fluvial

channels were preferentially localized by greater subsidence in tertiary peripheral sinks than in adjoining areas. Deflection of fluvial channels from the domal mounds allowed deposition of fine-grained floodplain sediments over the domes. The effects of these processes are well illustrated in the southern part of the East Texas Basin, where eight domes occupy the interaxial areas between major sand belts of the Wilcox Group (fig. 24).

Sand-body distribution in the Wilcox around Bethel (fig. 25) and Oakwood Domes (fig. 26) illustrates the effect of dome growth on coeval sedimentation (Seni and Fogg, 1982). The tertiary

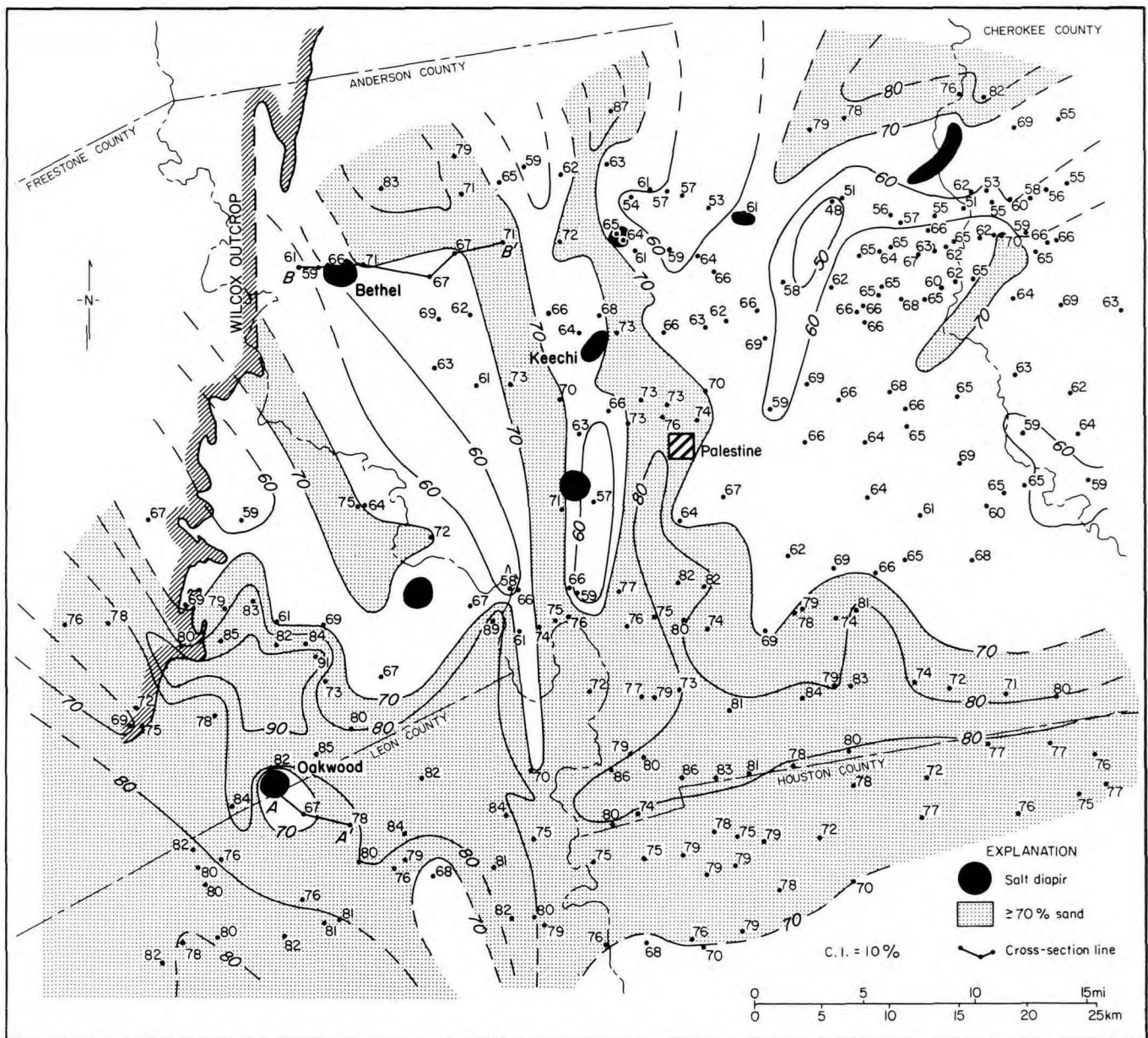
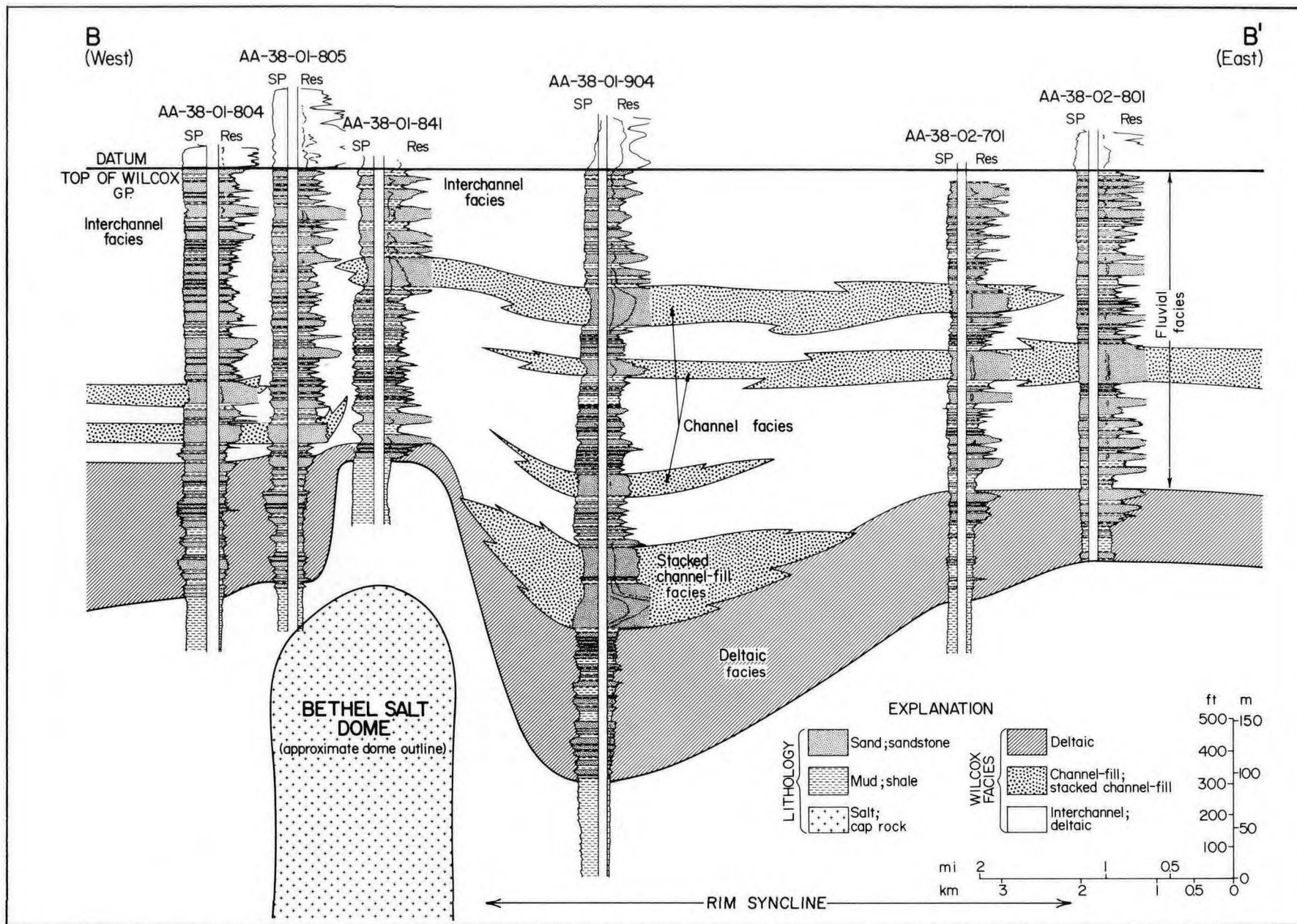


FIGURE 24. Sand-percent map, Wilcox Group, southern part of East Texas Basin. Eight diapirs in this area lie in interaxial areas containing relatively low percentages of sand.



**FIGURE 25.** Cross section B-B', Wilcox Group, Bethel Dome area (cross section located on figs. 2 and 24). Four channel-fill sandstones 15 m (50 ft) thick occupy the tertiary peripheral sink east of Bethel Dome. Five of the six sandstones pinch out over the diapir.

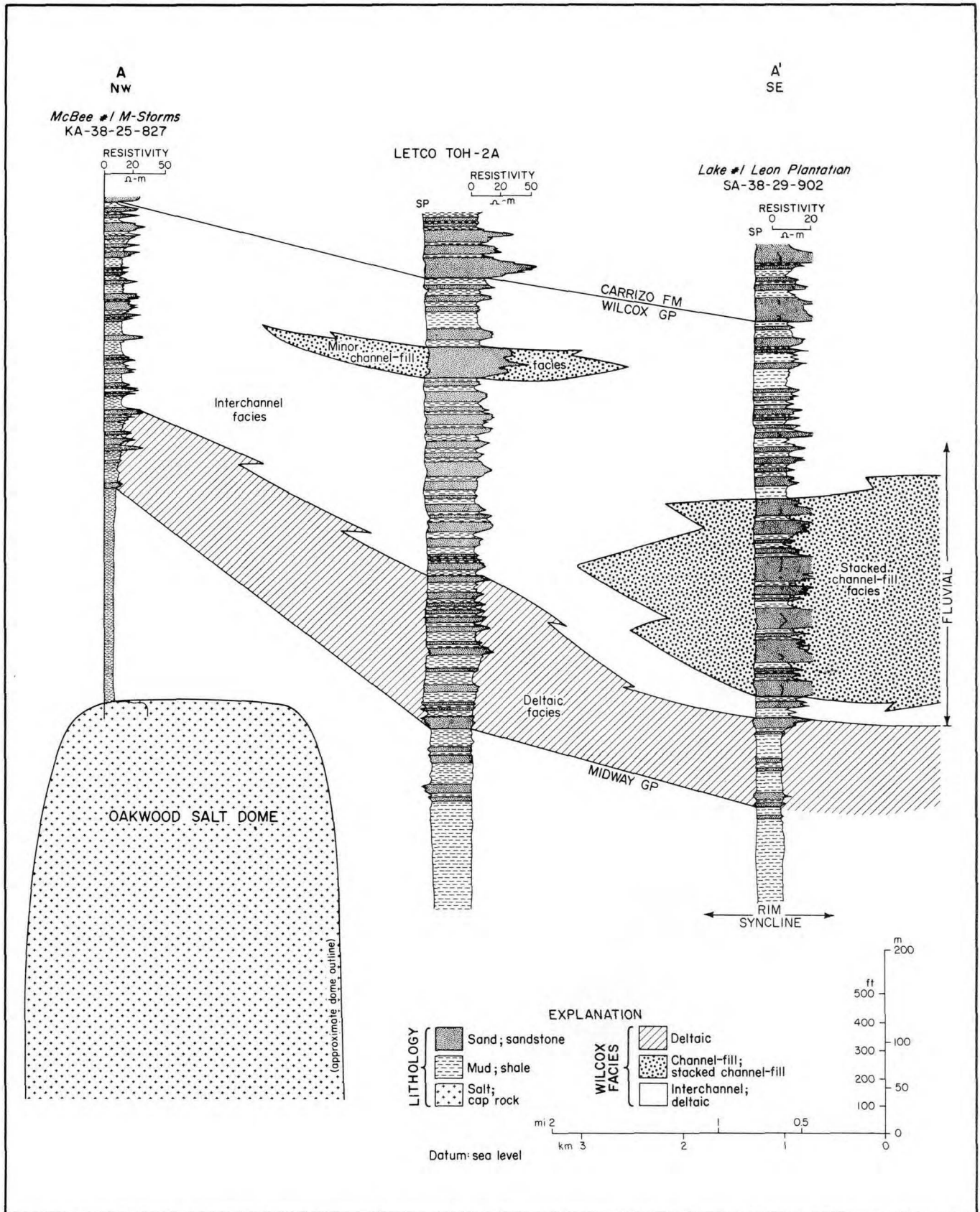


FIGURE 26. Cross section A-A', Wilcox Group, Oakwood Dome area (cross section located on figs. 2 and 24). The tertiary peripheral sink contains sand-rich facies. A paleotopographic mound over the dome deflected Wilcox fluvial systems, so that thinned strata over the crest of the dome comprise mud-rich, floodplain facies.

peripheral sink east of Bethel Dome (fig. 25) includes four stacked channel-fill sands, each more than 15 m (50 ft) thick. In contrast, uplifted strata over Bethel Dome are thinned and include only one sand body thicker than 15 m (50 ft), although percent sand is only slightly lower than in the peripheral sink. Vertically stacked, channel-fill sands also dominate the tertiary peripheral sink 3 to 10 km (2 to 6 mi) southeast of Oakwood Dome (fig. 26). Muddy sediments dominate the floodplain over the dome and are interbedded with crevasse-splay sands 0.3 to 4.0 m (1 to 13 ft) thick. F- and t-tests at the 95-percent confidence level indicate that strata over the diapirs contain 7 to 18 percent less sand than do strata in nearby channel axes.

### Holocene Analogs

Surface mapping of the Texas Coastal Zone (Fisher and others, 1972, 1973; McGowen and others, 1976; McGowen and Morton, 1979) provides valuable information on Holocene topography and surficial sediment distribution over coastal shallow domes. This information can then be used to draw analogies with early Tertiary deposition (fig. 27) over shallow domes in East Texas.

Fifty-six percent of the diapirs on the upper Texas coast have more than 1.5 m (5 ft) positive relief of sediments over their crests (fig. 27, inset C). This relief has apparently influenced the distribution of Holocene surficial sediments. Texas coastal diapirs generally occur in sand-poor areas or along sand-belt margins. Since the Tertiary, facies and environments of the Texas Coastal Zone have tended to stack vertically owing to rapid subsidence. For instance, sandstones are vertically stacked in the upper Pliocene and Pleistocene fluvial-deltaic sequences in the Houston-Galveston area (Kreitler and others, 1977). Thus the present association of coastal diapirs in mud-rich surficial deposits indicates a high probability that older deposits encasing the diapirs are also mud rich. The lack of relief over some salt structures is related either to greater depth of burial, to cessation of upward growth, or to dissolution.

The present Persian Gulf is a shallow epicontinental sea with many similarities to the East Texas Basin during the Mesozoic. Holocene sediments in the Persian Gulf are primarily carbonates similar to those in the Washita Group and Glen Rose Subgroup. Shallow salt domes form mounds on the seafloor, and particularly active diapirs form islands exposing salt at the surface (Purser, 1973; Kent, 1979). Some of the salt-dome islands, such as Yas Island (fig. 28), are flanked by arcuate depressions inferred to be the surface

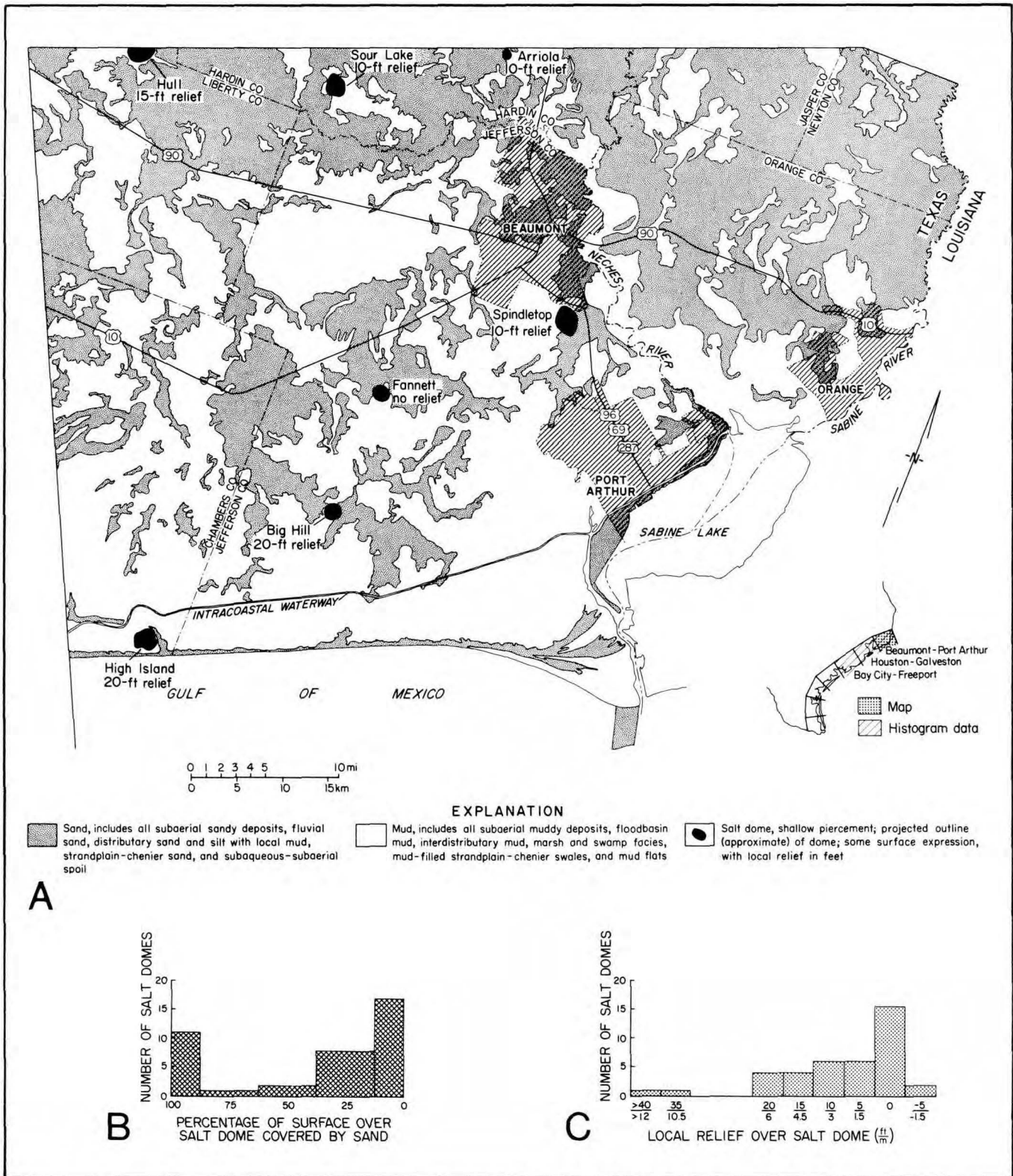
expression of rim synclines (Purser, 1973). Mud and muddy carbonate sand accumulate in topographic depressions of rim synclines located 1 to 5 km (0.6 to 3 mi) offshore (fig. 28). A zone of coral-algal reefs fringes many salt-cored islands and seafloor mounds. The seafloor around Hormuz Island, probably the most spectacular salt-dome island in the Persian Gulf, is littered with exotic blocks of late Precambrian Hormuz Formation that have been rafted up by the salt. The presence of late Precambrian blocks on the surface indicates that salt formerly extruded on the land and sea bottom (Kent, 1979).

### SUMMARY

Syndepositional lithostratigraphic variations caused by salt flow highlight the interdependence between sediment accumulation and dome evolution and their subsequent control on petroleum accumulation. These lithostratigraphic variations were primarily controlled by paleotopography. Salt uplift produced swells and mounds over salt pillows and diapirs, respectively. Concurrently, topographic and structural basins formed over zones of salt withdrawal, a process that formed saddles characterized by residual elevation between the basins. This salt-related topography influenced sedimentation patterns, which, in turn, enhanced continued salt flow through increased sedimentary loading in the basin.

In the East Texas Basin, salt-pillow growth was responsible for uplift and thinning in areas ranging from 100 to 400 km<sup>2</sup> (40 to 150 mi<sup>2</sup>), whereas diapir growth caused uplift and thinning in areas ranging from 8 to 50 km<sup>2</sup> (3 to 20 mi<sup>2</sup>). Continued domal "piercement" commonly destroyed the uplifted strata either by shoving the uplifted units aside in trapdoor manner or by pushing the units to the surface, where they were eroded. In contrast, much of the very broad, thinned zone over pillow crests was preserved after pillow collapse, when diapirism buried the thinned region deep below secondary and tertiary peripheral sinks.

Dome and pillow uplifts influenced net-sandstone trends because fluvial systems bypassed such mounds. Uplifted areas, therefore, tend to be thin and sand poor. Subsidence of the peripheral sinks, in turn, promoted aggradation of sand-rich, fluvial-channel facies. These variations are commonly illustrated in nonmarine facies deposited both in pillow-stage sinks (Paluxy Formation) and in postdiapir-stage sinks (Wilcox Group), but they are rare in marine facies deposited in diapir-stage sinks. Under marine conditions, sand can accumulate by winnowing on bathymetric shoals; consequently, salt domes having sufficient surface expression,

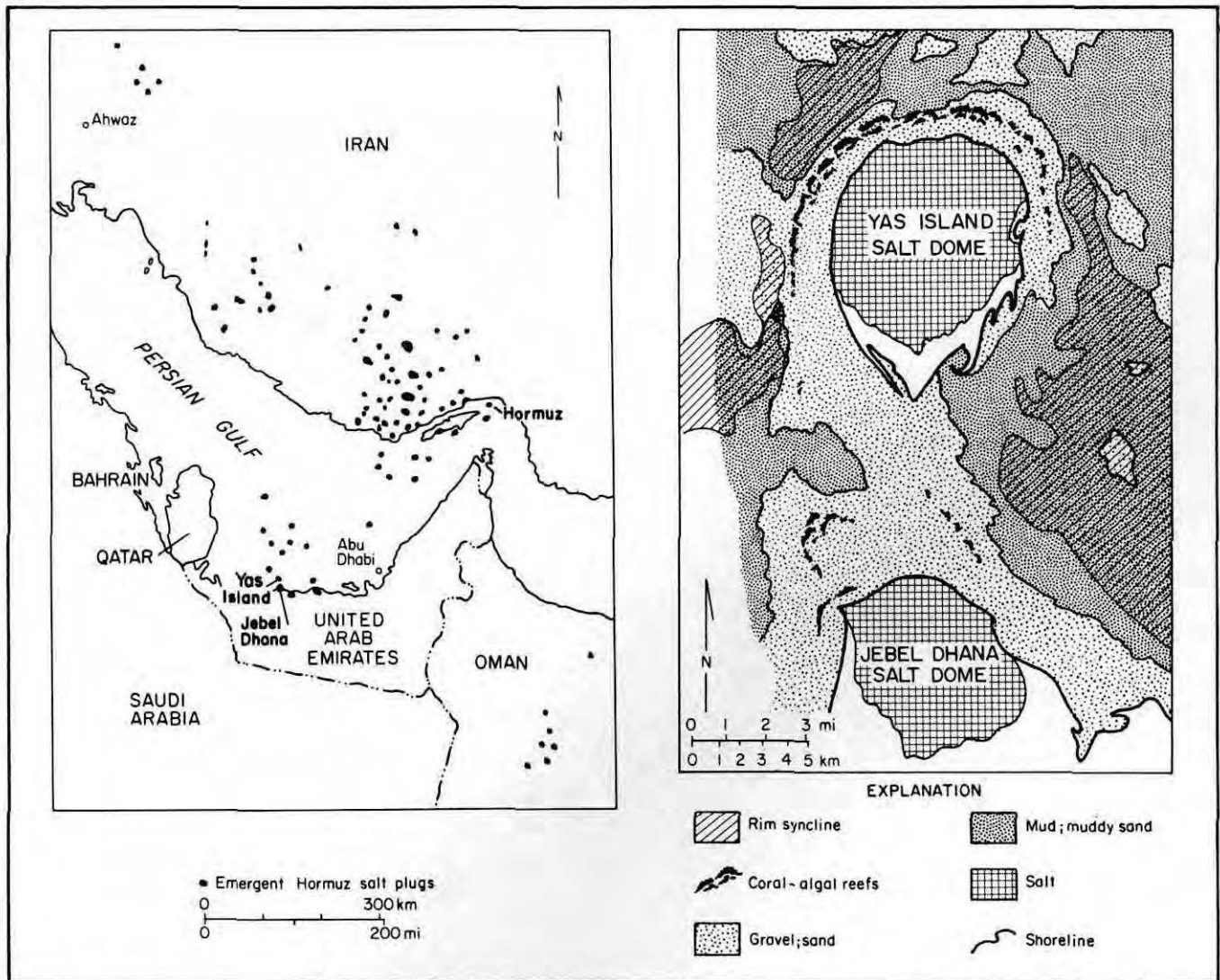


**FIGURE 27.** Relation between above-dome topography and surficial sand distribution, Upper Texas Gulf Coast. (A) Map of shallow salt domes and surficial sand and mud, Beaumont - Port Arthur area. Coastal diapirs are preferentially located along the margins of dip-oriented sand belts or in muddy, interaxial areas. Histograms (B and C) show percentage of surface over domes covered by sand and local relief, respectively. Abundant surficial sand (including eolian) blankets most of the Upper Texas Gulf Coast in the Bay City - Freeport area. Domes in this anomalously sandy area account for about half the domes in the 75- to 100-percent-sand class. (Histograms after Fisher and others, 1972, 1973; McGowen and others, 1976. Map after Fisher and others, 1973.)

such as those in the present Persian Gulf, are overlain by sand-rich sediments, in direct contrast to diapirs in fluviially dominated depositional environments (fig. 29). Small reefs might also be expected on topographic highs over dome crests, but these have not been discovered in East Texas. Such dome-crest reefs have been recognized in Oligocene sediments of the Texas Gulf Coast (Cantrell and others, 1959), in Holocene strata in the northwestern Gulf of Mexico (Bright, 1977; Rezak, 1977), and in the Persian Gulf (Purser, 1973). Lower Cretaceous reefs

have been found in East Texas on saddles between salt-withdrawal basins (fig. 29).

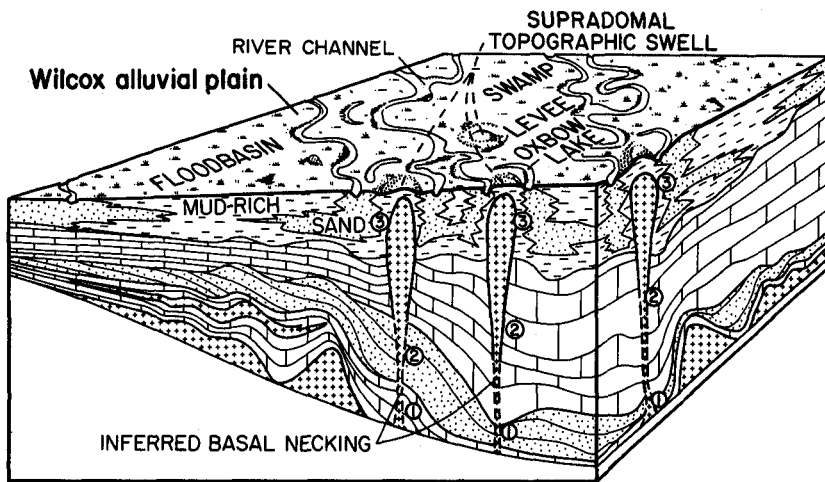
During diapirism, the lateral extent of the topographic depression in the peripheral sink is far greater than the extent of the area uplifted over the dome crest. Diapir growth is characterized by enormous secondary peripheral sinks. The largest secondary peripheral sink in East Texas, around Hainesville Dome, covers 1,000 km<sup>2</sup> (390 mi<sup>2</sup>). Low-energy marine facies characteristically dominate the fill of secondary peripheral sinks. In contrast to



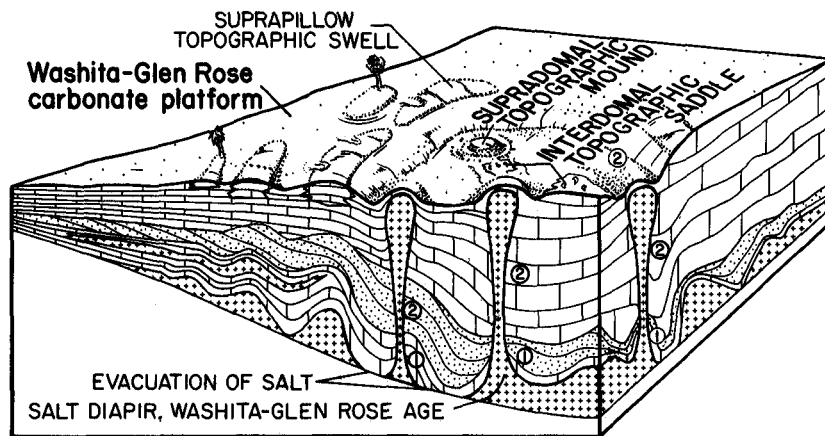
**FIGURE 28.** Location map showing the distribution of extrusive Hormuz salt plugs in the Persian Gulf and surrounding area. Geologic map shows Yas Island Dome, off the Trucial Coast, United Arab Emirates. The island is flanked by coral-algal reefs and carbonate sand and gravel. Areas designated "salt" include other rocks mantled by erosional debris from the salt plug. Bathymetry and distribution of Holocene carbonate sediments in the Persian Gulf are strongly

controlled by salt diapirism. The seafloor between Yas Island Dome and Jebel Dhana Dome, which is on the mainland, also contains coarse carbonate elastics and patch reefs. Farther offshore from Yas Island, rim synclines are expressed as topographic depressions on the seafloor in which carbonate mud and muddy sand are accumulating. (Yas Island Dome map modified from Purser, 1973; regional map modified from Kent, 1979.)



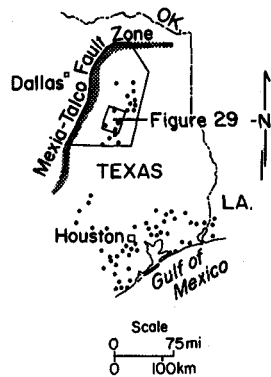


D



C

- EXPLANATION**
- ① Primary peripheral sink
  - ② Secondary peripheral sink
  - ③ Tertiary peripheral sink
  - Salt dome
  - ▨ Fault zone
- Index map



SYSTEM	SERIES	STAGE	UNIT	FIGURE	
TERTIARY	Eocene		Claiborne	D	
			Wilcox		
	Paleocene		Midway		
CRETACEOUS	UPPER CRETACEOUS	Senonian	Navarro	C	
			Taylor		
			Austin		
		Turonian	Eagle Ford		
		Cenomanian	Woodbine		
	LOWER CRETACEOUS	Albion			Washita
					Fredericksburg
					Paluxy
		Aptian			Glen Rose
					Hosston
JURASSIC	UPPER JURASSIC	Oxfordian	Schuler		
			Bossier		
			Gilmer		
			Buckner		
			Smackover		
			Norphlet		
	MIDDLE JURASSIC		Louann Salt		
TRIASSIC		Eagle Mills			
		Ouachita			

FIGURE 29. Schematic block diagrams of facies around salt structures showing the relation between salt flow and sediment accumulation during late evolution of the East Texas Basin. (C) Climax of group 2 diapirism in the Early Cretaceous, 115 to 98 Ma. (D) Deceleration of diapirism in the Tertiary, 56 to 48 Ma. (After Jackson and Seni, 1983b.) See figure 5 for earlier evolution, labeled (A) and (B).

secondary sinks, primary and tertiary peripheral sinks are usually difficult to map because they are only slightly thicker than surrounding strata, and because other, nearby active salt structures have a much greater influence on the thickness of surrounding strata.

The locations of sinks are related to evolutionary stage and regional dip. Axial traces of primary peripheral sinks are 5 to 20 km (3 to 12 mi) from the crest of the associated pillow and tend to be located updip of the structure. In contrast, secondary and tertiary peripheral sinks commonly encircle the diapir. This shifting of the peripheral sinks through time reflects the changes in salt migration through the various stages of dome growth, from predominantly downdip lateral flow in the pillow stage to a

combination of centripetal and upward flow in the diapir and later stages.

## FORMATION OF SUBTLE PETROLEUM TRAPS

Variations in thickness and syndepositional facies characterize near-dome strata during salt flow. These variations enable inference of dome growth stages and provide a framework to predict subtle hydrocarbon traps (fig. 30).

Pillow growth caused broad crestal uplift so that syndepositionally and postdepositionally thinned strata overlie the pillow crest. Fluvial and deltaic

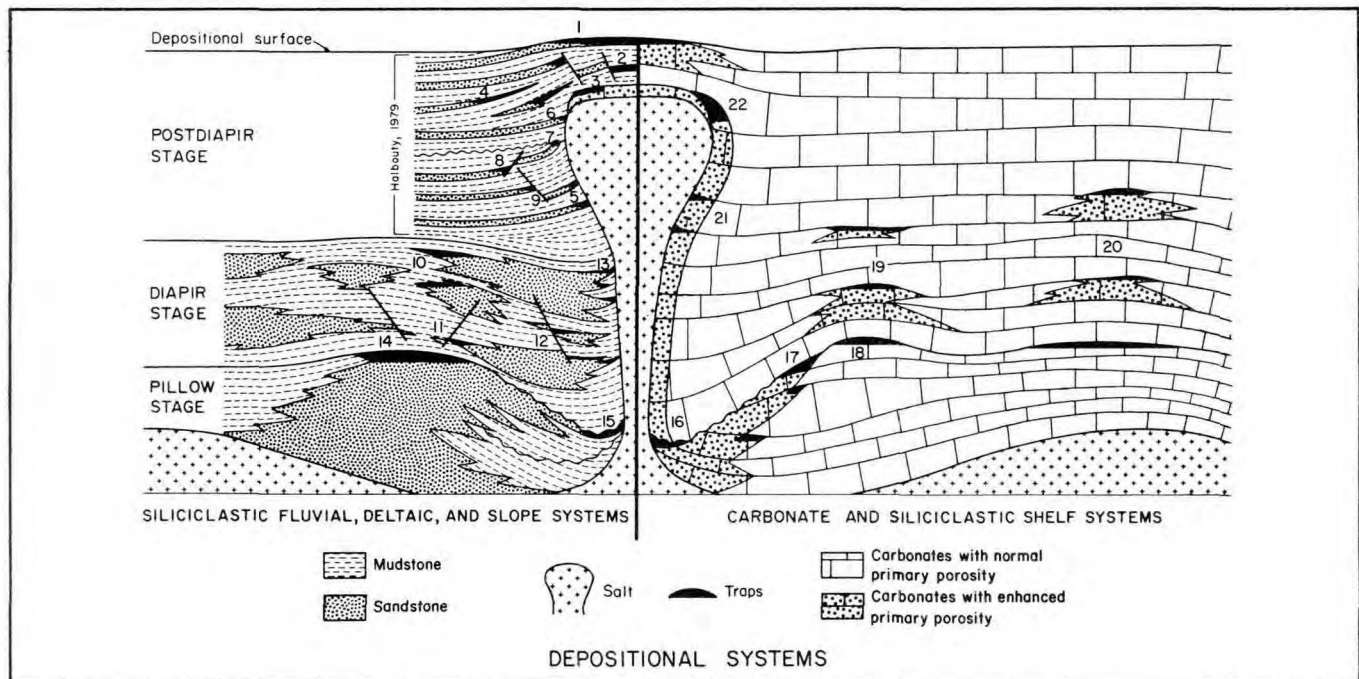


FIGURE 30. Schematic cross section through a mature diapir showing typical facies variations and potential petroleum traps (numbered) in siliciclastic fluvial, deltaic, and slope depositional systems and in carbonate and siliciclastic shelf depositional systems. Location of traps 1 through 9 and sand-body geometry in siliciclastic systems deposited during postdiapir stage are from Halbouty (1979). Various traps include: (1) combination trap in sandstone in anticline over crest of dome; (2) graben fault trap over dome; (3) porous cap rock; (4) stratigraphic trap in flank sandstone pinch-out; (5) structural trap beneath overhang; (6) structural trap uplifted and buttressed against salt stock; (7) unconformity trap; (8) fault trap downthrown away from salt stock; (9) fault trap downthrown toward salt stock; (10) combination trap in sandstone from updip pinch-out of porous facies in peripheral sink; (11) fault trap in sandstone over turtle structure; (12) fault trap in sandstone in peripheral sink;

(13) stratigraphic trap in sandstone from domeward pinch-out of porous facies in peripheral sink; (14) combination trap in sandstone at crest of turtle structure; (15) unconformity trap in sandstone over crest and flanks of precursor pillow; (16) unconformity trap in carbonates from enhanced porosity over crest and flanks of precursor pillow; (17) combination trap in carbonates from pinch-out of enhanced porosity zone on distal flanks of precursor pillow; (18) structural trap in carbonates over crest of turtle structure; (19) combination trap in carbonates from enhanced porosity due to paleotopography over turtle structure; (20) combination trap in carbonates from enhanced porosity due to paleotopography over raised saddle between peripheral sinks; (21) combination trap in carbonates from enhanced porosity near dome due to paleotopography and buttressing against salt stock; (22) combination trap in carbonates over crest of salt stock from enhanced porosity due to paleotopography and structure.

strata deposited over the crests of salt pillows are sand poor but are likely to be flanked by stratigraphic pinch-outs of sandy reservoirs. Sand-rich fluvial-channel systems bypassed pillow crests and occupied adjacent primary peripheral sinks. Under marine conditions, paleotopographic swells over pillows are potential hydrocarbon reservoirs because they were sites favorable for reef growth, high-energy grainstone deposition, and sand concentration by winnowing. Primary peripheral sinks formed preferentially updip of the salt pillows because of greater salt flow into the pillow from the updip side.

Structural reversal during diapirism transforms a primary peripheral sink into a turtle-structure anticline (figs. 8 and 14). Thus the location of a primary peripheral sink establishes the position of the core of the subsequent turtle-structure anticline as generally 5 to 20 km (3 to 12 mi) updip from the dome crest (fig. 11). This relationship is a valuable exploration guide for one of the most important salt-related structural traps, especially at the deeper, less explored horizons.

During diapirism, large secondary peripheral sinks enclosed or flanked the diapir. In East Texas, marine strata dominate the fill of secondary peripheral sinks and represent thickened, but otherwise normal, low-energy sequences. Because secondary peripheral sinks represented local sites of greater subsidence and hence were depressions, they were more likely to preserve marine sand bodies formed during transgressive reworking. These pinch-outs of marine sand bodies can subsequently act as subtle hydrocarbon traps.

Seafloor mounds over diapirs may become petroleum reservoirs because, as with pillows, they were sites of reef growth, grainstone deposition, and sand concentration by winnowing. However, these supradomal mounds were much smaller than analogous suprapillow swells. Furthermore, they were almost invariably destroyed by further uplift, erosion, and salt emplacement.

Another effective stratigraphic trap may be formed during diapirism. Raised saddles between secondary peripheral sinks allowed reef growth in the James Limestone (Lower Cretaceous Glen Rose Subgroup); both the structure and lithology of these saddles favored petroleum accumulation, such as occurred in the giant Fairway Field in Henderson and Anderson Counties.

Postdiapir growth had only minor effect on surrounding strata. Mounds over domes undergoing postdiapir growth deflected Wilcox fluvial-channel systems around supradome areas, so that mud-rich interaxial sediments were deposited over the diapir (fig. 29). Differential subsidence caused Wilcox fluvial-channel sandstones to

stack vertically in tertiary peripheral sinks. Subtle petroleum traps formed during this stage are probably much smaller than those formed during earlier stages of diapirism.

## **PATTERNS OF SALT MOVEMENT IN TIME AND SPACE**

Sixteen salt diapirs in the East Texas Basin constitute three groups defined by timing (fig. 31) and location (fig. 32) of diapirism:

Group 1 diapirs: Pre-Glen Rose Subgroup (pre-112 Ma), located on the periphery of the diapir province;

Group 2 diapirs: Glen Rose Subgroup to Washita Group (112 to 98 Ma), located on the basin axis; and

Group 3 diapirs: Post-Austin Group (86 to 56 Ma), also located on the periphery of the diapir province.

The following sections present a lithostratigraphic basis for this grouping. Two deep diapirs—Concord and Girlie Caldwell Domes—were not considered in this report because they do not intrude into the Glen Rose Subgroup, the deepest unit for which adequate subsurface data exist.

### **GROUP 1 DIAPIRS: PRE-GLEN ROSE SUBGROUP (pre-112 Ma)**

The seven diapirs of group 1 (figs. 31 and 32) can be divided spatially into three subgroups: Grand Saline Dome in the northwestern part of the province; Whitehouse and Bullard Domes on the eastern margin; and Oakwood, Butler, Palestine, and Keechi Domes in the southwestern part of the province (fig. 32).

Group 1 diapirs are the smallest of the dome groups in the East Texas Basin, having a mean volume of 21 km<sup>3</sup> (5.0 mi<sup>3</sup>). Diapir volumes were calculated using gravity-derived diapir models and a structure-contour map of the top of the Glen Rose Subgroup; thus all volumes refer to parts of the diapirs above the top of the Glen Rose Subgroup. The crests of all group 1 diapirs are less than 300 m (1,000 ft) deep. (Maximum depth to a group 1 crest is 244 m [800 ft] at Oakwood Dome. Minimum depth to a group 1 crest is 37 m [122 ft] at Palestine Dome. Mean depth of all group 1 crests is 122 m [401 ft].)

No primary or secondary peripheral sinks surround these domes in strata younger than 112 Ma because these diapirs had attained postdiapir stage by Glen Rose time (fig. 33). Influences on sedimentation and thickness range from effects so small that they cannot be detected using a contour interval of

100 ft (30 m) to minor effects of thickness on tertiary peripheral sinks in post-112 Ma strata. For example, Bullard and Whitehouse Domes have no discernible tertiary peripheral sinks in sediments that accumulated since 112 Ma. In contrast, sediments around Grand Saline Dome have small tertiary peripheral sinks in the time-equivalent facies of the Paluxy and Walnut Formations and in the Lower Taylor Formation and Austin Group strata (figs. 34 and 35).

Each of the three subgroups of group 1 diapirs consists of a cluster of coeval structures (fig. 32). In at least one of the clusters, the diapirs appear to have evolved from a single parental structure, thereby forming a "family" of related diapirs. The linear alignment and similar post-112 Ma growth histories of Oakwood, Butler, Palestine, and Keechi Domes suggest evolution from a single, parental, salt-cored anticline trending northeast. Seismic control around

Oakwood Dome discloses its growth history before 112 Ma, a growth history which may also be applicable to the three similar domes in this southern subgroup. Giles and Wood (1983) recognized domeward thinning of Smackover and Gilmer (Cotton Valley Limestone) carbonates and therefore inferred pillow growth during the Late Jurassic. Domeward thickening of post-Gilmer to pre-Pettet terrigenous elastics indicates that Oakwood Dome grew diapirically during the Late Jurassic to Early Cretaceous from 143 to 112 Ma ago.

The histories of Butler, Keechi, and Palestine Domes after the Early Cretaceous are broadly similar to that of Oakwood Dome. Butler, Keechi, and Palestine Domes had slightly higher growth rates than did Oakwood Dome during deposition of the Lower Cretaceous Paluxy and Walnut Formations and had slightly slower rates during subsequent deposition of the Washita Group.

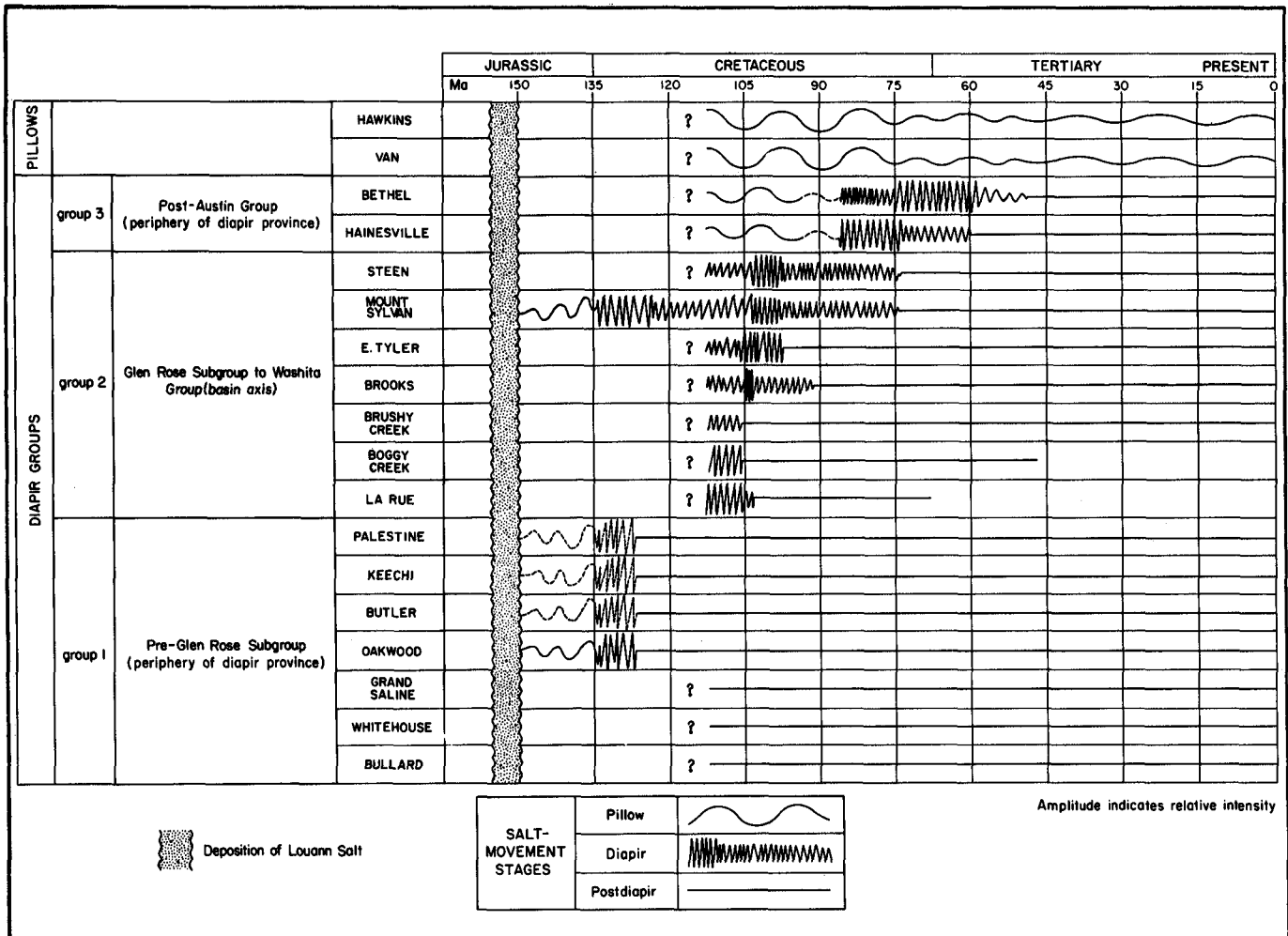


FIGURE 31. Three groupings of domes in the East Texas Basin based on the timing of stages of salt movement. Only the final evolutionary stage of the oldest diapirs (group 1) is preserved in Glen Rose and younger stratigraphic units. Where shown, pre-Glen Rose history is based on interpretation of available seismic sections.

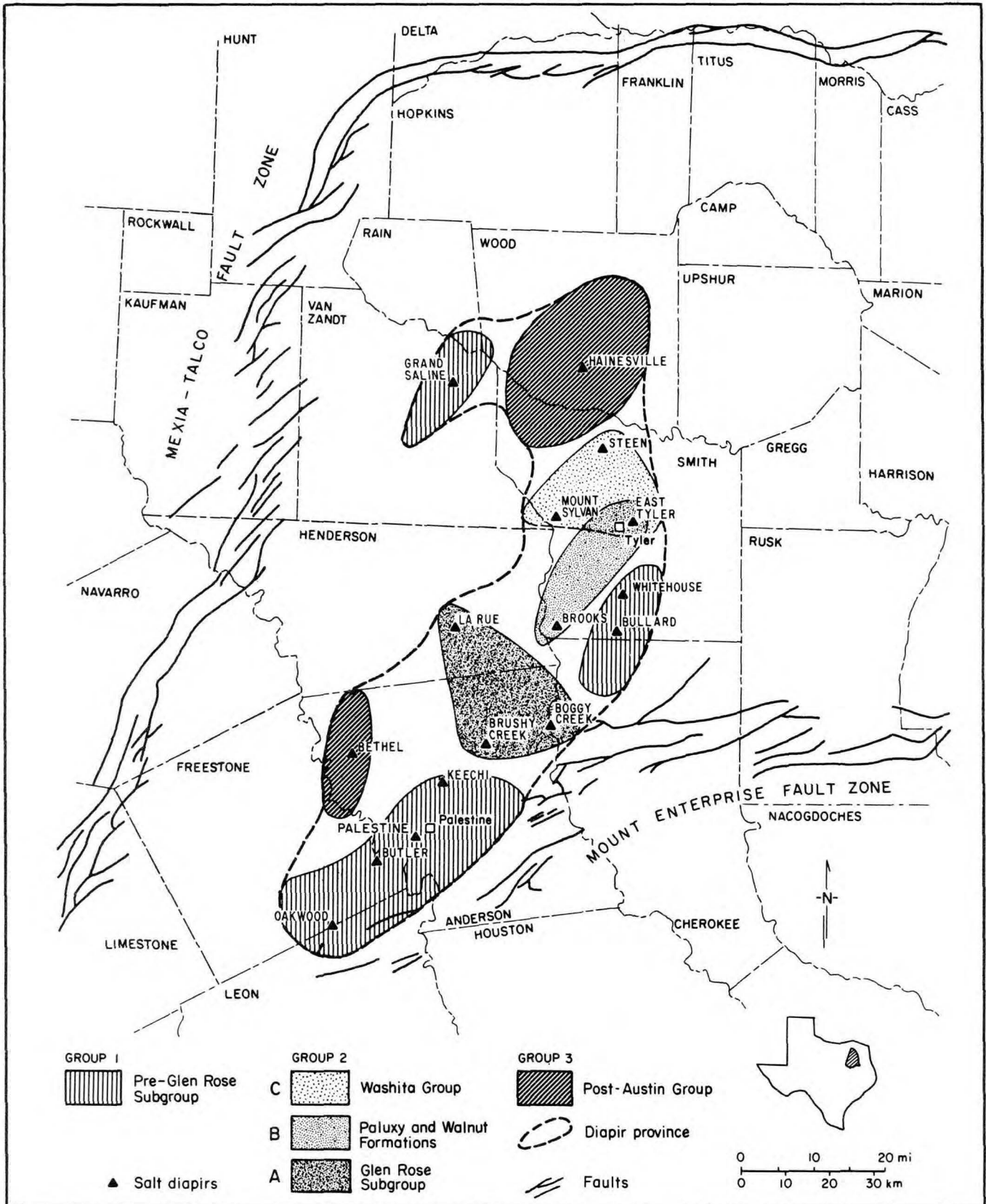


FIGURE 32. Map of three age groups of salt diapirs in the diapir province (dashed line), East Texas Basin. Patterned areas around diapirs correspond to outer limits of secondary peripheral sinks. Note gradual migration of group 2 subgroups A, B, and C toward group 3 areas. The Mexia-Talco Fault Zone defines the northern and western margins of the basin and marks the approximate updip limit of the Louann Salt.

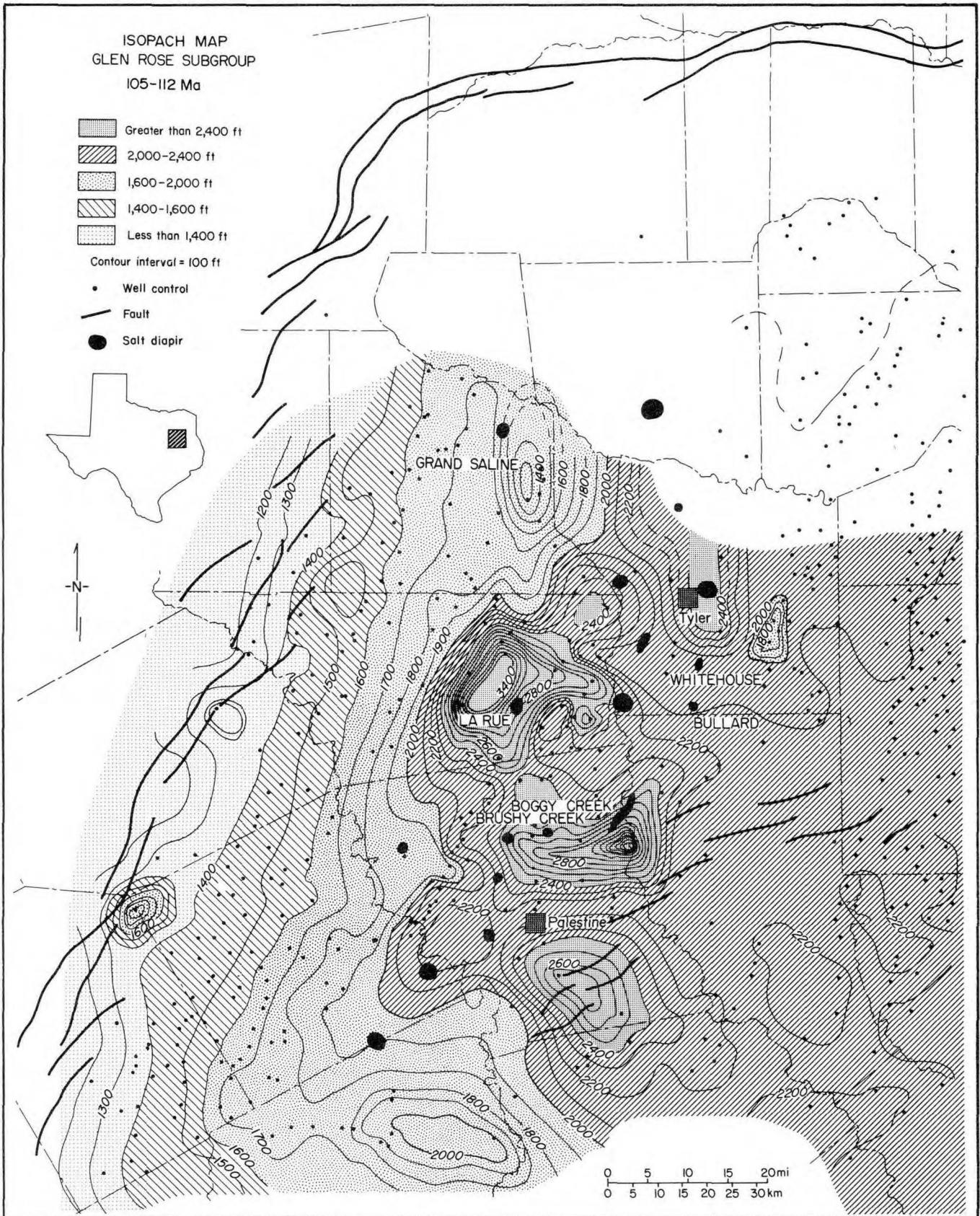
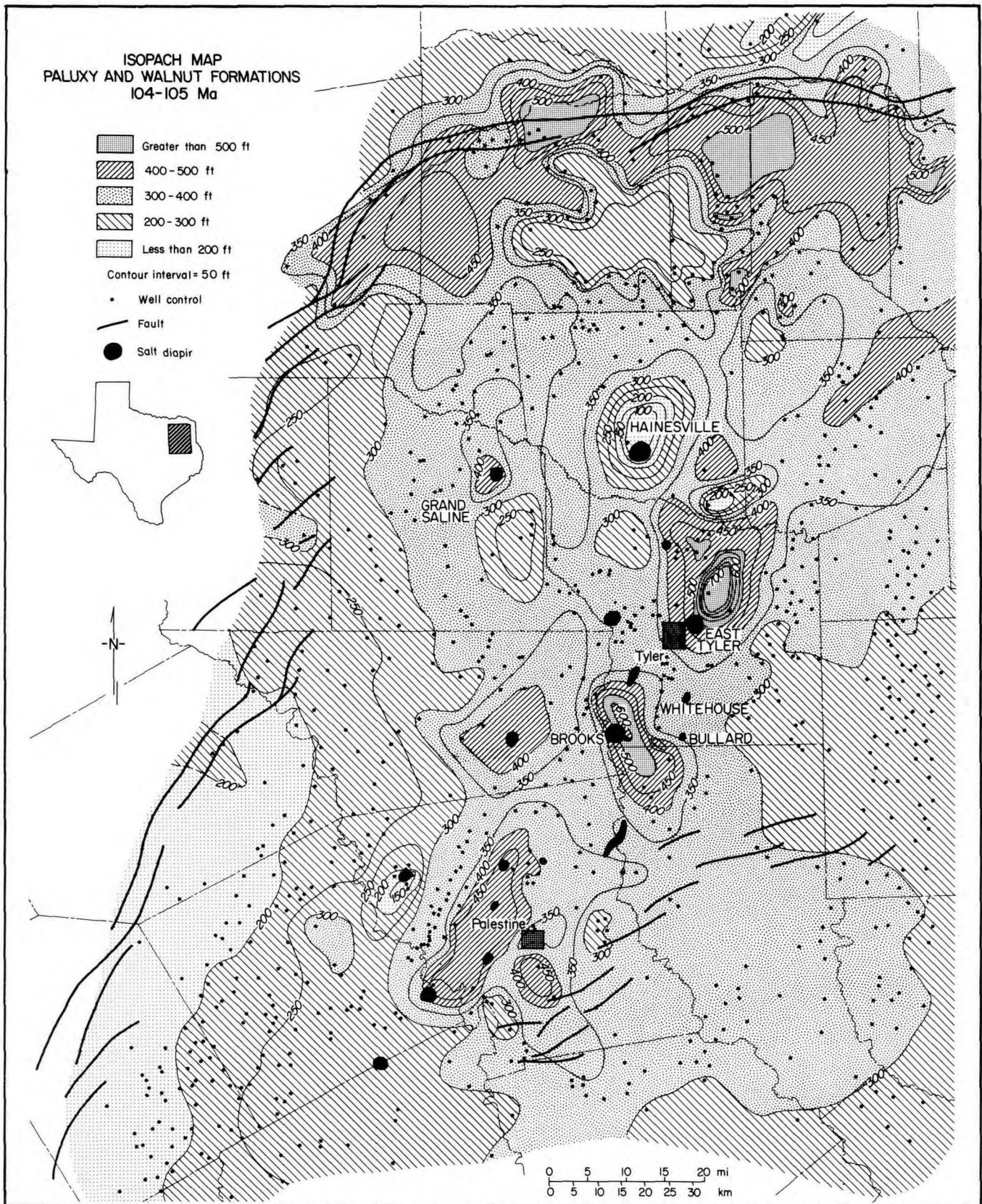


FIGURE 33. Regional isopach map of the Glen Rose Subgroup, East Texas Basin. Large secondary peripheral sinks in the central part of the basin indicate that La Rue, Brushy Creek, and Boggy Creek Domes grew diapirically during Glen Rose time.



**FIGURE 34. Regional isopach map of the Paluxy and Walnut Formations, East Texas Basin. The Walnut Formation is an offshore, time-equivalent facies of the Paluxy Formation. Small secondary peripheral sinks around Brooks and East Tyler Domes are in the central part of basin; large, thin areas formed in the northern part of basin over the crest of growing salt pillows like Hainesville Dome.**

## GROUP 2 DIAPIRS: GLEN ROSE SUBGROUP TO WASHITA GROUP (112 to 98 Ma)

The seven diapirs of group 2 (figs. 31 and 32) constitute three subgroups, all of which straddle the basin axis. The three subgroups are subgroup A, consisting of La Rue, Brushy Creek, and Boggy Creek Domes, all in the basin center; subgroup B, consisting of Brooks and East Tyler Domes, both north of the basin center; and subgroup C, consisting of Mount Sylvan, Steen, and East Tyler Domes, all farther north of the basin center (fig. 32). These subgroups exhibit progressively younger diapirism from the basin center to the northern part of the diapir province. The site of maximum diapirism shifted sequentially northward along the basin axis toward the margin of the diapir province from 112 to 98 Ma ago. During this period sediments accumulated fastest along the basin axis; this contrasts with group 1 diapirism, when sediments accumulated fastest around the margin of the diapir province. Group 2 diapirs are larger than group 1 diapirs, having a mean volume of  $31 \text{ km}^3$  ( $7.4 \text{ mi}^3$ ).

In the center of the basin, the subgroup A domes (La Rue, Brushy Creek, and Boggy Creek) are associated with two very large secondary peripheral sinks (figs. 20 and 33), indicating that diapir growth occurred 112 to 105 Ma ago during deposition of the shelf carbonates and thin evaporites of the Glen Rose Subgroup. The Glen Rose Subgroup exceeds mean regional thickness (571 m [1,873 ft]) by as much as 610 m (2,000 ft) in the secondary peripheral sinks. The area affected by salt withdrawal is  $1,900 \text{ km}^2$  ( $734 \text{ mi}^2$ ). La Rue Dome is surrounded by the largest salt-withdrawal basin ( $112 \text{ km}^3$  [ $27 \text{ mi}^3$ ]) of any of the group 2 diapirs.

The crests of La Rue, Brushy Creek, and Boggy Creek Domes are currently 1,356 m (4,450 ft), 1,088 m (3,570 ft), and 557 m (1,829 ft) deep, respectively. The net rate of postdiapiric growth of these domes in the basin center was slower than regional depositional rates, thus resulting in burial. This lag in upward dome growth may be related to (1) the deposition of massive, resistant carbonate strata around and above the diapirs, (2) rapid deposition in the center of the basin, (3) depletion of the salt source layer, or (4) some combination of these processes.

The diapirs of subgroup B, Brooks and East Tyler Domes, were active during deposition of the Paluxy and Walnut Formations, from 105 to 104 Ma ago. Secondary peripheral sinks ( $486 \text{ km}^2$  [ $188 \text{ mi}^2$ ] and  $727 \text{ km}^2$  [ $281 \text{ mi}^2$ ] in extent) are filled with Paluxy to Walnut strata (fig. 34). The Paluxy and Walnut sequence is relatively thin, having a mean thickness

of only 88 m (289 ft) and a maximum thickness of only 219 m (720 ft). This thinness and the absence of evidence of pillow-phase thinning during the preceding Glen Rose time indicate that Brooks and East Tyler Domes probably did not evolve from a pillow phase during deposition of Paluxy and Walnut strata; the domes are thus inferred to have been diapirs before that time. A renewed surge of diapiric growth, initiated by unknown causes during Paluxy and Walnut time, is indicated by the localized, massive thickening of the secondary peripheral sinks.

Mount Sylvan, East Tyler, and Steen Domes constitute subgroup C and are surrounded by secondary peripheral sinks filled with Washita Group carbonates (104 to 98 Ma ago) (fig. 19). Salt-withdrawal basins in Washita strata are similar in size and geometry to basins formed during Paluxy and Walnut time, suggesting that Washita dome growth was also caused by rejuvenation of pre-existing diapirs. East Tyler Dome is included in both subgroups B and C because it showed rapid rates of growth during both Paluxy deposition (subgroup B) and Washita deposition (subgroup C). Another similarity between subgroups B and C is the shallow depth of their diapir crests. The mean depths of the crests of subgroup B and C diapirs are 168 m (550 ft) and 183 m (601 ft), respectively.

## GROUP 3 DIAPIRS: POST-AUSTIN GROUP (86 to 56 Ma)

Hainesville and Bethel Domes are groups diapirs (figs. 31 and 32); their crests are 366 m (1,200 ft) and 488 m (1,600 ft) deep, respectively. Because of their youth, these are the only domes in the East Texas Basin having a complete history of salt movement preserved in strata younger than 112 Ma (fig. 35). Group 3 diapirs are by far the largest diapirs in the East Texas Basin, having a mean volume of  $47 \text{ km}^3$  ( $11 \text{ mi}^3$ ). According to Loocke (1978), approximately  $78 \text{ km}^3$  ( $19 \text{ mi}^3$ ) of salt constitutes the Hainesville salt stock.

Seismic control (Loocke, 1978) and well data indicate that pillow growth of Hainesville Dome occurred from 112 to 92 Ma ago during Glen Rose to Woodbine time. Diapir growth took place from 86 (or possibly 92) to 56 Ma ago during post-Woodbine to Midway time.

The evidence of late growth of group 3 diapirs and their location on the periphery of the diapir province (fig. 32) suggest that these diapirs have a growth history significantly different from that of group 1 and 2 diapirs. Group 1 and 2 diapirs grew fastest during rapid regional sediment accumulation (see following discussion), but group 3 diapirs grew



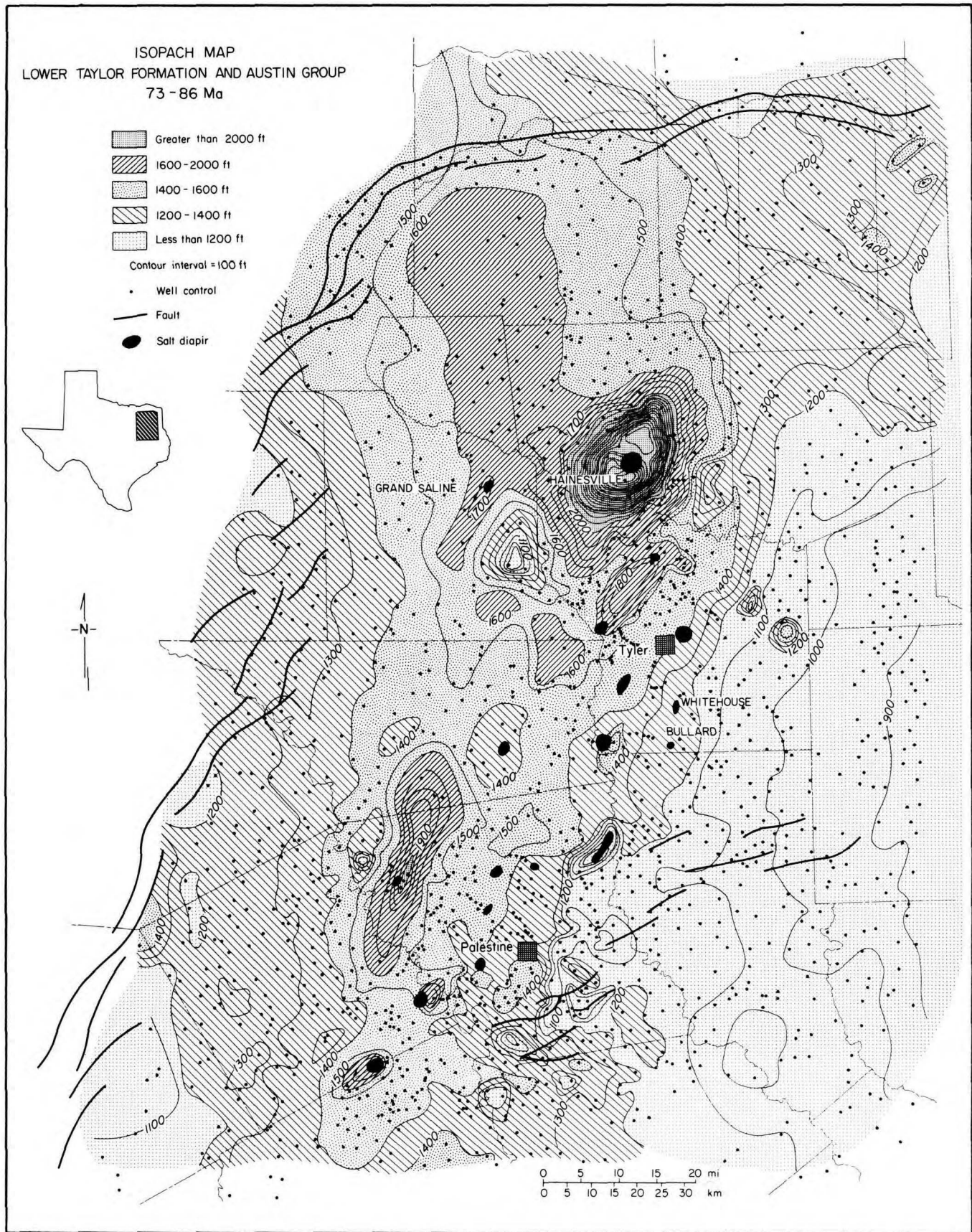


FIGURE 35. Regional isopach map of the Lower Taylor Formation and Austin Group, East Texas Basin. A large secondary peripheral sink around the diapiric Hainesville Dome dominates the northern part of the basin.

fastest when regional rates of sedimentation had significantly declined. This paradox is explained by examining formation of local angular unconformities over Hainesville Dome during the pillow-growth stage.

## INITIATION AND ACCELERATION OF SALT FLOW

The pre-Glen Rose history of diapirism in the East Texas Basin, described by Jackson and Seni (1983a) and McGowen and Harris (1982), is summarized here to provide an overview of salt movement in the area. Figure 7 shows salt-structure provinces 1 through 4 in the East Texas Basin.

The earliest record of movement in the Louann Salt is in the shallow-marine interval below the top of the Gilmer Limestone. This seismic unit thins over salt anticlines of province 2 (fig. 7), indicating the growth of low-amplitude salt pillows in pre-Gilmer time (Jackson and Harris, 1981). Pillows grew along the western margins of the basin in pillow provinces 2 and 3. On the western fringe of diapir province 4, Oakwood Dome and possibly Grand Saline Dome also began to grow as pillows in pre-Gilmer time.

The overlying Upper Jurassic marine strata formed an aggrading and slowly prograding, carbonate wedge that loaded the salt fairly uniformly (Bishop, 1968). Differential loading by the carbonate platform would have operated at maximum effectiveness along the shelf edge beneath ooid shoals. But this mechanism would have been less effective than differential loading by fan deltas in Schuler-Hosston time. Gravity gliding of the post-Louann section over the salt décollement zone may have contributed to Gilmer folding. The growth of periclinal salt pillows can also be ascribed to the inverse density layering of carbonates (density, 2.3 to 2.7 g/cm<sup>3</sup>) on salt (density, 2.0 to 2.2 g/cm<sup>3</sup>). In Gilmer time, the basin was still starved and the slope sediments were thin (fig. 5A). This explains the lack of contemporaneous halokinesis in the central basin despite the great thickness of salt there.

In the Late Jurassic and Early Cretaceous, the Schuler-Hosston elastics prograded rapidly across the carbonate platform, forming coalescing, sand-rich deltas. Progradation slowed seaward of the shelf break, but the thick deltas continued to advance as a linear front into the previously starved basin (fig. 5B). Loading of the pre-Schuler substrate by the advancing linear depocenters squeezed salt ahead in a frontal bulge to form salt anticlines (fig. 5B). Increase in either sediment supply or progradational rate buried the frontal anticlines,

thereby initiating parallel, but more distal, salt anticlines (fig. 5B). These anticlines, which may have been formed partly by gravity gliding as well as by differential loading, were ridges of source rock from which the salt diapirs grew by budding upward.

## OVERVIEW OF DOME HISTORY

Location of diapirism in the East Texas Basin varied through time. Against a background of basin infilling, the areas of dome movement shifted in an orderly progression. Diapirism was concentrated first along the western and eastern edges of the diapir province (represented by group 1 diapirs) and then in the basin center and northward along the basin axis (represented by group 2 diapirs) in response to the shifting of depocenters from the basin margin to the center. Basin-edge tilting and erosion over pillow crests localized the final episode of diapiric activity (represented by group 3 diapirs) on the western and northern updip margins of the diapir province.

Rapid peripheral filling of the previously starved basin during Hosston - Glen Rose deposition may explain the location of the three subgroups of group 1 diapirs around the margin of the diapir province. The distribution and ages of group 1 diapirs suggest that uneven loading by thick terrigenous elastics of the Schuler and Hosston Formations, prograding toward the basin center, triggered diapirism in the Jurassic and Early Cretaceous (fig. 5B). Group 1 diapirs grew in sites of maximum regional sedimentation.

Group 2 diapirs underwent diapirism along the basin axis as sedimentation and subsidence rates peaked from 112 to 98 Ma ago in the Early Cretaceous (figs. 31 and 32). It is uncertain whether diapirs of groups 1 and 2 "pierced" their overburden by subsurface intrusion or by erosional breaching. But the growth of group 2 diapirs during rapid regional sedimentation and subsidence suggests that erosion was not the prime cause. Rather, uneven sediment loading (both thickness and lithofacies) was probably responsible for initiating diapirism.

Group 3 diapirs grew on the northern and western margins of the diapir province in the Late Cretaceous when regional sedimentation rates were significantly reduced from former levels. Loading of the lithosphere in the center of basins commonly causes basin-edge tilting, making locally elevated areas, over pillow crests, prone to erosion between episodes of sedimentation (Boillet, 1981). Erosion could therefore have exposed and breached salt pillows on the updip margin of the East Texas diapir province. This breaching initiated diapirism in at

least one dome. Local unconformities show that Hainesville Dome reached the surface by erosional exposure of the salt pillow (Loocke, 1978; fig. 10). Salt extrusion, probably forming salt-cored islands, allowed massive diapirism because of the lack of vertical constraint on the rise of salt (Bishop, 1978). The minor amount of cap rock present over the dome supports the conclusion that most salt was removed by extrusion and erosion rather than by ground-water dissolution.

## RATES OF SALT MOVEMENT AND DOME GROWTH

Syn depositional thickness variations in surrounding strata allow us not only to recognize the timing and patterns of halokinesis but also to measure the volumes and rates of salt flow. All previous estimates of the growth rate of pillows and diapirs (for example, Trusheim, 1960; Ewing and Ewing, 1962; Sannemann, 1968; Kupfer, 1976; Motherland, Sewell and Associates, 1976; Kumar, 1977; Jaritz, 1980) relied on certain basic propositions, and the present study is no exception; these propositions are discussed below.

### PROPOSITIONS

In assessing the times, rates, and volumes of salt movement, we have relied on three proven propositions, three unproven propositions, and two simplified propositions, that while simplified, introduce negligible error to quantitative assessments.

### Proven Propositions

(1) *The upper surfaces of mapped units were originally horizontal and planar.* The absence of deep-water (more than 200 to 300 m [650 to 980 ft] deep), post-Aptian deposits indicates that on a regional scale, the depositional surface was nearly horizontal.

(2) *Contour intervals less than 100 ft (30 m) provide little increase in accuracy of computed volumes.* Closed isopach contours around salt structures delineate the area influenced by local salt flow in different stratigraphic intervals. The total volume of a salt-withdrawal basin is calculated by using planimetry of hand-drawn isopach maps and the technique shown in figure 36. Making the contour interval less than 100 ft has little effect on the calculated volume. In this type of integration, errors due to approximation cancel out except at the boundary of the basin (perimeter of area  $A_1$  in fig. 36), where the maximum vertical error is  $\pm 100$  ft. However, because the actual basin edge is equally likely to lie on either side of the outermost contour, errors will also tend to nullify each other.

Errors may be classed as relative (if compared with the volume of an individual salt-withdrawal basin) or absolute (if compared with the total volume of all salt-withdrawal basins). Maximum relative error in calculating the volume of an individual salt-withdrawal basin is greatest in the smallest basins. However, because such basins constitute a small percentage of the total volume of all salt-withdrawal basins, the absolute error is small.

(3) *Deformation around and above salt structures resulted directly from gravity-induced salt tectonics (halokinesis).* The tectonic setting of

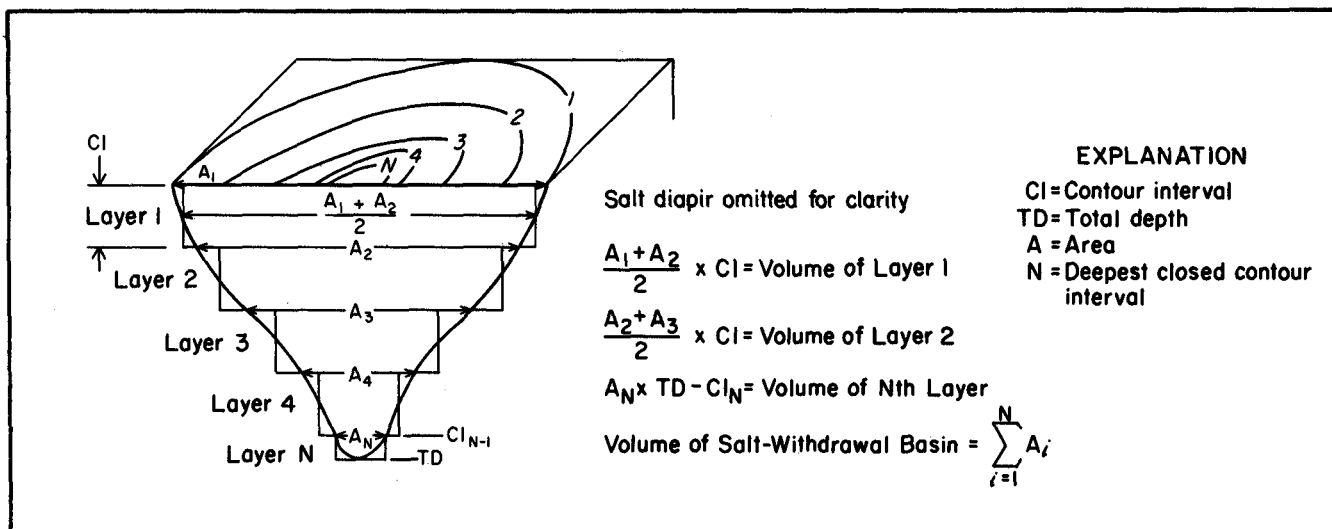


FIGURE 36. Technique for calculating the volume of a salt-withdrawal basin.

the evolving East Texas Basin is that of a subsiding passive margin or aulacogenic reentrant (Dennis and others, 1979). Regional crustal shortening in such a setting is improbable, and there is no evidence for its occurrence. Approximately 740 km (444 mi) of seismic data indicate that the Louann Salt is a décollement zone separating deformed overburden from the nearly planar upper surface of the pre-Louann basement (Jackson and Harris, 1981; Jackson and Seni, 1983a; McGowen and Harris, 1982).

### Unproven Propositions

(4) *The geochronology is reasonably accurate.* Acknowledging that no single time scale is universally accepted (Baldwin and others, 1974), we used the Jurassic-Cretaceous time scale of van Hinte (1976a, b), which includes radiometric, paleomagnetic, and faunal data. A single age from van Eysinga (1975) was used for the top of the Eocene Wilcox Group.

(5) *The upper surfaces of mapped units are essentially isochronous.* Variations in rates of progradation and transgression result in small variations in age along the upper surface of a stratigraphic unit due to dipping bedding surfaces. Because the study area is relatively small and the mapped units have a long depositional history, these age variations are negligible.

(6) *The stratigraphic record is sufficiently complete to allow recognition of long-term trends.* We recognize that the geologic record includes periods of nondeposition, erosion, and removal of stratigraphic section. Dome uplift caused local angular unconformities around Hainesville and Butler Domes. Only one regional unconformity (the base of the Austin Chalk) truncates a significant thickness of stratigraphic section. Halbouty and Halbouty (1982) saw evidence for an additional regional unconformity (the base of the Woodbine Group) in the eastern part of the East Texas Basin. Even in a highly explored and relatively small area like the East Texas Basin, it is doubtful that all unconformities, especially disconformities, have been recognized. We have diminished the problem associated with intermittent dome growth by averaging time intervals. The Cretaceous-Tertiary growth history was divided into seven consecutive time intervals, each having a duration of 1 to 17 Ma. We recognize that the time intervals for which mean dome growth rates were calculated may include periods of growth and nongrowth. These mean rates are therefore less than actual rates over shorter durations of intermittent sedimentation and dome growth. Nevertheless, long-term growth trends can

be clearly recognized by comparing the mean rates of the seven consecutive intervals.

### Simplified Propositions

This category includes simplified propositions that we have adopted to make quantitative assessments possible. Accepting proposition 7 is justified because, although it is manifestly false, we demonstrate that it is irrelevant to long-term historical trends of growth rates and to short-term prediction of growth rates. Proposition 8 is a simplification of the interaction of three complex processes. We show that the effects of two of these processes are negligible, and that the effects of the third are impossible to quantify.

(7) *The effects of compaction were negligible.* During burial, expulsion of pore fluids by compaction progressively reduces the volume and porosity of sediments. Our calculations of volumes and rates of salt flow are based on the present (compacted) volumes of sediments rather than on the original (uncompacted) volumes. Compactional effects on shale can be assessed for various burial depths. Depths of 152 m (500 ft), 1,524 m (5,000 ft), and 3,048 m (10,000 ft) are the limits of burial for strata studied in this paper. Using averaged porosity-depth data from Magara (1980), we calculated volume loss for shale at depths of 152 m (500 ft), 1,524 m (5,000 ft), and 3,048 m (10,000 ft) to be 5 percent, 35 percent, and 39 percent, respectively. Fine-grained elastics are the most common type of sediment in the East Texas Basin. They are also likely to be the most compacted. The calculated volume losses therefore are the probable maxima of the entire stratigraphic section studied. On the basis of these maximum volume losses, true rates of dome growth, calculated for original, decompacted sediment thicknesses (1/[100-volume percentage loss]), are estimated to exceed compacted rates by, at most, 1.05, 1.54, and 1.64 (at depths of 152 m [500 ft], 1,524 m [5,000ft], and 3,048 m [10,000 ft], respectively).

Figure 37 demonstrates two important relationships. First, the long-term historical trends of both the compacted and decompacted curves are similar. Second, because the most recent dome growth rates were calculated from the least compacted sediments, the decompacted curve for the past 56 Ma yields a rate only 5 percent higher than that of the compacted curve. In anticipating future dome growth rates by extrapolating historical trends, the difference between the compacted and decompacted techniques is negligible.

(8) *The volume of sediments in a salt-withdrawal basin is equivalent to the volume of salt that flowed into the diapir during filling of that basin.* This

proposition is based on propositions 5, 6, and 7 and on the principle of conservation of volume. Under this proposition the evacuation of salt from a particular zone allows the accumulation of an equivalent volume of extra-thick sediments (in a salt-withdrawal basin) above the zone. Other studies have equated the volume of sediments in a salt-withdrawal basin with the volume of salt that migrated into the diapir (Trusheim, 1960; Crowe, 1975; Kupfer, 1976; Reese, 1977). The concept is also used for various purposes in the oil industry. To our knowledge, this is the first study to use volumes measured by planimetry to calculate volumes and rates of dome growth.

Despite acceptance of this proposition in the literature, three general processes, in addition to compaction, reduce its reliability: (1) structural thickening by folding, (2) dissolution below the withdrawal basin, and (3) centrifugal salt flow (away from diapir).

The influence structural thickening by folding has on volume calculations is thoroughly discussed in the following section. Our data indicate that

theoretical and experimental effects of fold thickening are much less than the observed thickening in withdrawal basins.

Dissolution and collapse of the salt source layer below a withdrawal basin could potentially yield erroneously high rates of diapir growth if the salt dissolved and entered the basinal ground-water regime instead of migrating to feed the diapir. Average values of ground-water salinity do increase with depth in the East Texas Basin; for example, the average salinity of the Hosston Group is 200,000 mg/L (sea water is 35 to 40 mg/L). There is no evidence of differential salt dissolution in withdrawal basins. Therefore we cannot estimate the degree to which sedimentary volume might be affected by dissolution of salt before it migrated into the diapir. In contrast, volumetric changes in the withdrawal basin register the dissolution of salt at the diapir crest and flank if further diapir growth replaced the lost salt.

Centrifugal flow of salt from below a withdrawal basin and away from a diapir could cause

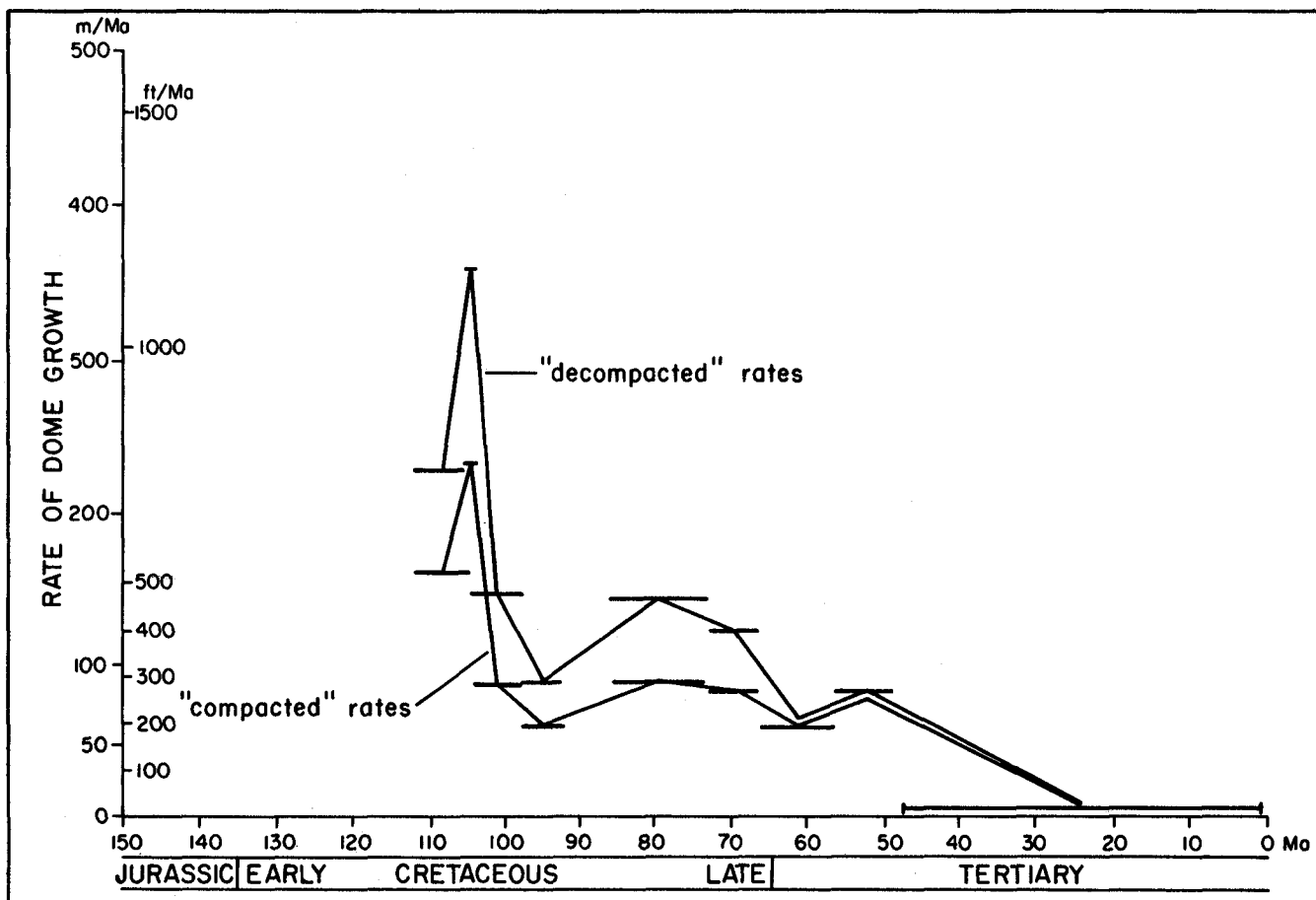


FIGURE 37. Dome-growth-rate curve calculated on the basis of compacted sediments (bottom line) (fig. 47) and curve calculated on the basis of decompacted sediments, East Texas Basin (top line). At the youngest stage of dome growth, the two curves differ by only 5 percent.

erroneously high estimates of diapir growth rates. Centrifugal salt flow has been experimentally produced in diapir models by Dixon (1975, his fig. 21). Seismic reflection data do not indicate rings of salt structures around salt-withdrawal basins; rather, salt is largely absent between diapirs (figs. 6A and 6B). Such peripheral salt rings would be expected if centrifugal flow had occurred. Furthermore, the salt rings could not have subsequently been dissolved because their removal would be recorded by anomalously thickened sediments above them, and there is no evidence for this.

## DISTINGUISHING BETWEEN SYNDEPOSITIONAL AND POSTDEPOSITIONAL THICKNESS VARIATIONS

### The Problem

This report extensively analyzes thickness variations in strata around and above growing salt structures. The origin of these thickness variations is debatable (Bishop, 1978); they may arise either syndepositionally or postdepositionally. Recognition of a specific origin is critical because only syndepositional thickness variations can document the flow of salt during deposition of a particular stratigraphic unit and thereby provide a time frame for the history of diapirism.

Thickness variations of strata over and around salt structures can be ascribed to four processes: (1) local rise or fall of the sedimentation surface during deposition (which results in syndepositional thickness variations), (2) postdepositional erosion, (3) structural distortion of strata caused by stresses imposed by growth of nearby salt structures, or (4) increased compaction of sediments draping a virtually incompressible salt body (which results in postdepositional thickness variations). The effects of these processes are broadly similar. For instance, thinning of strata over a salt pillow can be caused by syndepositional rise of the pillow, by erosion, or by increased drape compaction over the rigid, relatively incompressible salt body, analogous to draping of varvite laminae over dropstones. Thickening of strata in a rim syncline around a diapir can be caused either by syndepositional deepening of the syncline or by postdepositional ductile folding of poorly consolidated sediments around the salt stock.

Postdepositional strain of originally planar layers overlying a rising buoyant mass has been documented by scaled centrifuge modeling (Dixon,

1975; Ramberg, 1981). In addition, Talbot (1977) modeled strongly inclined diapirs by building models having lateral changes in thickness, viscosity, or density. In the case of a low-viscosity, low-density body such as rock salt, the overburden above the crest of a circular rising dome distorts by oblate flattening and by horizontal extension. This distortion is identical to nontectonic compactional strain and therefore cannot be differentiated from compaction above the crest. Furthermore, if traced laterally, tectonic flattening diminishes because rise of the underlying salt in the flanks is less than in the dome axis. Compactional strain also diminishes laterally because the sediments are not directly overlying virtually incompressible salt. Differentiating between tectonic and compactional thinning over a salt dome is therefore difficult. There are also practical problems in detecting lateral changes in strain where strain gradients are minute. Figure 38 shows the percentage thickness change,  $\Delta h$ , in sedimentary units near East Texas salt domes. Maximum thinning averages only about 0.75 percent per 100 m of lateral distance. Strain analysis is currently inadequate to identify these small changes in strain and to filter out background variations.

Centrifuge modeling also shows that overburden is tectonically thickened in rim synclines around both low-viscosity diapirs (those formed of salt, for example) and high-viscosity diapirs (such as those formed of gneiss). This thickening counteracts the effects of compaction, so can be differentiated from it. Nevertheless, the combination of vertical shortening (induced by compaction) and oblique shortening (induced by folding of planar layers) of constant lateral thickness would be extremely difficult to differentiate from an analogous combination of compaction and folding of syndepositionally thickened layers of variable lateral thickness. Apart from this inherent problem of differentiation, there is, again, the practical problem of detecting strain gradients averaging as low as 1.5 to 1.0 percent per 100 m in rim synclines (fig. 38).

If syndepositional thickness changes cannot be differentiated from postdepositional thickness changes by strain analysis, are other means available? We believe that the changes can be differentiated by structural and sedimentological criteria discussed in the following two sections.

### Structural Evidence

The structural criteria for distinguishing syndepositional from postdepositional thickness changes are based on comparison of the geometry of folds around natural salt domes with that of folds around experimental models of domes. Ramsay (1967, p. 359-362) recognized two types of thickness

measurements in the profile of a folded layer (fig. 39A): orthogonal thickness,  $t_\alpha$ , and thickness parallel to the axial surface,  $T_\alpha$ , where  $\alpha$  refers to the dip of a folded surface relative to the axial trace. Of more practical use in subsurface geology is the isochore thickness,  $IT_\alpha$ , which differs slightly from the  $T_\alpha$  thickness in all folds except true similar folds (fig. 39A). All three thickness measurements are equal along the axial trace in the profile plane. On the basis of the relation between the limb dip,  $\alpha$ , and  $t' = t_\alpha/t_0$  or  $T' = T_\alpha/T_0$ , all classes of folds can be precisely classified (figs. 39B and 39C). Class 1B (parallel folds) and Class 2 (similar folds) are the most widely known classes, but are fairly rare in nature (Hudleston, 1973; Powell, 1974; Gray, 1979,

1981; Orozco and Galvez, 1979). Each half fold (quarter wavelength) can be plotted on these graphs, as depicted by curves  $I_t$  and  $I_T$  for the fold illustrated in figure 39A.

Certain fold profiles are characteristic of certain models of formation. Thus the mechanics of fold formation can be inferred from fold morphology in some cases (Ramsay, 1967, p. 366-372, 391-415). For example, consider folds II and III, which represent experimentally modeled domes analogous to gneiss domes (stiff, buoyant layer) and salt domes (soft, buoyant layer), respectively (fig. 40). The  $t'/\alpha$  and  $T'/\alpha$  plots for each fold are shown in figure 39. They indicate that both are Class 1C folds. Accepting the consensus that Class 1C folds form

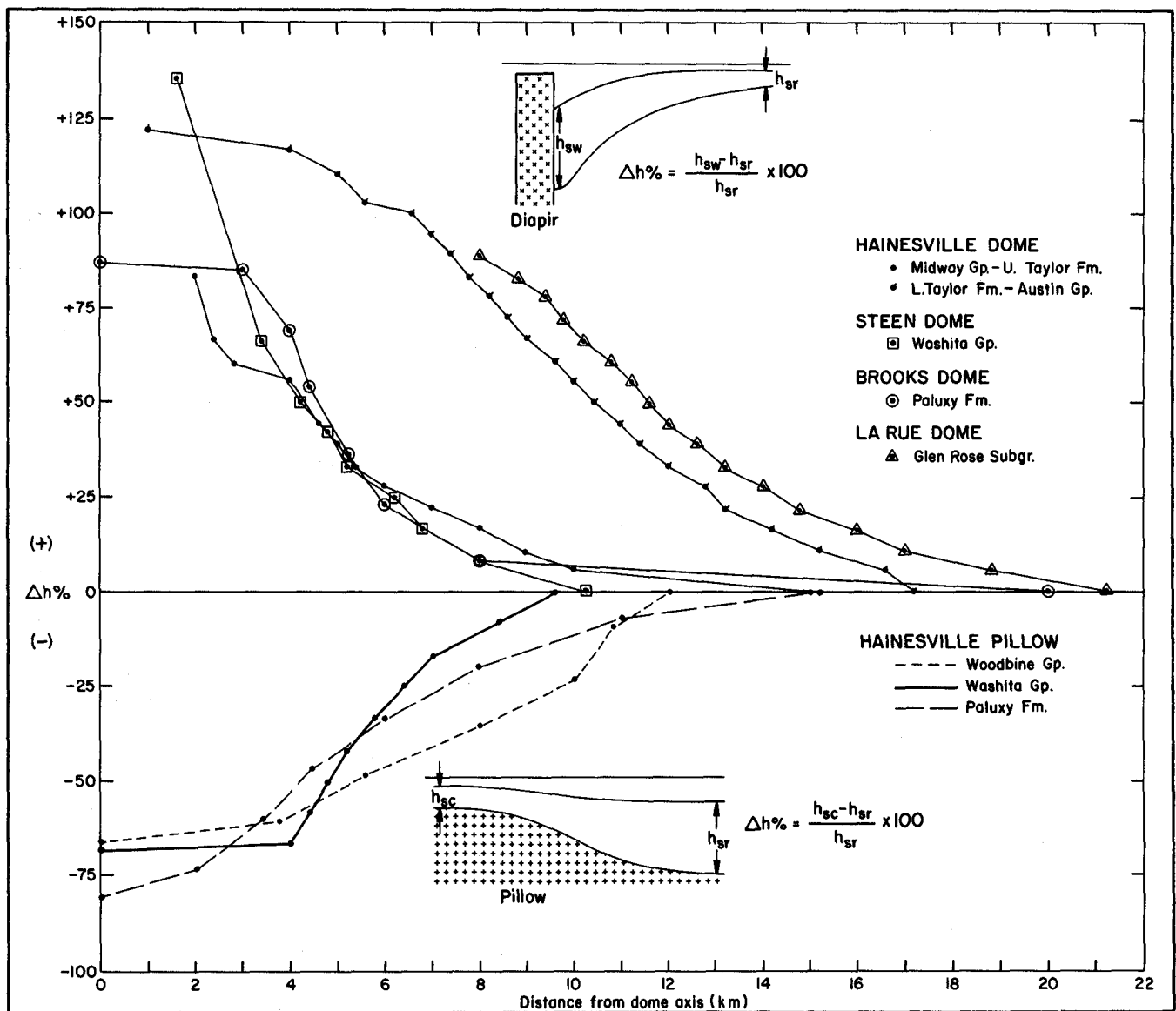


FIGURE 38. Percentage thickness change ( $\Delta h\%$ ) around selected diapirs and pillows in the East Texas Basin. Diagrammatic insets show methods of calculating  $\Delta h\%$ .

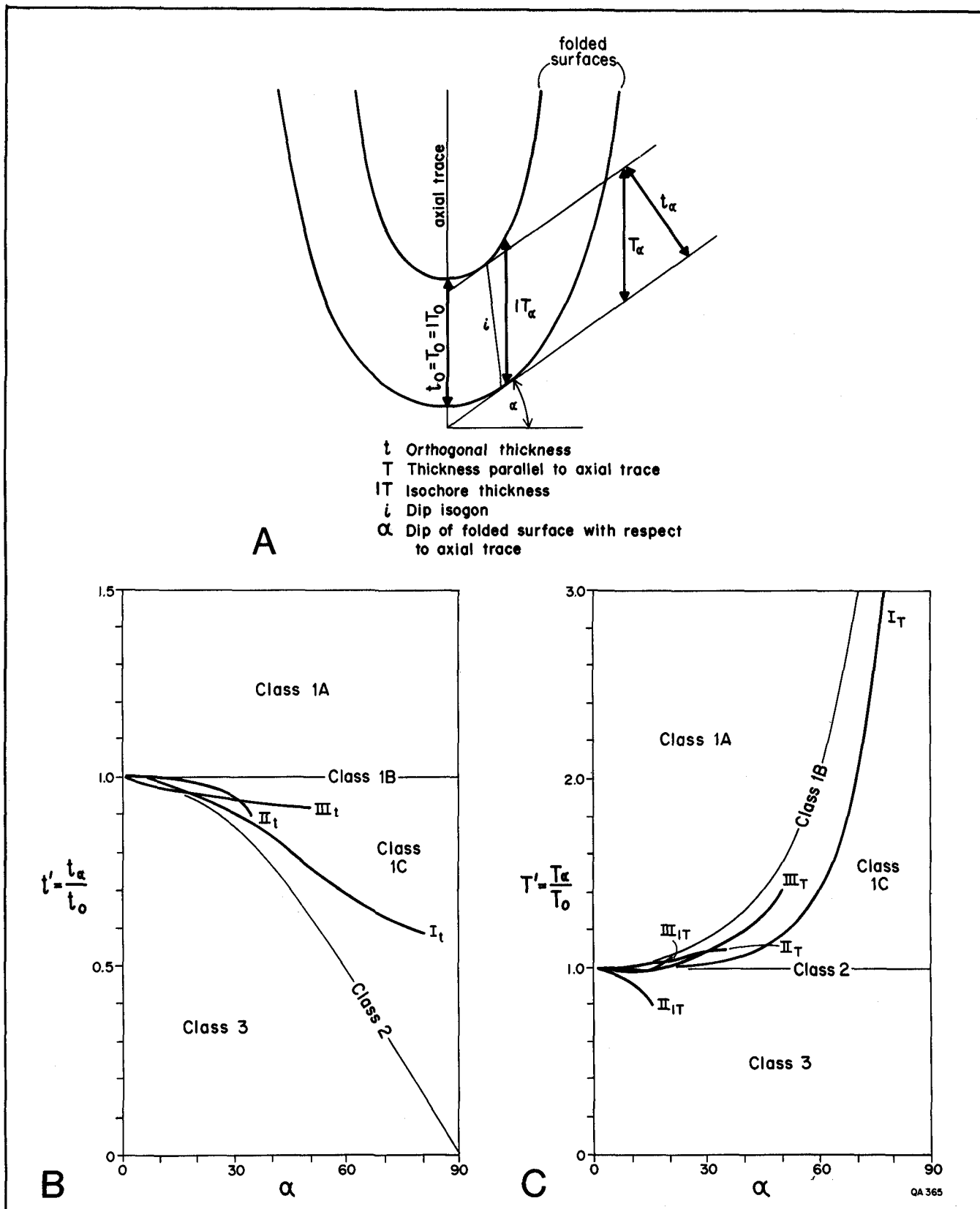


FIGURE 39. Fold-shape analysis of Ramsay (1967, p. 359-372). (A) Thickness parameters of a folded layer (fold I) in profile. (B, C) Fundamental fold classes on the  $t'/\alpha$  and  $T'/\alpha$  graphs showing plots for fold I (fig. 39A) and folds II and III (fig. 40). Curves marked  $II_{IT}$  and  $III_{IT}$  are based on isochore thickness rather than on  $T_\alpha$ , so do not represent the true fold shape.



by a combination of layer-parallel shortening before folding, homogeneous flattening strain during folding, and class 1B parallel folding (Ramsay, 1967, p. 411-415; Hobbs and others, 1976, p. 196-199), folds II and III formed by a combination of buckling and homogeneous shortening normal to their axial traces. The isochore thicknesses of these two inclined folds (right side of fig. 40) do not reveal their true morphologic class. Nevertheless, a plot of  $IT/\alpha$  (fig. 39C) indicates an important point about fold III: its  $IT/\alpha$  curve is largely horizontal, illustrating negligible change in isochore thickness up to limb dips of nearly 20 degrees. This model was constructed by Dixon (1975) specifically to simulate salt-dome growth, so this observation of negligible change in isochore thickness due to postdepositional folding is relevant to the problem discussed in this section.

Many domes have been experimentally modeled by the centrifuge technique pioneered by Hans Ramberg. These domes record deformation in originally planar layers overlying a buoyant source layer. This deformation is commonly extreme because the models were allowed to evolve to highly mature structural stages to illustrate a full range of strain states. The strain states appropriate to this discussion can be readily correlated with dip. The maximum dip of the Louann Salt indicated by seismic reflection data is 25 degrees on the flanks of the Van-Ash salt pillows. But the maximum large-scale dip of strata younger than 112 Ma old (the subject of this paper) in the rim synclines is 9.7 degrees. A 10-degree dip therefore represents the steepest major structure (with the exception of the zone of contact strain sheathing the domes) in the basin.

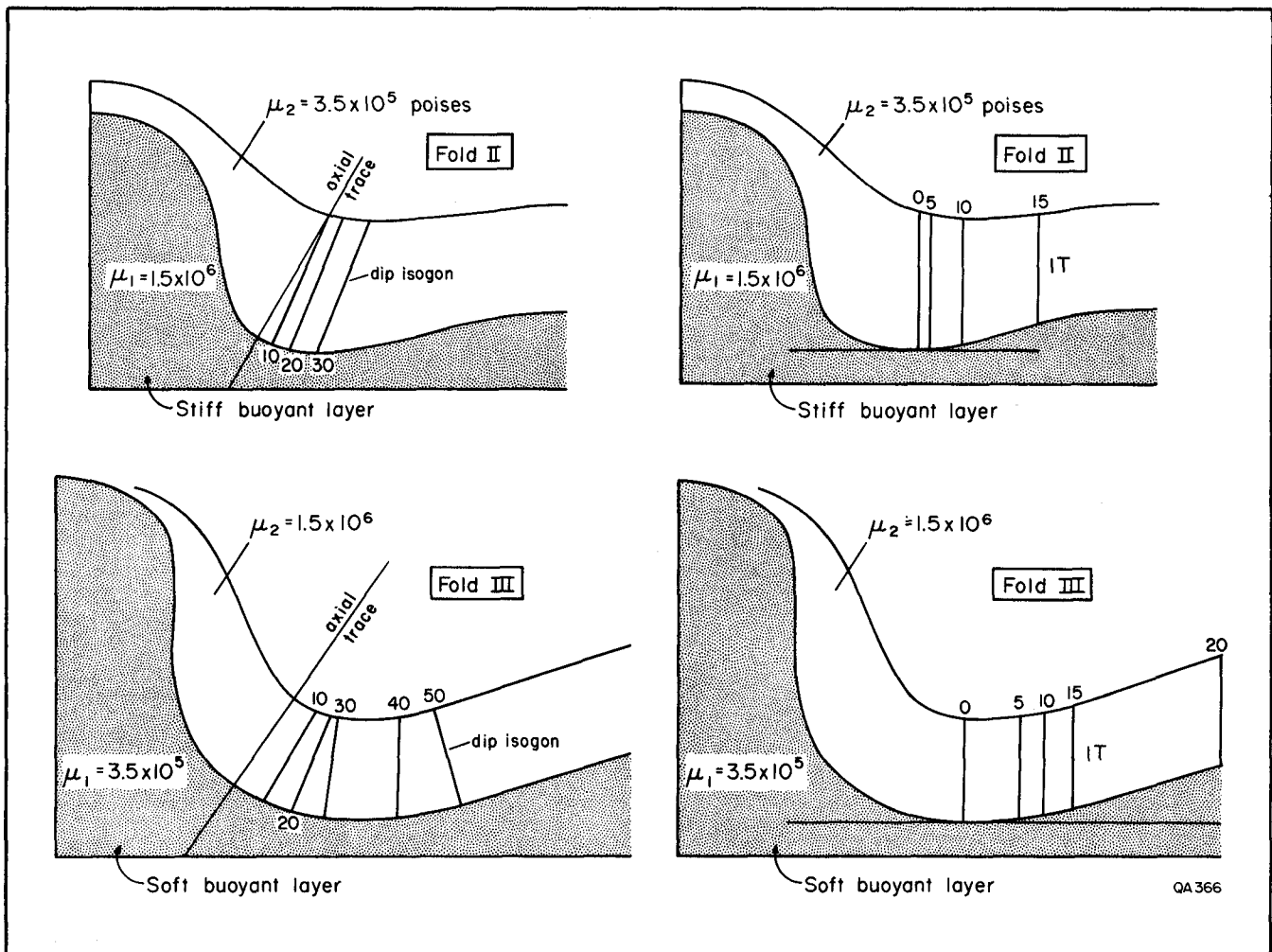
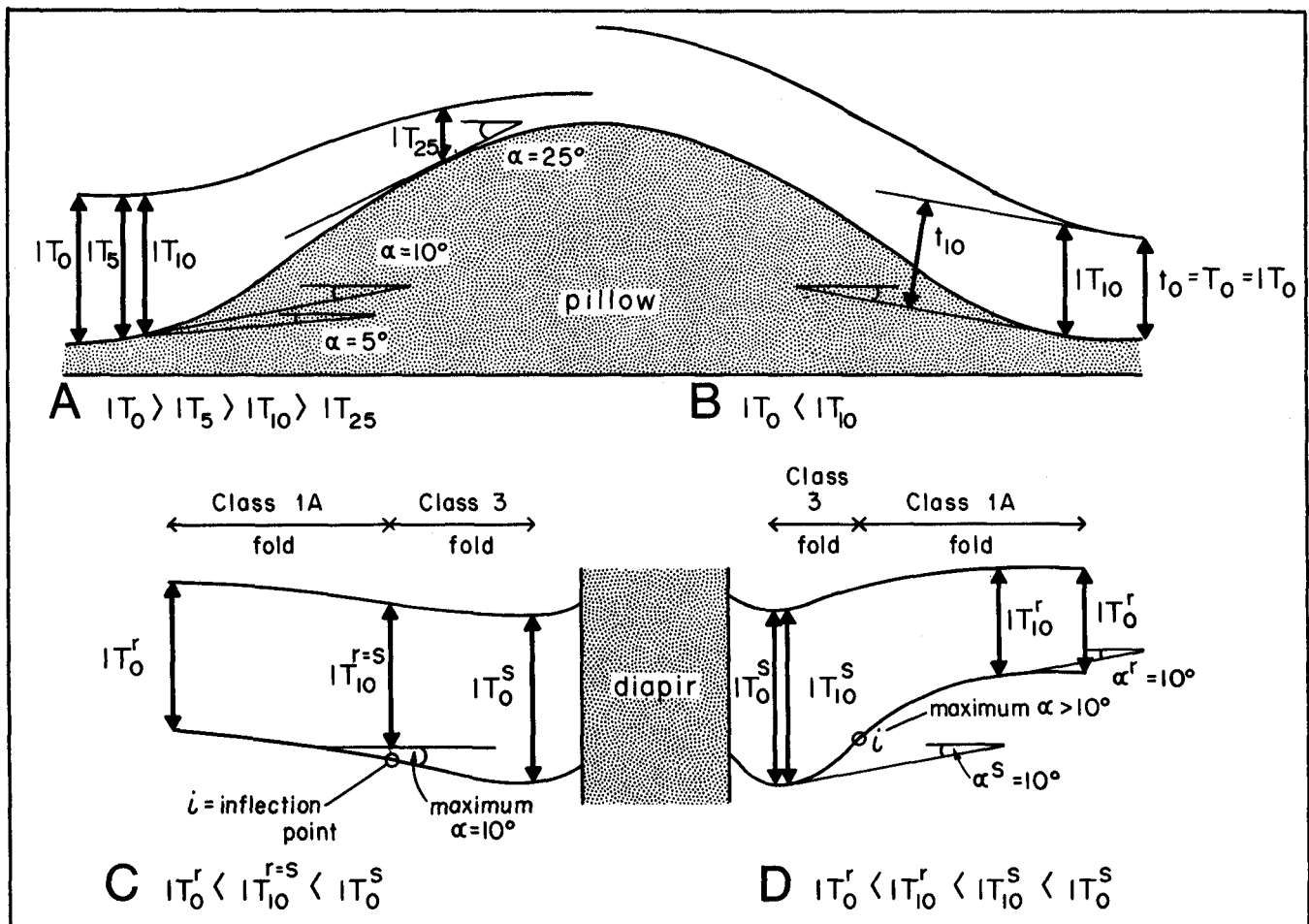


FIGURE 40. Cross sections (folds II and III) of model domes WD-4 (II) and WD-6 (III) of Dixon (1975, his figs. 6A and 21A). The models were constructed to simulate growth of gneiss domes and salt domes, respectively. The symbol  $\mu$  represents the viscosity of a particular layer. Dip isogons are shown in the left-hand figures; isochore thicknesses (IT) are shown in the right-hand figures. (Isochore thicknesses are plotted as curves II<sub>IT</sub> and III<sub>IT</sub> in fig. 39.)

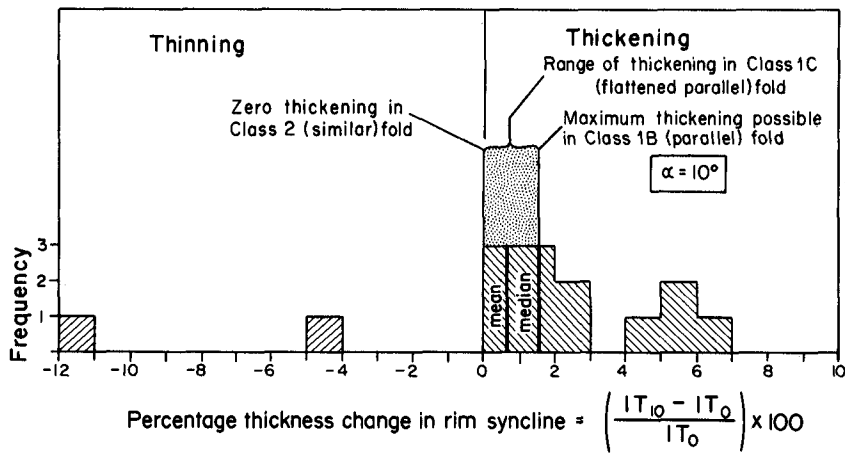
Proportional thinning above experimentally modeled pillows is easily calculated from measurements of the parameters  $IT_0$ ,  $IT_5$ ,  $IT_{10}$ , and  $IT_{25}$  (fig. 41A). In most cases the maximum thickness is  $IT_0$ . However, where the dip steepens more rapidly than the layer thins (fig. 41B), the isochore thicknesses ( $IT_\alpha$ ) increase up the flank of the pillow, although the orthogonal thicknesses ( $t_\alpha$ ) decrease, causing apparent thickening over the pillow. Ideally, thicknesses in diapir rim synclines should be measured from models having maximum dips of 10 degrees (fig. 41C). Such models are not available, so the parameters  $IT_0^r$  and  $IT_{10}^r$  were measured (fig. 41D) to enable comparison with the parameters  $h_{sr}$  and  $h_{sw}$  in figure 38.

Thickness changes induced by folding were measured from 14 model diapirs (toward rim synclines) and 11 model pillows (toward crests); the

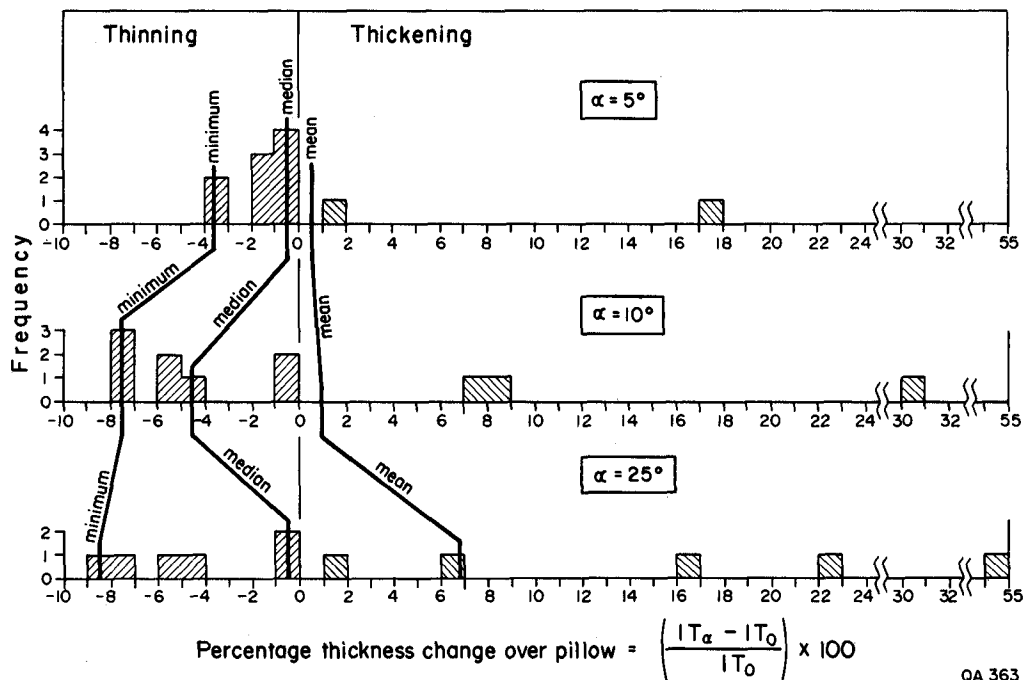
results are shown in figure 42. Both the mean and median values of thickness change in rim synclines are less than 2-percent thickening; maximum is 7-percent thickening and minimum is -12-percent thinning. The median value is identical to the maximum thickening theoretically possible in a limb dipping 10 degrees in a fold formed by buckling ( $T'_\alpha = \sec \alpha$ , Ramsay, 1967, equation 7-6). Higher values suggest either errors in model construction or measurement, or the action of a different folding mechanism. In the case of thickness changes over a pillow (fig. 42) the maximum thinning increases from -3.5-percent change at a flank dip of 5 degrees to -8.5-percent change at a flank dip of 25 degrees; the maximum thinning at 10 degrees of dip is -7.5 percent. With increasing flank dip, the distributions are skewed to the right by the geometric effect illustrated in figure 41 B.



**FIGURE 41.** Measurement of isochore thickness parameters in model domes. (A) Changes in thickness up the flanks of a pillow at dips of  $\alpha = 0, 5, 10,$  and  $25$  degrees. Percentage thickness change is  $[(IT_\alpha - IT_0)/IT_0] \times 100$ . (B) The effect of increasing flank dip of a pillow. Even though orthogonal thickness,  $t_\alpha$ , decreases up the flank, the isochore thickness,  $IT_\alpha$ , increases in the same direction. (C) Thickness variations in an ideal model, whose maximum dip of 10 degrees on the flanks of the rim syncline is the same as the maximum dip in East Texas rim synclines. (D) Measurement of thickening in a rim syncline whose maximum limb dip is greater than 10 degrees. Percentage thickness change is  $[(IT_{10} - IT_0)/IT_0] \times 100$ .



A



QA 363

B

FIGURE 42. Histograms showing frequency distribution of thickness changes measured (A) in rim synclines of model domes (14 layers) and (B) over model pillow crests (11 layers). Models are illustrated in Dixon (1975, his figs. 6A and 21A) and Ramberg (1981, his figs. 11.13, 11.17, 11.38, 11.46, 11.58, 11.80, 11.81, 11.83, 11.93, and 12.1). (A) The median thickness change of 1.5 percent thickening is identical to the maximum thickening theoretically possible at this limb dip in a fold formed by buckling, as calculated by the equation  $T_\alpha = \sec \alpha$ . Maximum thickening is 7 percent. (B) Increased thinning with increased steepness of pillow flanks is reflected by the decreasing minimum curve; maximum thinning at 10 degrees dip is -8 percent. The mean and median curves are skewed rightward with increasing dip because of the geometric effect illustrated in figure 41B.

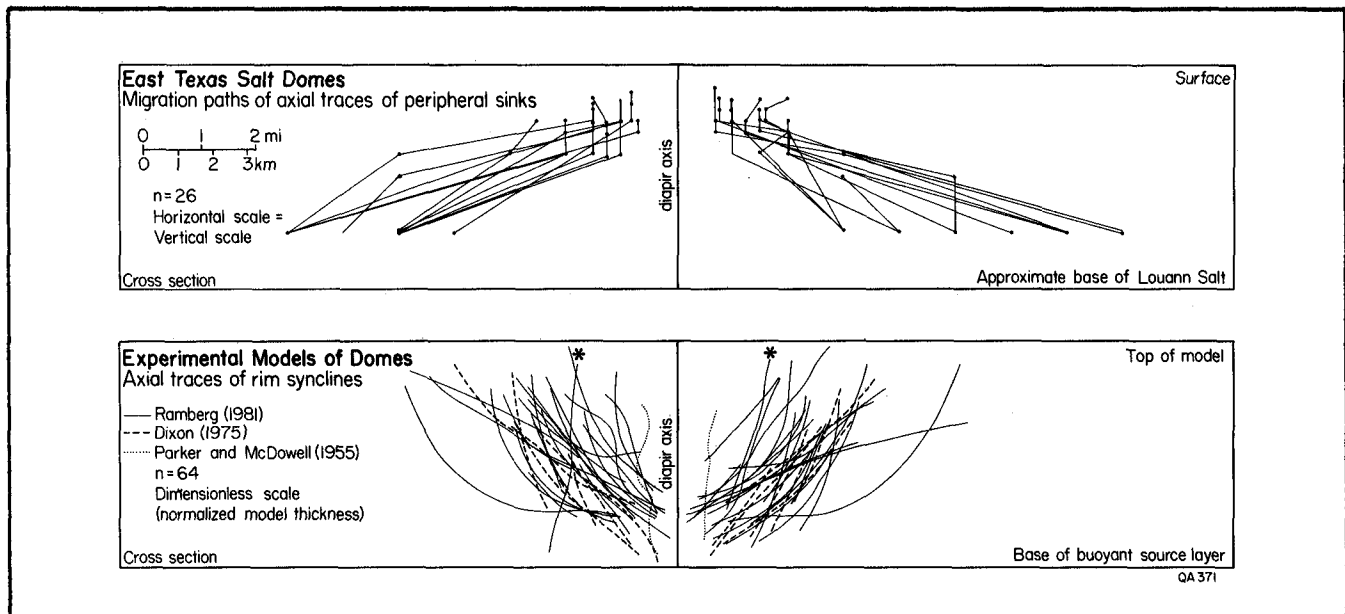
In summary, the *maximum* thickness changes induced by growth of experimentally modeled domes at comparable maximum dips of 10 degrees are (1) 7-percent thickening in rim synclines of diapirs and (2) -9-percent thinning above pillows. These thickness changes are far less than those actually measured around the salt domes of the East Texas Basin (compare figs. 38 and 42). Equivalent thickness changes in figure 38 are (1) 135-percent thickening and (2) -80-percent thinning. These findings suggest that because of the comparatively low dips within the basin, folding could have caused only a small fraction of the observed thickness changes. Rise and fall of the depositional surface induced by flow of underlying salt remains the only reasonable explanation for huge thickness changes induced over wide areas of gentle dip.

Further structural evidence that thickness changes around the East Texas salt domes are largely syndepositional, rather than postdepositional, results from comparing the positions of axial traces with those of experimental models. The axial traces of experimental dome models are shown in cross section in figure 43. Their shapes vary widely, but they share one important characteristic. All but one of the axial traces curve away from the diapir as they ascend through higher layers. The exception is marked by the asterisk in the left-hand part of the

figure. This particular example from Ramberg (1981, his fig. 11.93) is not representative because the diapir consists largely not of buoyant material but of a dense material below the buoyant layer. This trend of inward curvature in experimentally modeled domes is quite different from the pattern shown by the axial traces of the East Texas salt domes (fig. 43). There the axial traces of the primary, secondary, and tertiary peripheral sinks progressively migrate toward the diapirs, so axial traces in younger units are closer to their diapirs. This migration is caused by shrinkage of a broad salt pillow as salt was evacuated up a central diapir and is an inherent characteristic of the stages of dome growth shown in figure 8.

### Sedimentological Evidence

The syndepositional nature of dome-related thickness changes is also supported by sedimentologic evidence including changes in patterns of sandstone distribution, depositional facies, and localized reef growth near domes in East Texas. These changes, all documented in this paper, reflect the influence of syndepositional topographic variations that were controlled by salt flow. In other basins, ancient examples are provided by facies



**FIGURE 43.** Comparison of axial-trace positions in vertical cross sections through 14 of the 16 East Texas Basin salt domes (Bullard and Whitehouse Domes have a measurable sink at only one level) (top figure) and 23 model domes (illustrated in Parker and McDowell, 1955, their fig. 21; Dixon, 1975, his figs. 2B, 3B, 4B, 5B, 21A, 21B, and 21C; Ramberg, 1981, his figs. 11.2, 11.13F, 11.16, 11.17, 11.19, 11.25, 11.32, 11.38, 11.39, 11.45, 11.50, 11.58B, 11.93, 11.95, and 12.1B). Axial traces of primary, secondary, and tertiary sinks (measured from maps) of the East Texas diapirs migrate progressively closer to the diapirs through the evolutionary stages of growth. In contrast, axial traces in the model-dome cross sections curve away from the dome as they ascend; one unrepresentative model is marked by asterisks.

variations associated with salt structures, including sand-body pinch-outs, changes in sand-body geometry, and preferential growth of reefs over domes and pillows (Halbouty and Hardin, 1951; Cantrell and others, 1959; O'Neill, 1973; Stude, 1978; Elliot, 1979; Trippet, 1981). Holocene examples of analogous topographic, lithologic, and faunal variations associated with salt structures have also been recorded (Ewing and Ewing, 1962; Fisher and others, 1972, 1973; Purser, 1973; McGowen and others, 1976; Bright, 1977; Rezak, 1977; Kent, 1979).

On the basis of these structural and sedimentological observations, we have concluded that most thickness variations in the East Texas Basin are syndepositional in origin. For the purposes of estimating dome growth rates, all thickness variations are assumed to be syndepositional in origin.

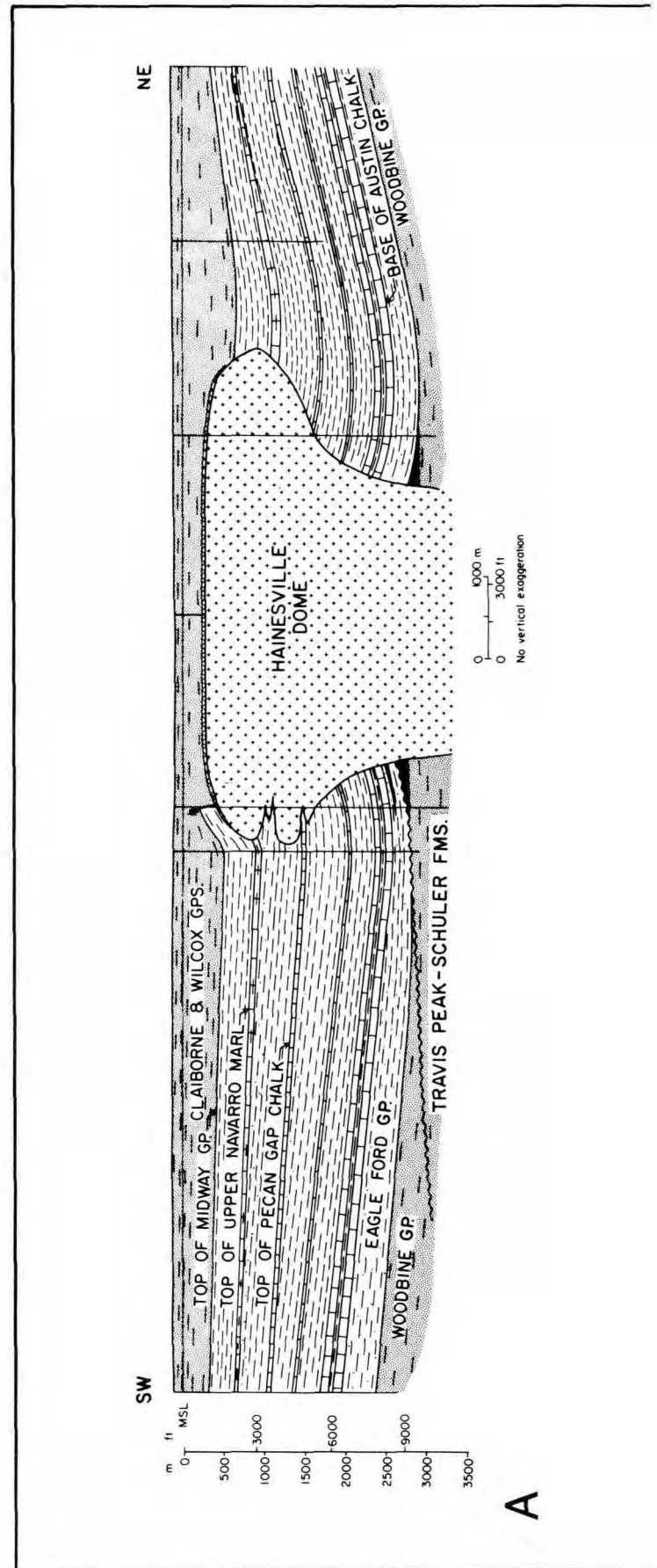
## METHODOLOGY

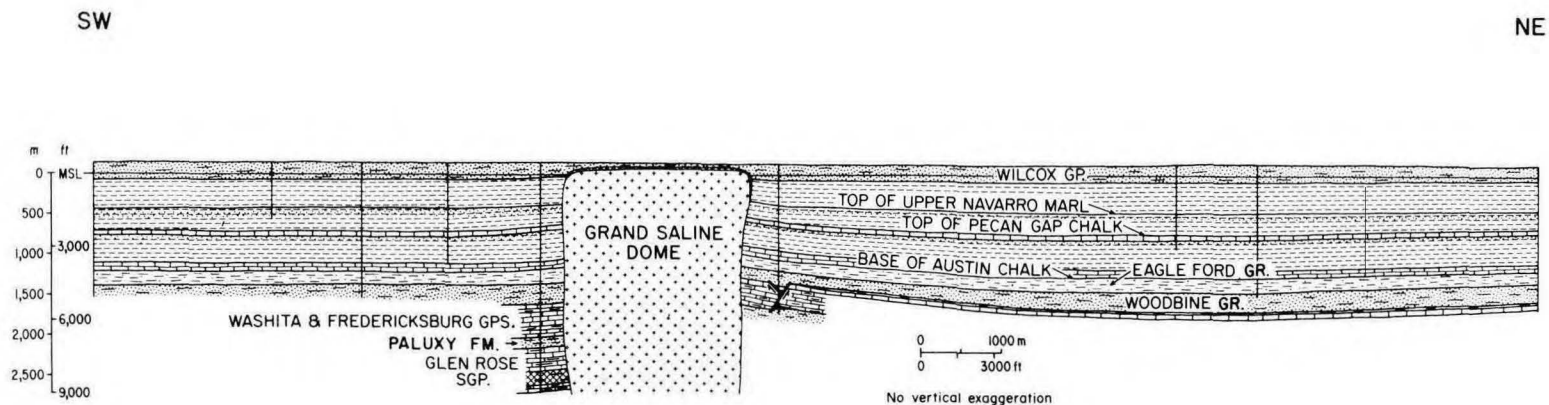
Methods used to assess rates of salt movement vary widely in their elegance and applicability. Some are based solely on structural uplift through time, an approach fraught with complications such as the possibility of collapse of marker beds because of salt dissolution. Cross sections from three domes (fig. 44) illustrate how dome growth rates based on the rate of uplift of flank strata are equivocal. The dip of strata flanking a salt structure is affected by geometry of the salt stock as well as by uplift of the salt crest and subsidence of the salt source layer. Quantifying rates of dome growth by dip changes is applicable only in areas where strata overlie the salt crest and where strata are not intruded or pierced by the salt stock. This method also requires wells very close to the diapir contact to record maximum dips, a severe restriction.

The difference between gross rate of growth and net rate of growth is of fundamental importance but has almost invariably been ignored in the literature. Gross rates are a function of the volume of salt evacuated from the withdrawal basin and mobilized up the diapir. Net rates are a function not only of this process but also of all other processes that affect diapir height and growth rate, such as salt dissolution, extrusion, and lateral intrusion. Thus, gross rates of growth approximate the true rate of salt flow regardless of the independent motion of the diapir crest. On the other hand, net rates of growth approximate the actual movement of the diapir crest.

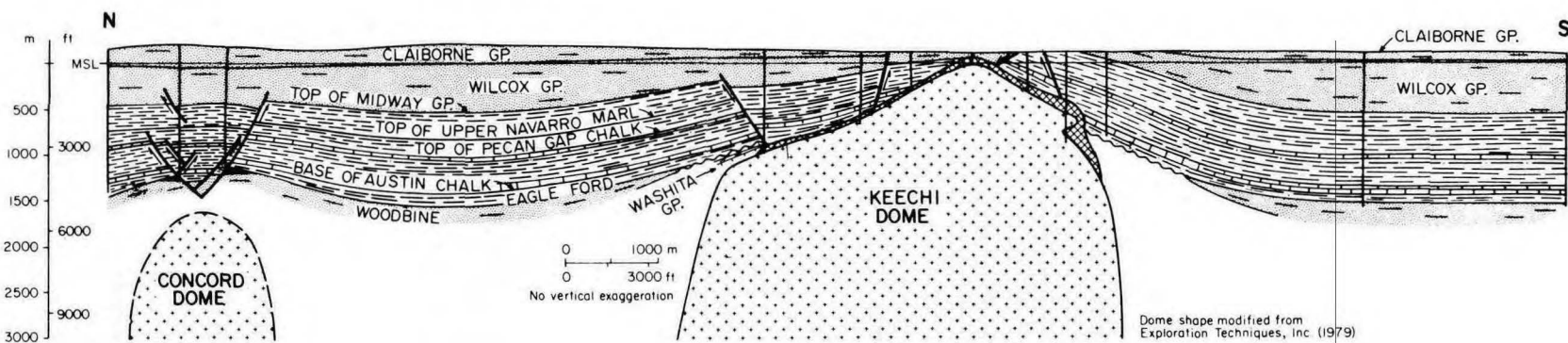
Stratigraphic data were used in four types of calculations; the first is self-explanatory, and the other three are explained in figure 45.

(1) The volume of sedimentary fill in a salt-withdrawal basin is equated with the volume of salt

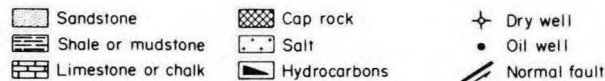




**B**



**C**



**FIGURE 44. Cross sections showing the relation between structural attitude of strata flanking diapirs and the geometry of (A) Hainesville, (B) Grand Saline, and (C) Keechi Domes. Unpierced strata arch over diapirs having gently dipping margins, like Keechi Dome. Structurally based methods of measuring dome growth, such as stratal uplift per time (reflected in increasing dip with depth) are useful where dome flank strata are not pierced by the dome. But the growth rates of Grand Saline and Hainesville Domes could not be measured accurately by a similar structural technique because flank strata have been pierced and are not uplifted around these domes. Dome uplift has been accommodated by faulting along the contacts of the salt stocks. (After Wood and Giles, 1982.)**

that migrated during filling of that basin (fig. 36). Dividing this volume by the duration of withdrawal-basin activity quantifies the rate of salt movement as volume through time.

(2) Net rates of salt-pillow uplift are calculated by equating the rate of salt-pillow uplift with the rate of stratigraphic thinning over the crest of salt pillows through time (fig. 45A; table 1). The upward growth of nonpiercement salt pillows resulted in thinning of strata over the pillows. Rate is obtained by dividing the amount of growth by duration.

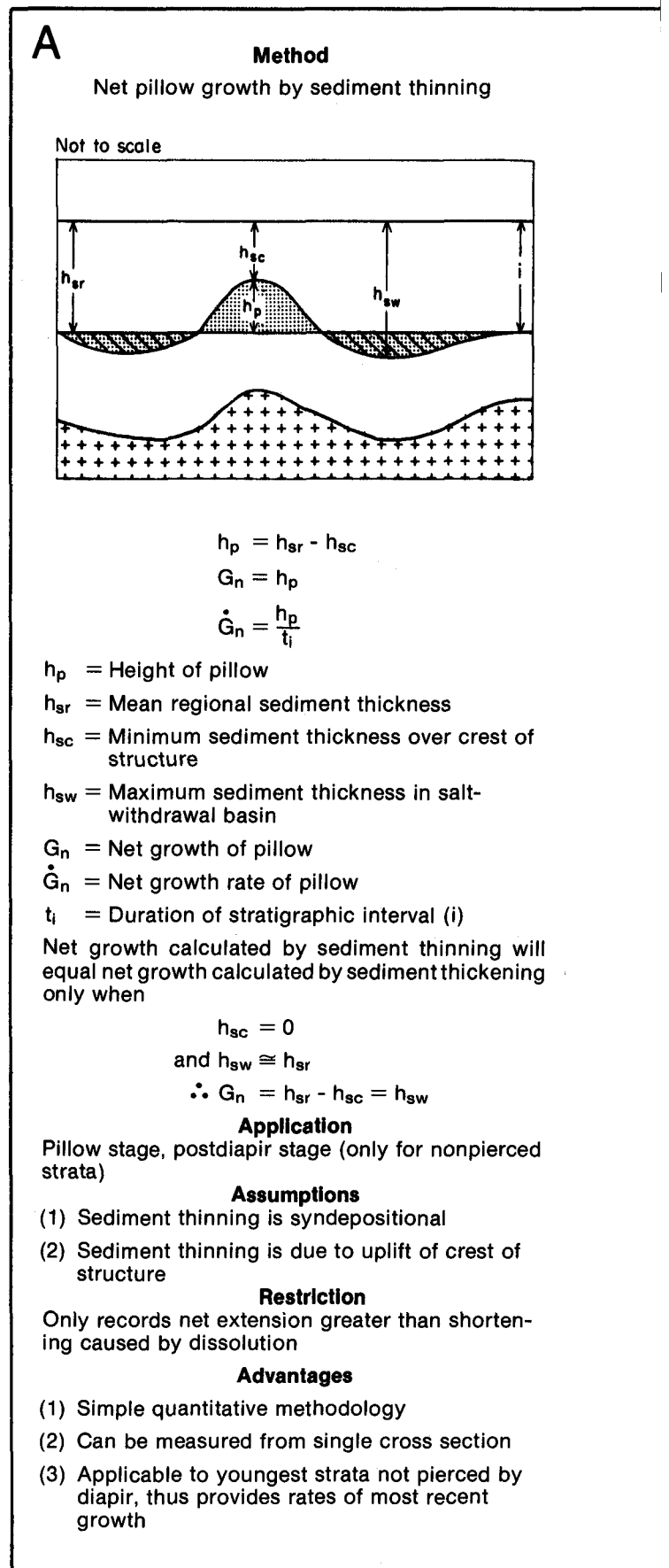
(3) Net rate of dome-crest uplift (or net rate of dome growth) is calculated by equating the rate of dome-crest uplift with the maximum rate of sediment accumulation in the associated withdrawal basin (fig. 45B; table 2). This technique assumes that salt remained at or near the depositional surface through most of the growth of the diapir, representing a balance between basin subsidence, ground-water dissolution, and extrusion on the one hand, and upward movement of the diapir crest on the other hand. Again, rate is obtained by dividing the amount of growth by duration.

(4) Gross rate of diapir elongation is calculated by dividing the volume of salt moved (estimated by method 1 above) by the maximum cross-sectional area of the diapir neck (fig. 45C; table 3). This technique assumes that all salt migrated from below the withdrawal basin into the diapir and rose through a constriction defined by the cross-sectional area of the stock, thereby lengthening the stock. Rate is obtained by dividing amount of growth by duration.

### Distinguishing Between Regional and Salt-Related Thickness Variations

Regional isopach maps (figs. 33, 34, and 35) and statistical analysis of thickness data were used to differentiate changes in interval thickness caused by basinwide subsidence from those caused by salt-related local subsidence. In the East Texas Basin, local, salt-related thickness changes are evident on regional isopach maps as isolated perturbations of regional trends. This contrasts sharply with the Tertiary section of the Upper Texas Gulf Coast, where regional isopach trends are strongly influenced across a large area by salt migration or growth faulting (Galloway and others, 1982; Bebout

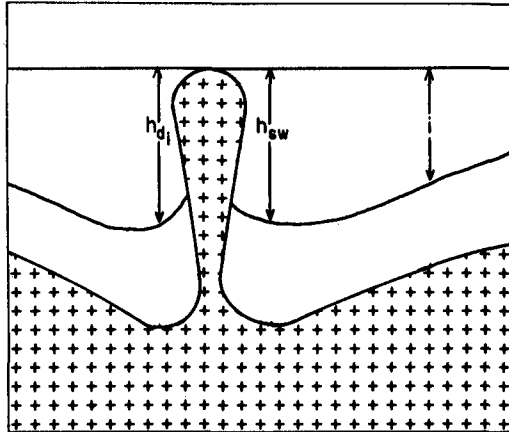
**FIGURE 45. Methods of calculating net and gross rates of dome growth, and applications, assumptions, restrictions, and advantages of each method. (A) Net pillow growth equated with sediment thinning. (B) Net diapir growth equated with sediment thickening. (C) Gross diapir growth calculated by dividing volume of salt moved by the maximum cross-sectional area of the diapir neck.**



**B****Method**

Net diapir growth by sediment thickening

Not to scale



$$G_n = h_{d_i} = h_{sw}$$

$$\dot{G}_n = \frac{h_{sw}}{t_i}$$

 $h_{d_i}$  = Height of diapir $h_{sw}$  = Maximum sediment thickness in salt-withdrawal basin $G_n$  = Net growth of diapir $\dot{G}_n$  = Net growth rate of diapir $t_i$  = Duration of stratigraphic interval (i)**Application**

Pillow stage, diapir stage, postdiapir stage

**Assumptions**

- (1) Diapir remains near sediment surface during deposition
- (2) Rate of deposition controls or is controlled by diapir growth

**Restriction**

Only records net extension greater than shortening caused by diapir extrusion or dissolution

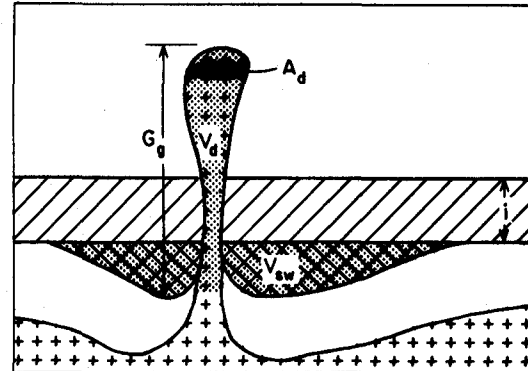
**Advantages**

- (1) Simple quantitative methodology
- (2) Can be measured from single cross section

**C****Method**

Gross diapir growth by volume and area

Not to scale



$$V_{sw} = V_d$$

$$G_g = \frac{V_{sw}}{A_d}$$

$$\dot{G}_g = \frac{V_{sw}/A_d}{t_i}$$

 $V_{sw}$  = Volume of sediments in salt-withdrawal basin $V_d$  = Volume of diapir $A_d$  = Maximum cross-sectional area of diapir $G_g$  = Gross growth of diapir $\dot{G}_g$  = Gross growth rate of diapir $t_i$  = Duration of stratigraphic interval (i)**Application**

Diapir stage only

**Assumptions**

- (1) Present cross-sectional area of diapir equals cross-sectional area of diapir during filling of withdrawal basin
- (2) Volume of withdrawal basin equals volume of salt mobilized during filling of withdrawal basin
- (3) All salt mobilized during filling of withdrawal basin migrated into diapir

**Restrictions**

- (1) Requires measuring volume of withdrawal basin and area of diapir, which requires close well spacing for map construction
- (2) Growth by tear-drop detachment of diapir base is not measurable

**Advantage**

Records total extension independent of possible dissolution or extrusion



and others, 1978). Isopach maps of strata in the East Texas Basin clearly show that local thickness anomalies around salt domes shifted with time (figs. 33, 34, and 35). For instance, Austin Group strata are thin (figs. 33 and 34) around Bethel and Hainesville Domes, whereas younger strata are massively thickened (fig. 35) around these domes. Whitehouse and Bullard Domes have had little effect on the thickness of adjacent post-112 Ma strata.

Statistical data on thickness of each isopach interval, obtained from wells, are shown in table 4. Each isopach interval was treated as a separate population and analyzed by the procedures described in the following paragraph.

The effect of salt tectonics on thickness and on rate of sediment accumulation is illustrated by histograms, cumulative-probability curves, and contour maps (figs. 46 through 48) showing rate of

TABLE 1. Net rate of pillow growth (m/Ma), East Texas Basin, equated with rate of sediment thinning over pillow crests and with rate of sediment accumulation in primary peripheral sinks.

	Pillows	Midway and Navarro Groups and Upper Taylor Formation	Navarro Group and Upper Taylor Formation	Lower Taylor Formation and Austin Group	Woodbine Group	Washita Group	Paluxy and Walnut Formations	Glen Rose Subgroup
Net growth equated with rate of sediment thinning over pillow crests	Hainesville	----	----	----	54	54	104	----
	Bethel	----	----	----	22	34	89	45
	Hawkins	----	----	13	22	30	80	31
	Van	----	----	26	28	31	36	22
Net growth equated with rate of sediment accumulation in primary peripheral sinks	Hainesville	----	----	----	58	73	129	101
	Bethel	----	----	----	38	49	113	95
	Hawkins	----	----	40	39	73	125	101
	Van	----	----	41	42	53	109	77

TABLE 2. Net rate of diapir growth (m/Ma), East Texas Basin, equated with rate of maximum sediment accumulation in salt-withdrawal basin.

Domes	Wilcox Group	Midway and Navarro Groups and Upper Taylor Formation	Navarro Group and Upper Taylor Formation	Lower Taylor Formation and Austin Group	Woodbine Group	Washita Group	Paluxy and Walnut Formations	Glen Rose Subgroup
Bethel	----	43	64	51	----	----	----	----
Hainesville	----	59	87	94	----	----	----	----
Mount Sylvan	----	32	31	41	50	81	104	102
Steen	----	34	37	44	51	45	149	105
East Tyler	----	32	33	33	40	87	219	105
Brooks	----	34	30	40	55	65	185	100
Boggy Creek	----	30	30	34	47	52	122	161
Brushy Creek	----	33	27	33	41	57	128	132
La Rue	----	27	26	43	48	65	131	156
Keechi	----	32	27	37	40	50	141	114
Palestine	----	33	28	34	43	61	139	100
Butler	----	35	34	42	35	50	148	95
Oakwood	----	36	34	43	32	58	85	87
Grand Saline	----	36	38	41	42	60	123	77
Whitehouse	----	36	27	30	45	68	100	87
Bullard	----	30	27	30	45	68	100	87
Mean		34	36	42	44	62	134	108
Standard deviation		7	16	15	6	12	35	25

sediment accumulation and standard deviation of that rate. These methods allow salt-induced thickness variations to be treated statistically. Figure 46 is a histogram of measured thicknesses and calculated rates of sediment accumulation for various isopach intervals. Increased thicknesses and rates of sediment accumulation on the right side of the histograms are especially evident for the Glen Rose Subgroup and Paluxy Formation. These skewed values are known to be salt induced because they represent areas adjacent to salt diapirs. Cumulative-probability curves (fig. 47) were constructed using the procedures of Folk (1980) for analysis of grain populations. These curves approach a straight-line (normal or Gaussian) distribution over the central 16th to 84th percentiles. The tails of the distribution above the 95th to 98th percentiles (stippled area, fig. 47) are associated with much greater rates of accumulation in withdrawal basins. Thickness and rates of sediment accumulation in diapir-stage withdrawal basins are typically three standard deviations (3  $\sigma$ ) more variable than are such values on a regional scale (fig. 48). Figure 48 illustrates thickness variability around Bethel and Hainesville Domes, which were the only active (diapir-stage) diapirs during Lower Taylor to Austin deposition. At this time, Oakwood, Grand Saline, and Mount Sylvan were in the postdiapir stage and sediments deposited around the domes during this stage show little thickness variation.

### Calculating Volumes of Salt Mobilized and of Salt Lost

Basinwide summation of the volumes of salt-withdrawal basins (table 5) shows a general decline in the rates of salt movement from the Early

Cretaceous to the Eocene (fig. 49). The volume of mobilized salt peaked during deposition of the Lower Cretaceous Glen Rose Subgroup, when 276 km<sup>3</sup> (67 mi<sup>3</sup>) of sediment accumulated in withdrawal basins. Salt apparently moved fastest (65 km<sup>3</sup>/Ma [15 mi<sup>3</sup>/Ma]) during deposition of the Paluxy and Walnut Formations approximately 105 Ma ago (fig. 49). However, this estimate appears to be somewhat high, and is probably the result of Paluxy deposition being so short-lived that small errors are magnified. Actual rates of salt movement were probably similar to rates during deposition of the Glen Rose Subgroup, about 40 km<sup>3</sup>/Ma ago (10 mi<sup>3</sup>/Ma).

A subsidiary peak of salt movement coincided with filling of the large salt-withdrawal basin (Mineola Basin) around Hainesville Dome in the Late Cretaceous. The proportion of the volume of salt mobilized to the total volume of sediments accumulated during the Eocene is  $2.0 \times 10^{-3}$ , one order of magnitude lower than the equivalent proportion over a similar interval of time in the Early Cretaceous ( $2.0 \times 10^{-2}$ ).

The volumes of withdrawal basins for individual diapirs in the East Texas Basin are given in figure 50. Hainesville and Bethel Domes have a complete growth history from pillow to postdiapir stages preserved in post-Glen Rose strata; thus, large primary peripheral sinks can be mapped. Only the latest stage of the growth history of older domes is preserved in post-Glen Rose strata. Because this stage is characterized by slow growth, the salt-withdrawal basins of older domes are small (less than 15 km<sup>3</sup>, or 4 mi<sup>3</sup>).

The volume of all salt-withdrawal basins is much greater than the total volume of salt in stocks projecting above the Glen Rose Subgroup (table 5). The volume of known and probable withdrawal

TABLE 3. Gross rate of diapir growth (m/Ma), East Texas Basin, calculated by dividing volume of salt moved by maximum cross-sectional area of diapir neck.

Domes	Wilcox Group	Midway and Navarro Groups and Upper Taylor Formation	Navarro Group and Upper Taylor Formation	Lower Taylor Formation and Austin Group	Woodbine Group	Washita Group	Paluxy and Walnut Formations	Glen Rose Subgroup
Bethel	60	20	180	150	----	----	----	----
Hainesville	----	120	210	460	----	----	----	----
Mount Sylvan	----	----	----	10	10	80	----	60
Steen	----	----	----	40	90	310	420	----
East Tyler	----	----	----	----	----	----	----	----
Brooks	----	----	----	----	40	30	530	80
Boggy Creek	----	----	----	----	----	----	----	----
Brushy Creek	----	----	----	----	----	----	----	----
La Rue	----	----	----	----	----	----	----	----
Keechi	----	----	----	----	----	----	----	----
Palestine	----	----	----	----	----	----	----	----
Butler	----	----	----	----	----	----	----	----
Oakwood	----	----	----	20	----	100	----	----
Grand Saline	----	----	----	----	----	----	----	----
Whitehouse	----	----	----	----	----	----	----	----
Bullard	----	----	----	----	----	----	----	----

TABLE 4. Statistical analysis of data on thickness (m) and rate of regional sediment accumulation (m/Ma) for major stratigraphic units in the East Texas Basin from 112 to 48 Ma.

Isopach interval		Wilcox Group	Midway and Navarro Groups and Upper Taylor Formation	Navarro Group and Upper Taylor Formation	Lower Taylor Formation and Austin Group	Woodbine Group	Washita Group	Paluxy and Walnut Formations	Glen Rose Subgroup
	Duration (Ma)	8	17	7	13	6	6	1	7
	No. of wells	413	1,001	1,370	1,815	950	997	839	544
	No. of grid elements having data	171	443	629	727	533	564	483	319
	No. of classes having data	25	17	15	23	12	13	11	23
Thickness	Mode ( $M_0$ )	503	465	259	411	198	290	99	655
	Median ( $M_{50}$ )	591	485	218	387	163	259	88	600
	Mean ( $M_2$ )	596	494	189	383	151	255	88	571
	Standard deviation ( $\sigma_0$ )	171	53	68	69	74	60	22	105
	Standard deviation ( $\sigma_1$ )	168	52	68	68	69	60	24	102
	Coefficient of variance ( $\frac{\sigma_1}{M_2}$ )	0.28	0.10	0.36	0.18	0.46	0.23	0.27	0.18
	Skewness ( $SK_0$ )	+0.36	+0.28	-0.32	-0.10	-0.24	-0.11	-0.03	-0.42
	Skewness ( $SK_1$ )	+0.94	+0.26	-0.32	-0.66	-0.23	-0.04	-0.03	-0.30
	Kurtosis ( $K_0$ )	0.95	0.96	0.99	1.01	0.80	0.94	1.17	0.83
Rate of sediment accumulation	Mode ( $M_0$ )	63	27	37	32	33	48	99	94
	Median ( $M_{50}$ )	74	28	28	30	27	43	88	86
	Mean ( $M_2$ )	74	29	27	30	25	42	88	81
	Standard deviation ( $\sigma_0$ )	21	3	10	5	12	10	22	15
	Standard deviation ( $\sigma_1$ )	21	3	10	5	12	10	24	48
	Coefficient of variance ( $\frac{\sigma_1}{M_2}$ )	0.28	0.10	0.36	0.18	0.46	0.23	0.27	0.18
	Skewness ( $SK_0$ )	+0.04	+0.43	-0.20	-0.16	-0.21	-0.11	-0.03	-0.44
	Skewness ( $SK_1$ )	+0.10	+0.36	-0.14	-0.11	-0.22	-0.05	-0.02	-0.30
	Kurtosis ( $K_0$ )	0.95	0.85	0.98	0.98	0.82	0.86	1.26	0.85

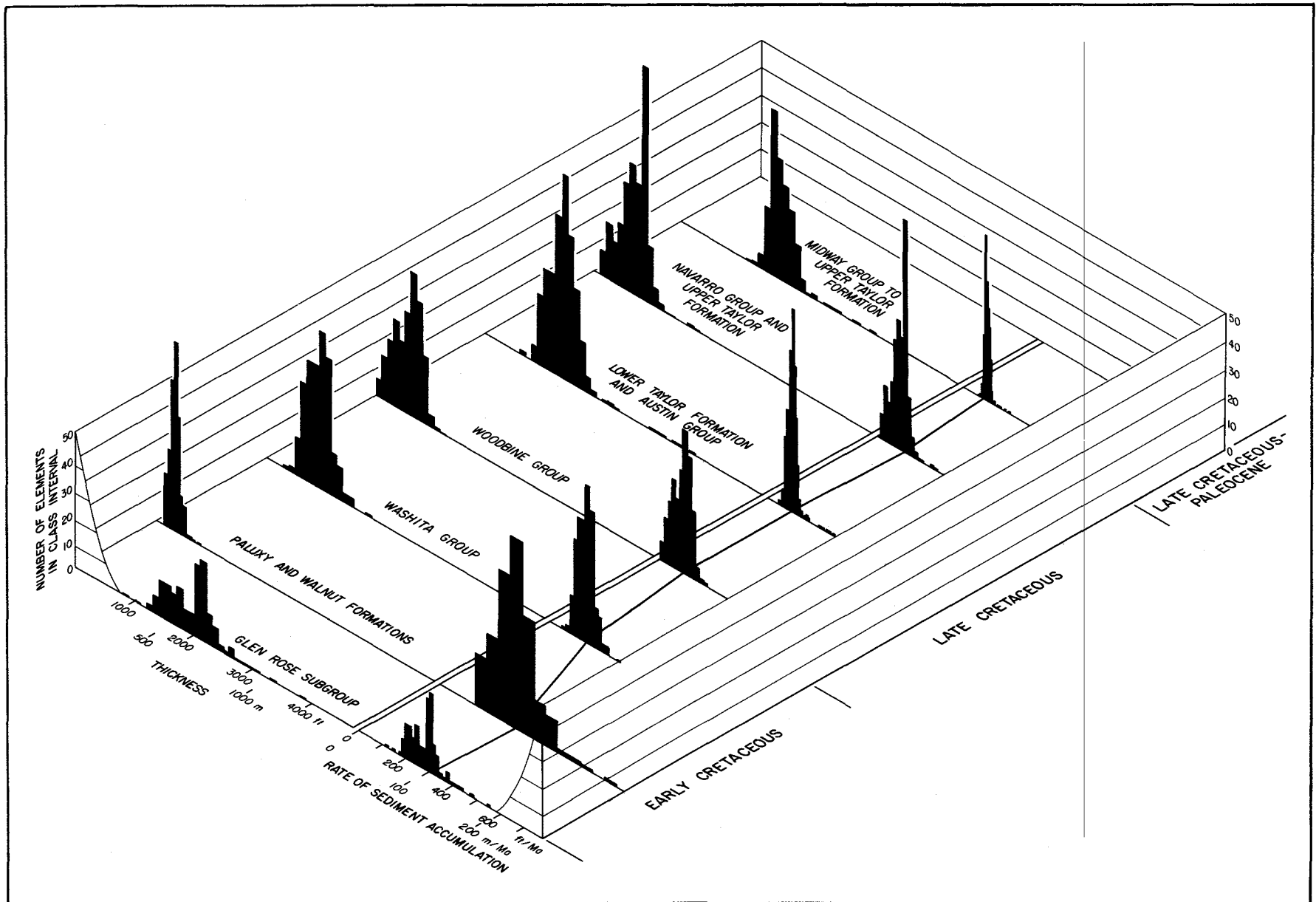
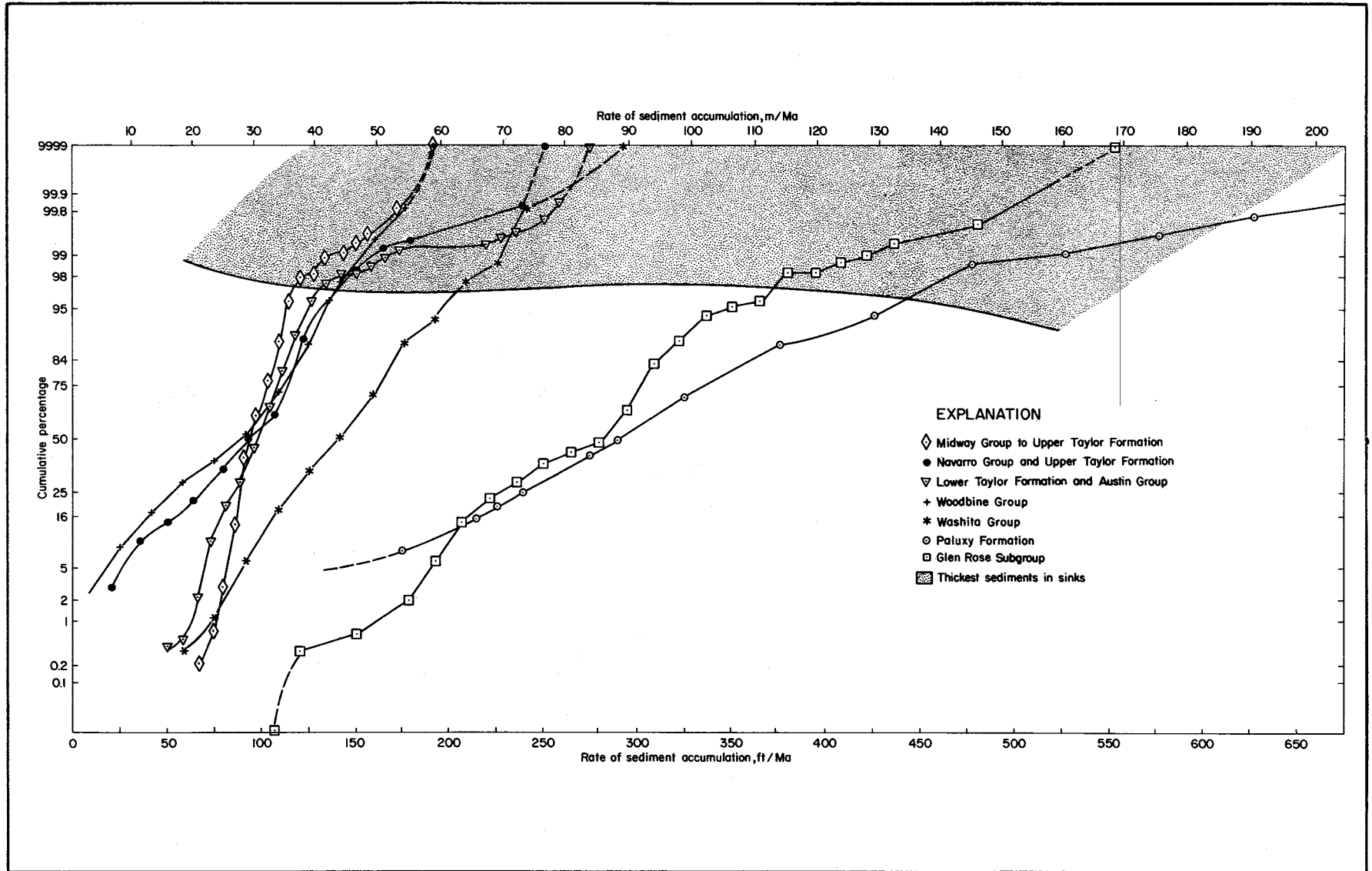


FIGURE 46. Histograms of thickness and rate of regional sediment accumulation of major stratigraphic units in the East Texas Basin from 112 to 56 Ma ago. Rate of sediment accumulation equals vertical thickness divided by duration of each unit. Crooked horizontal line connects modes of sediment accumulation rates and reveals a systematic decline in accumulation rates over time. Salt-influenced values of increased thickness and rate form tails on the right side of each histogram.



**FIGURE 47.** Cumulative-probability curves of sediment-accumulation rate in the East Texas Basin. Declining regional accumulation rates are evidenced by displacement of curves of younger units to the left. The increase in slope of the curves of younger strata compared with older strata reflects less variable sediment accumulation rates. Salt-induced skewness is clearly evident by decreasing slopes above the 95th or 98th percentile (stippled zone). These thickest parts of each unit accumulated in peripheral sinks. Salt-induced thinning over pillows is not apparent at the lower parts of curves in this diagram because of the small number of post-Glen Rose pillows compared with post-Glen Rose diapirs. Wilcox data are omitted because the Wilcox Group is restricted to the southernmost part of the basin.

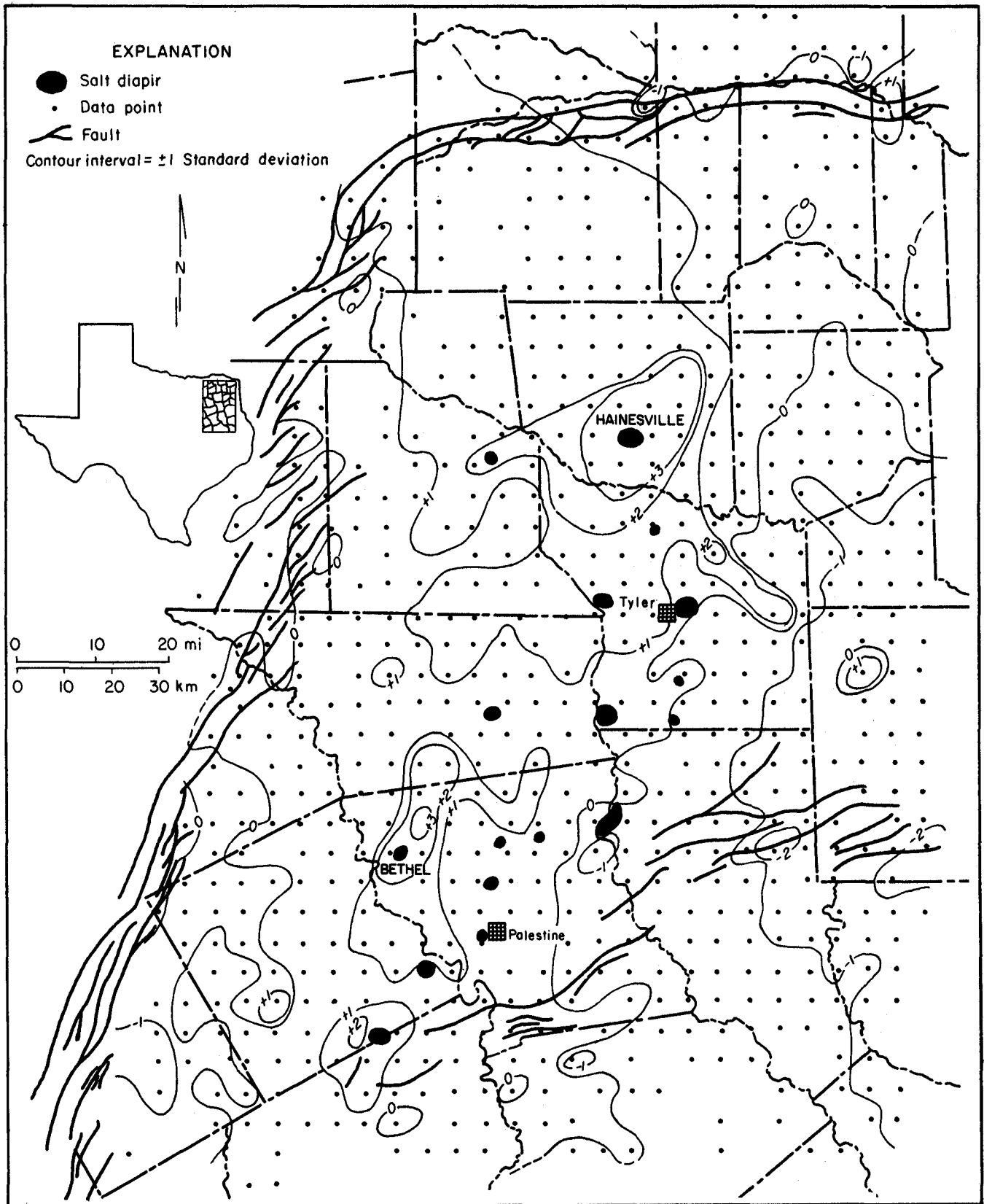


FIGURE 48. Contour map showing sample grid spacing and standard deviation of sediment-accumulation rate for the Lower Taylor Formation and Austin Group. Secondary peripheral sinks around Hainesville and Bethel Domes exhibit rates of sediment accumulation three standard deviations more variable than regional values, indicating the high degree of local variability induced by salt flow. Compare with the isopach map in figure 35.

**TABLE 5. Volume (km<sup>3</sup>) of salt-withdrawal basins in various stratigraphic intervals around individual diapirs in the East Texas Basin.**

Basin areas	Wilcox Group	Midway and Navarro Groups and Upper Taylor Formation	Navarro Group and Upper Taylor Formation	Lower Taylor Formation and Austin Group	Woodbine Group	Washita Group	Paluxy and Walnut Formations	Glen Rose Subgroup	All intervals	Volume of salt in diapirs above the Glen Rose Subgroup (km <sup>3</sup> )
Oakwood	----	----	----	3.4	----	9.3	----	----	12.7	18.2
Butler	----	----	----	1.2	----	----	3.9	----	5.1	17.8
Palestine	----	----	----	----	3.9	7.8	3.9	----	15.6	22.0
Keechi	----	----	----	----	----	7.8	3.9	4.6	16.2	55.4
Bethel	4.5	15.6	12.9	19.6	----	----	----	----	52.6	16.4 (e)
Boggy Creek	----	----	----	3.2	----	----	----	73.5	76.7	71.3
Brushy Creek	----	----	----	3.2	----	----	4.6	9.2	17.0	13.1 (e)
Whitehouse	----	----	----	----	----	----	----	----	----	10.2
Bullard	----	----	----	----	----	----	----	----	----	8.4
La Rue	----	----	----	12.1	----	22.0	6.3	111.8	152.2	12.3 (e)
Brooks	----	----	----	----	5.1	4.6	12.0	12.4	34.1	41.0 (e)
Mount Sylvan	----	----	----	2.1	1.1	8.0	----	6.4	17.6	28.0
East Tyler	----	----	----	----	----	10.6	20.1	----	30.7	28.4 (e)
Steen	----	----	----	4.1	4.5	15.6	3.6	----	27.8	20.5 (e)
Grand Saline	----	----	----	3.5	----	----	----	----	3.5	16.4 (e)
Hainesville	----	73.3	40.8	169.6	12.8	11.4	5.9	----	272.9	41.0 (e)
Other basins	7.0	----	----	----	----	7.8	2.3	4.6	14.8	----
Withdrawal-basin volume	11.5	88.9	53.7	222.0	27.4	104.9	66.5	222.5	749.4	420.4
Basins of unknown affinity	----	----	----	----	----	----	3.5	53.2	----	----
<b>Total</b>	<b>11.5</b>	<b>88.9</b>	<b>53.7</b>	<b>222.0</b>	<b>27.4</b>	<b>104.9</b>	<b>70.0</b>	<b>275.7</b>	<b>806.1</b>	<b>420.4</b>

(e) Estimated by extrapolation of residual-gravity data.

┌ Domes that share a single withdrawal basin.

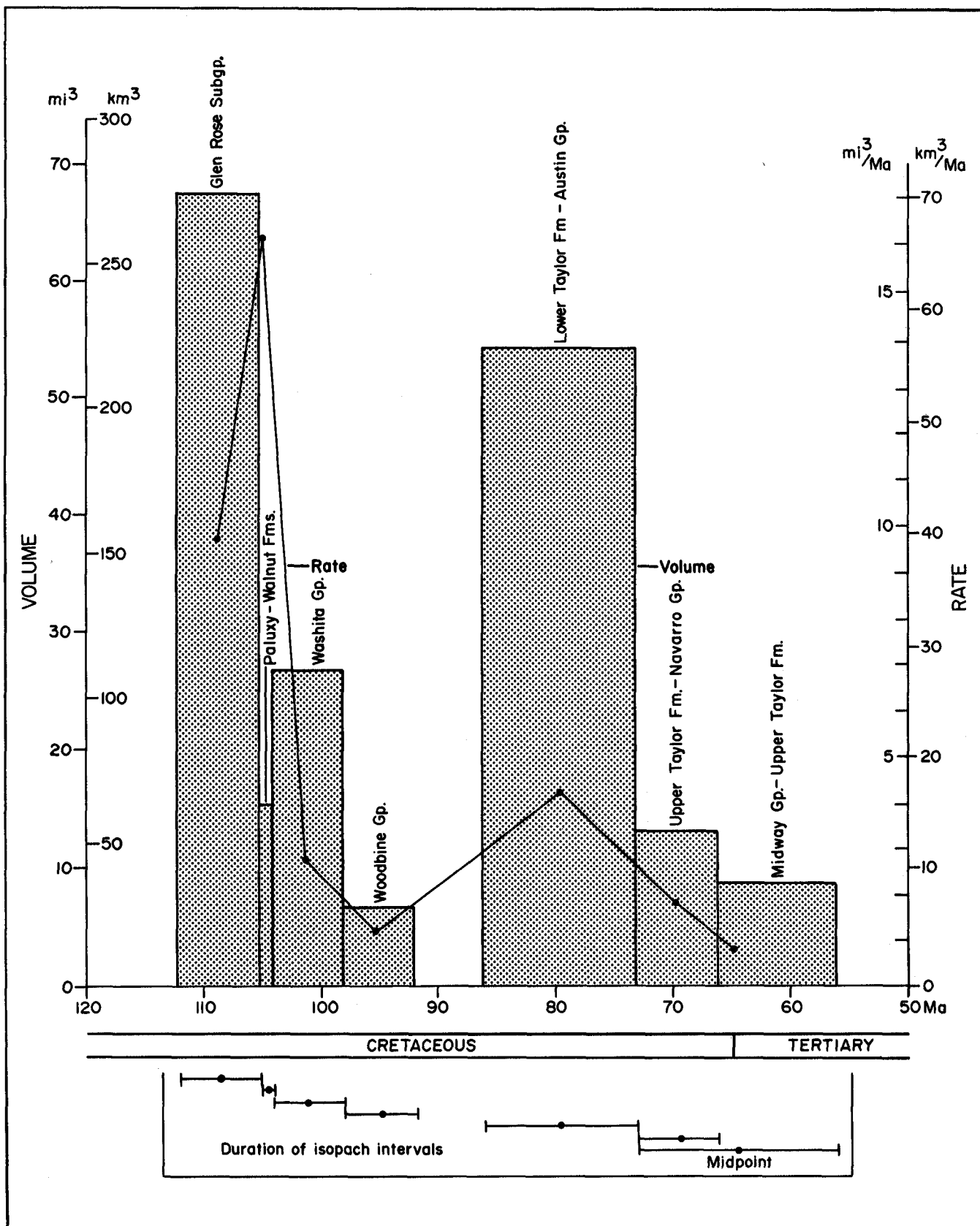
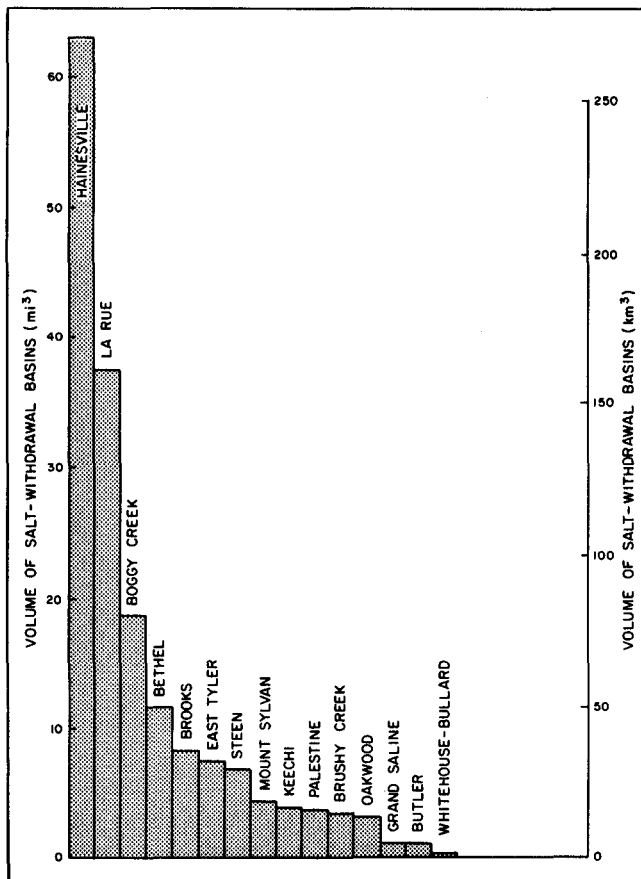


FIGURE 49. Histogram of the volumes of salt-withdrawal basins and the volumetric rates at which salt-withdrawal basins were filled in the East Texas Basin. The rate and volume of sedimentary fill in salt-withdrawal basins are equal to the rate and volume of salt flow, respectively.



basins indicates that approximately 800 km<sup>3</sup> (193 mi<sup>3</sup>) of salt migrated during deposition of Lower Cretaceous to Eocene strata. Subtracting from this quantity the volume of salt in stocks above the Glen Rose Subgroup indicates that approximately 380 km<sup>3</sup> (90 mi<sup>3</sup>) of salt has been lost by either ground-water dissolution, extrusion, or erosion. This loss of salt and the abundance of anhydrite and calcite cap rock over most East Texas salt domes support a residual origin for cap-rock formation by salt dissolution. Hainesville Dome is surrounded by the largest withdrawal basin (243 km<sup>3</sup>, or 58 mi<sup>3</sup>) in the East Texas Basin. Subtracting the volume of the Hainesville salt stock (40 to 78 km<sup>3</sup>, or 10 to 19 mi<sup>3</sup>) from the volume of the withdrawal basin indicates that 165 to 203 km<sup>3</sup> (40 to 49 mi<sup>3</sup>) of salt is missing from Hainesville Dome. Loocke (1978) estimated salt loss around Hainesville Dome by interpreting seismic data showing original and residual salt volumes. He deduced that 92 to 133 km<sup>3</sup> (22 to 32 mi<sup>3</sup>) of salt was missing, a comparable estimate. Extrusion and erosion of salt are the most likely explanations for the tremendous loss of salt around Hainesville Dome because the cap rock of that dome is much too thin to have formed from ground-water dissolution of vast volumes of salt.



## RATES OF DOME GROWTH

Methods of calculating rates of dome growth are based on different inferred mechanisms of dome growth. Different methods yield different estimates of growth rate for the same dome in the same time interval (tables 1, 2, and 3). The reliabilities of these methods depend on the validity of the inferred mechanism of dome growth and on the accuracy of the estimates of volume, area, thickness, and duration.

Calculating gross rates of dome growth requires reliable estimates of volumes and areas (fig. 45C). Calculating net rates of dome growth (fig. 45B) assumes that the diapir crest remains at or near the sediment surface. In the case of pillows, only net rates can be calculated.

### Net Rates of Pillow Growth

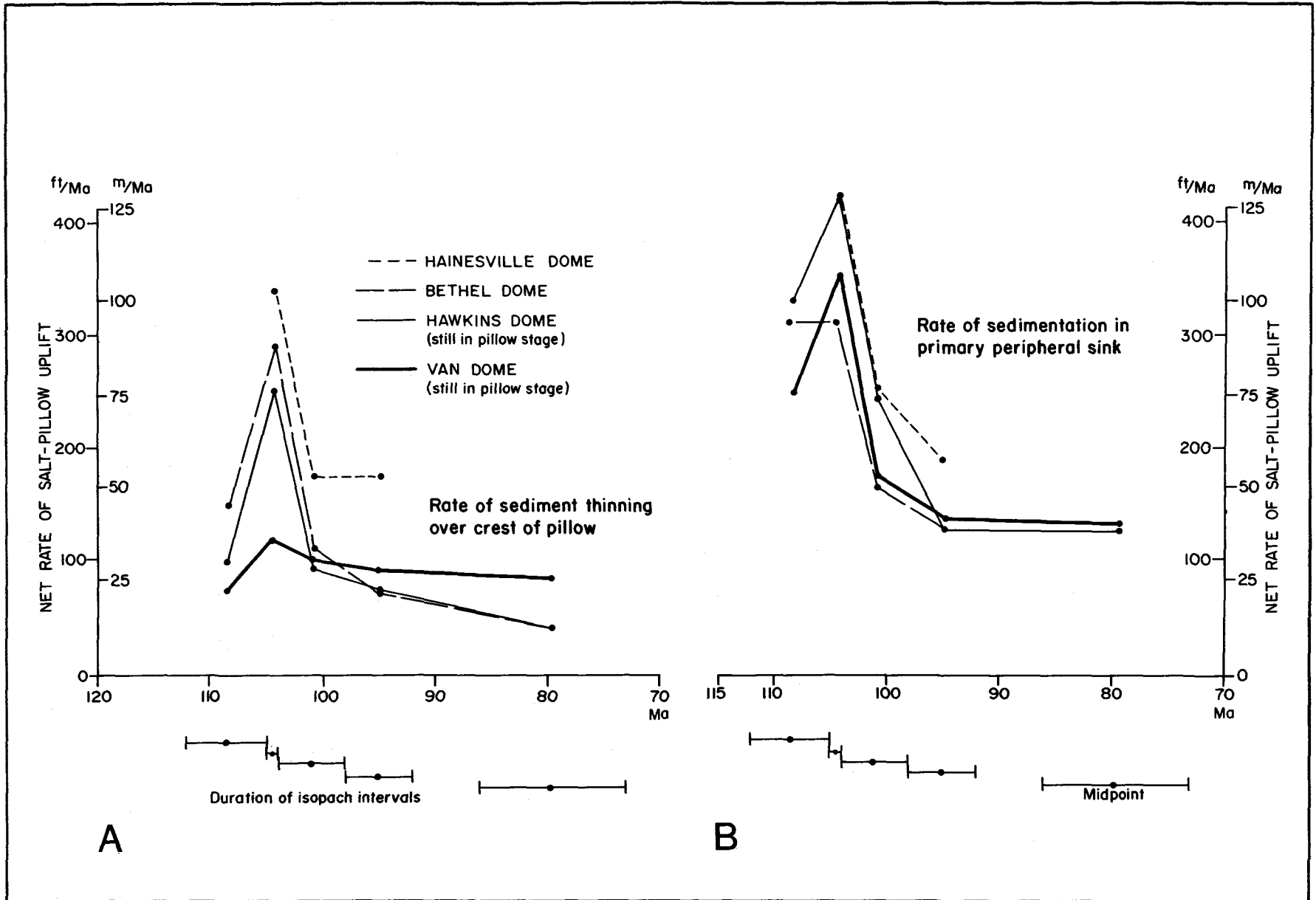
Net rates of pillow growth were calculated both by equating the rate of pillow-crest uplift with (1) the rate of sediment thinning over pillow crests and (2) the maximum rate of deposition in primary peripheral sinks (figs. 45A and 51; table 1). The rate of sediment thinning yields maximum net rates of 40 to 100 m/Ma (130 to 330 ft/Ma) for pillow uplift (fig. 51A). In comparison, the rate of sedimentation in primary peripheral sinks yields net rates of uplift ranging from 100 to 130 m/Ma (330 to 427 ft/Ma) (fig. 51B). The two methods of calculation yield the same growth rate only when sediments over the pillow crest are thinned to zero thickness and when the thickness of the primary peripheral sink is approximately equal to the regional thickness.

Generally, the growth rate of those salt pillows that later evolved into diapirs exceeded the growth rate of pillows still in a pillow stage. Perhaps a certain threshold value of geologic momentum (a function of velocity times mass) must be exceeded for a pillow to evolve into a diapir.

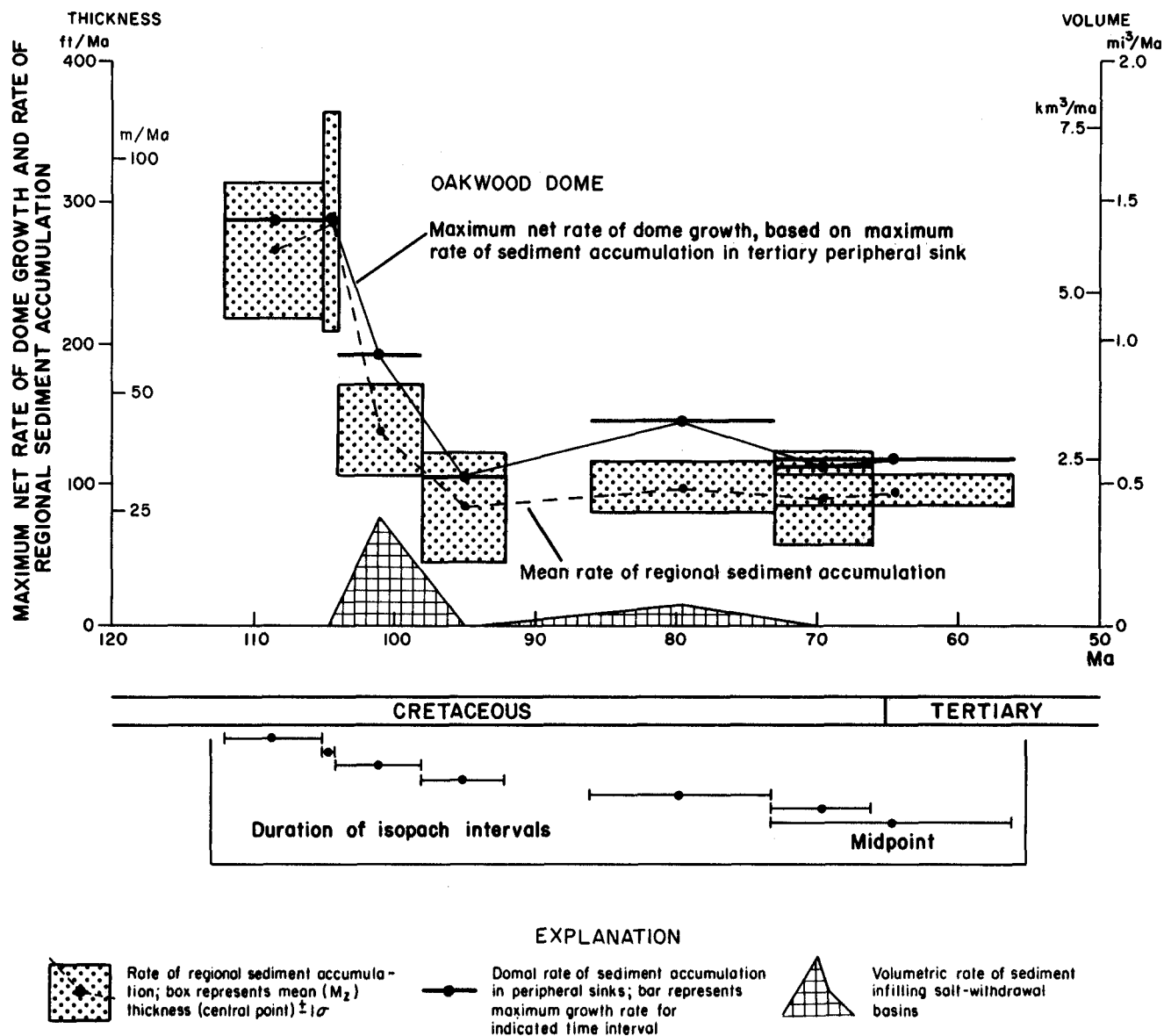
### Net Rates of Diapir Growth

Net rates of diapir growth are calculated by equating the rise of the diapir crest with the maximum rate of sediment accumulation in secondary and tertiary peripheral sinks (figs. 45B, 52A, and 52B; table 2). These rates are similar to those of salt movement and to regional sediment accumulation (fig. 53). Maximum

**FIGURE 50.** Histogram of the volumes of salt-withdrawal basins around individual diapirs of basins formed since 112 Ma ago (early Glen Rose time) in the East Texas Basin.



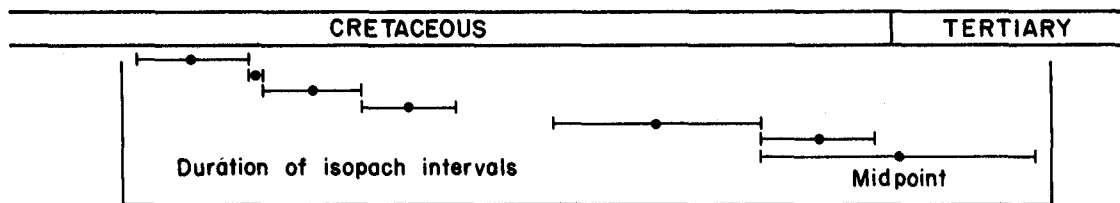
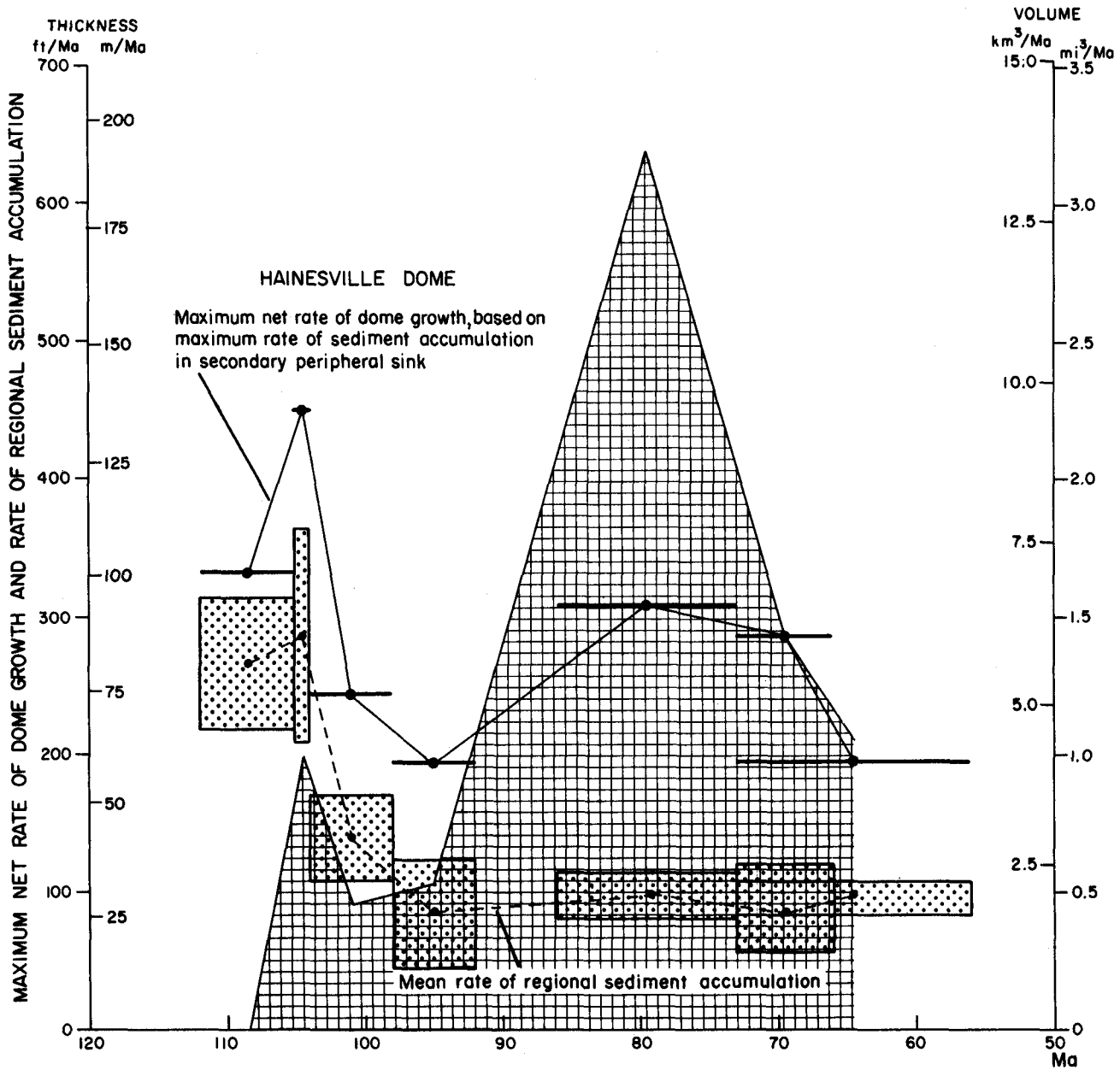
**FIGURE 51.** Net rates of salt-pillow growth, East Texas Basin, calculated by equating pillow-crest uplift with (A) the rates of sediment thinning over the crests of pillows (compare with fig. 54) and (B) the rates of sedimentation in primary peripheral sinks. Rates calculated by sediment thickening always exceed those calculated by sediment thinning (see fig. 45). Both graphs show that pillows grew fastest during the Early Cretaceous.



A

FIGURE 52. Maximum net rates of dome growth from 112 to 56 Ma ago for Oakwood and Hainesville Domes, calculated by equating the rise of the diapir crest with the rate of sediment accumulation in secondary (Hainesville Dome) and tertiary (Oakwood Dome) peripheral sinks. Mean regional rate ( $\pm 1\sigma$ ) of sediment accumulation (dashed line) is shown. Volumetric rate of sedimentary filling of salt-withdrawal basins (crosshatched area) is inferred to be equal to the volumetric rate of salt flow into the salt structure. Volumetric rate was calculated by dividing planimetered volumes of salt-withdrawal basins (fig. 36) by the duration of the isopach interval. (A) Oakwood Dome is a group 1 diapir that exhibits little difference between regional rates of sediment

accumulation and net rates of dome growth. This reflects the absence of thick secondary peripheral sinks in stratigraphic units younger than 112 Ma, which indicates the absence of large volumes of salt flow and rates of dome growth roughly equivalent to mean rates of regional sediment accumulation. Therefore, the period of greatest diapiric growth for Oakwood Dome predated 112 Ma ago (see figs. 31 and 32). (B) In contrast, the younger Hainesville Dome is a group 3 diapir that exhibits a large difference between mean rates of regional sediment accumulation and net rates of dome growth. Hainesville Dome is surrounded by the largest secondary peripheral sink in the East Texas Basin. The sink was filled from 86 to 56 Ma ago (see figs. 4 and 10).



**EXPLANATION**

- Rate of regional sediment accumulation; box represents mean ( $M_2$ ) thickness (central point)  $\pm 1\sigma$
- Domal rate of sediment accumulation in peripheral sinks; bar represents maximum growth rate for indicated time interval
- Volumetric rate of sediment infilling salt-withdrawal basins

**B**

net rates of dome growth ranged from 150 to 230 m/Ma (490 to 755 ft/Ma) during deposition of the Lower Cretaceous Glen Rose Subgroup and the Paluxy and Walnut Formations. Growth rates then generally declined into the Eocene. Mean net rates of growth were 30 m/Ma (100 ft/Ma) from 73 to 56 Ma. Except at Hainesville and Bethel Domes, maximum net rates of dome growth accompanied or coincided with high rates of regional sediment accumulation (figs. 52B and 53).

Subtracting mean rates of regional sediment accumulation from maximum rates of sediment accumulation in withdrawal basins yields residual rates of dome growth independent of the background effects of regional sedimentation. Figure 54 shows that most domes have an initially rapid growth rate in the Early Cretaceous even after subtracting the effects of rapid sediment accumulation during that time.

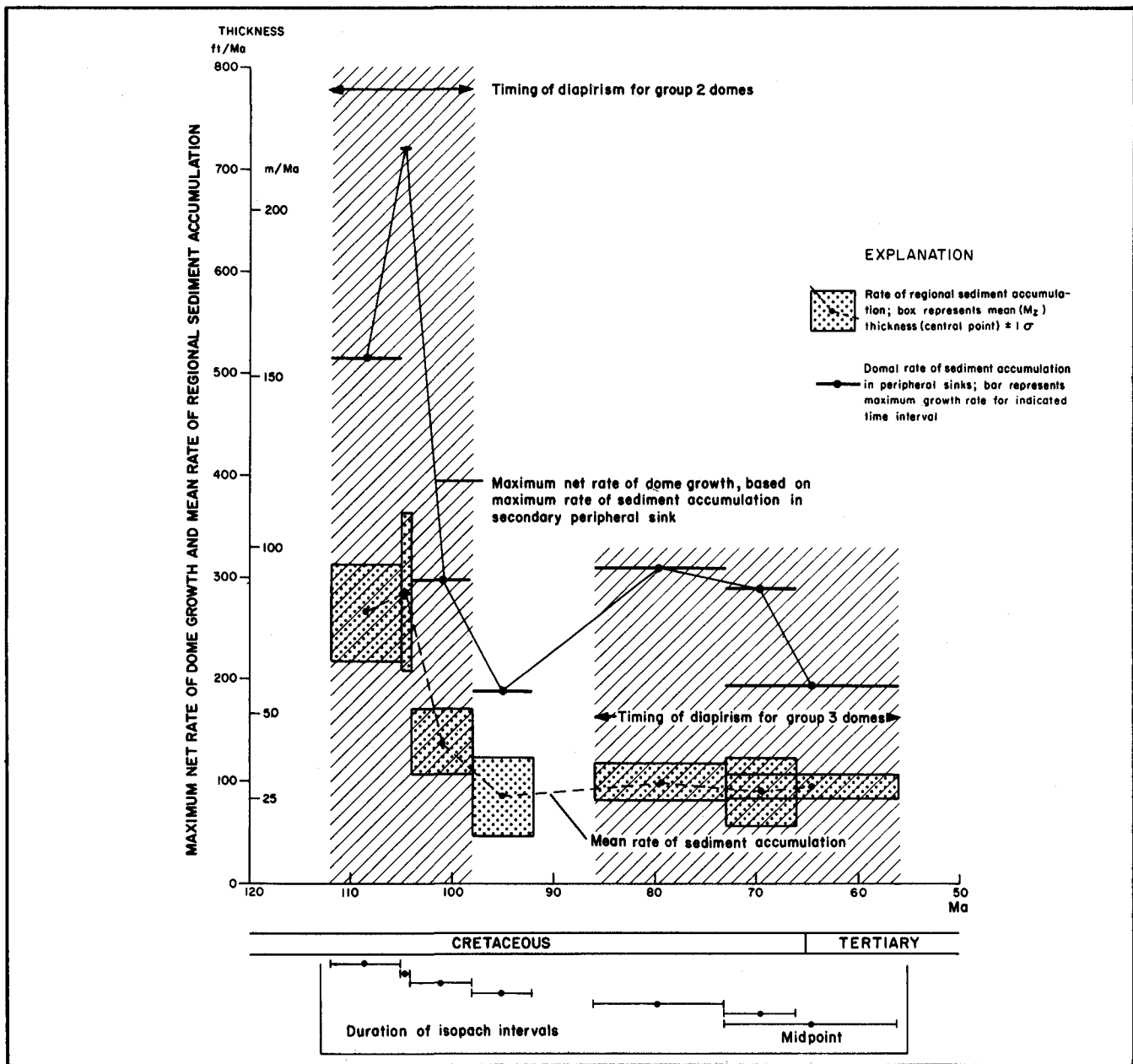


FIGURE 53. Maximum net rates of dome growth (solid line represents the growth rate of the most rapidly growing diapir during deposition of any given stratigraphic unit) and mean rate of regional sediment accumulation in the East Texas Basin from 112 to 56 Ma ago. Dome-growth rates of group 2 diapirs peaked in the Early Cretaceous during a time of high regional sediment accumulation. In contrast, subsequent growth of group 3 diapirs, associated with the growth of Hainesville and Bethel Domes in the Late Cretaceous, was accompanied by low rates of regional sediment accumulation.

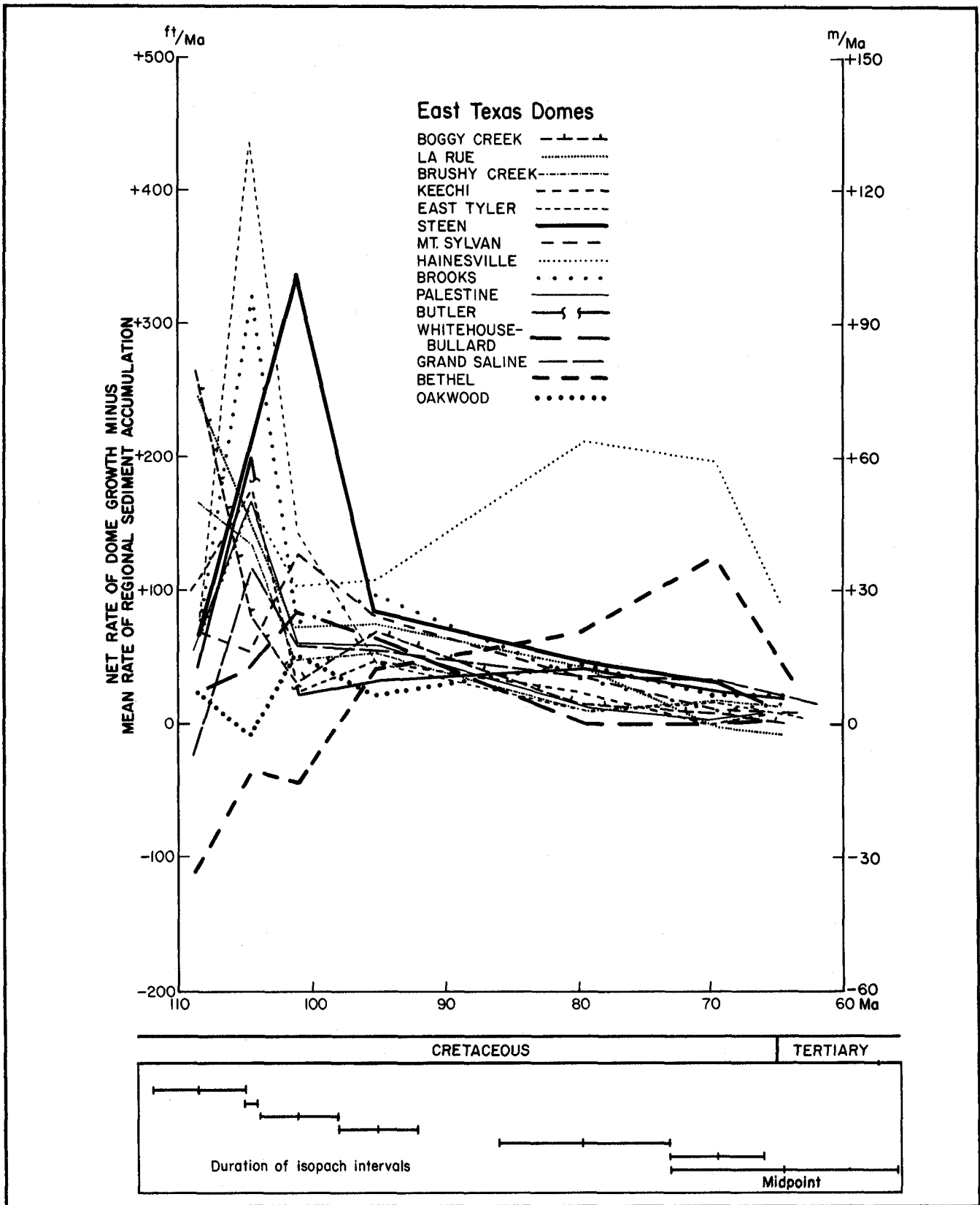


FIGURE 54. Residual rates of dome growth for 16 East Texas salt domes calculated by subtracting mean rate of regional sediment accumulation from net rate of dome growth. Residual rates of dome growth are independent of regional sediment-accumulation rates. Even with removal of high rates of regional sedimentation (compare fig. 53), most domes grew fastest during the Early Cretaceous.

## Gross Rates of Diapir Growth

Gross rates of diapir growth are calculated on the basis of the volume of salt passing through the maximum cross-sectional area of the diapir neck. The salt volume is equated with the volume of the secondary or tertiary peripheral sink, and the cross-sectional area of the diapir neck is calculated from gravity-derived models of present dome shape (Jackson and Seni, in press). Dome growth rates calculated by this method (figs. 45C and 55; table 3) are generally the highest for early growth, but show a rapid decrease with time. Brooks, Steen, and Hainesville Domes thus show peak rates of 530 m/Ma (1,740 ft/Ma), 420 m/Ma (1,380 ft/Ma), and 460 m/Ma (1,510 ft/Ma), respectively. Minimum

growth rates for these domes range from 10 to 20 m/Ma (33 to 66 ft/Ma); these estimates are probably too low because some salt-withdrawal basins escape detection, thereby effecting low estimates of salt volume mobilized. The growth rates given here are based on the maximum cross-sectional area of the stock, which yields minimum growth rates.

The hypothetical gross heights of six East Texas diapirs are shown in figure 56. Estimated gross heights of Brooks, Mount Sylvan, and Oakwood Domes are less than the thickness of the enclosing strata above the Glen Rose datum surface. This is either because some withdrawal basins are too thin to be detected or because the cross-sectional area of the stock was smaller during diapirism than at present. The short gross length of these domes also

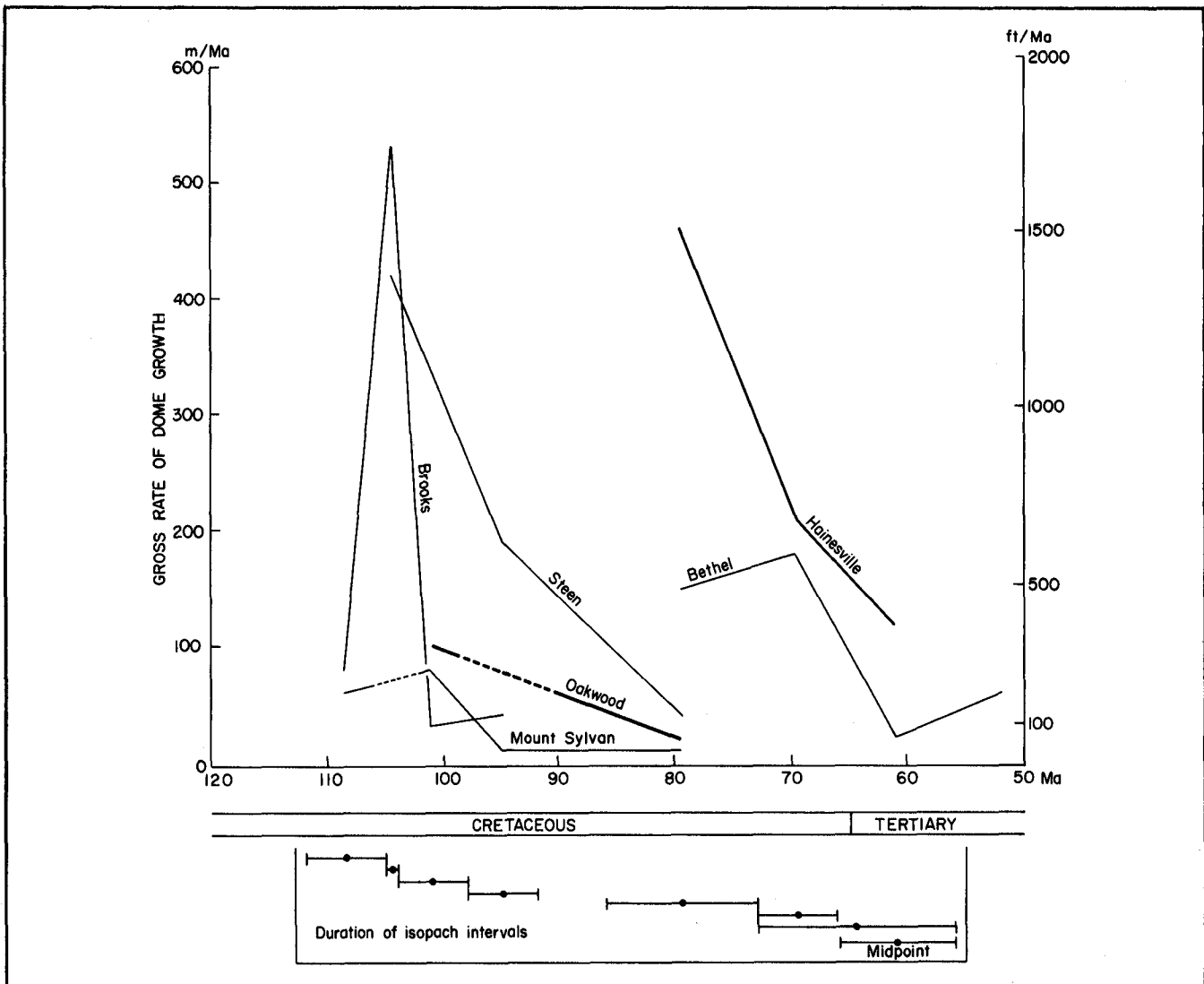


FIGURE 55. Gross rates of dome growth in the East Texas Basin calculated by dividing volume of salt moved by the maximum cross-sectional area of the diapir neck. Relatively rapid vertical growth rates greater than 300 m/Ma (1,000 ft/Ma) are estimated for several domes by this approach.

indicates little salt loss by dissolution or extrusion since Glen Rose time. In contrast, the gross heights of Hainesville, Bethel, and Steen Domes are 48 to 163 percent higher than the thickness of enclosing strata (equivalent to net column length), indicating abundant loss of salt during deposition of post-Glen Rose strata.

## GROWTH RATES AND STRAIN RATES

Given the current state of knowledge, rates of dome growth are at best semiquantitative. None of these methods can determine absolute movement of dome crests—that is, the movement of the crest relative to the topographic surface and the geoid. For instance, the dome crest can remain stationary relative to the geoid (no absolute movement) while undergoing relative upward movement with respect to strata subsiding around the dome. Geologic evidence of absolute rise of salt structures is known—for example, uplifting of abyssal-plain sediments by dome growth in the Gulf of Mexico, described by Ewing and Ewing (1962).

As discussed above, there are two main ways of estimating rates of diapir growth: those that estimate net rates and those that estimate gross rates. Which way is better depends on the intended purpose of the estimates. For instance, gross rates of growth are especially appropriate for feasibility studies of nuclear waste repositories in salt domes because they provide estimates of the rate of salt flow within diapirs. Diapiric salt around a repository could conceivably carry a repository upward (at the gross rate of growth), while the diapir crest remains stationary (zero net rate of growth) because of salt dissolution.

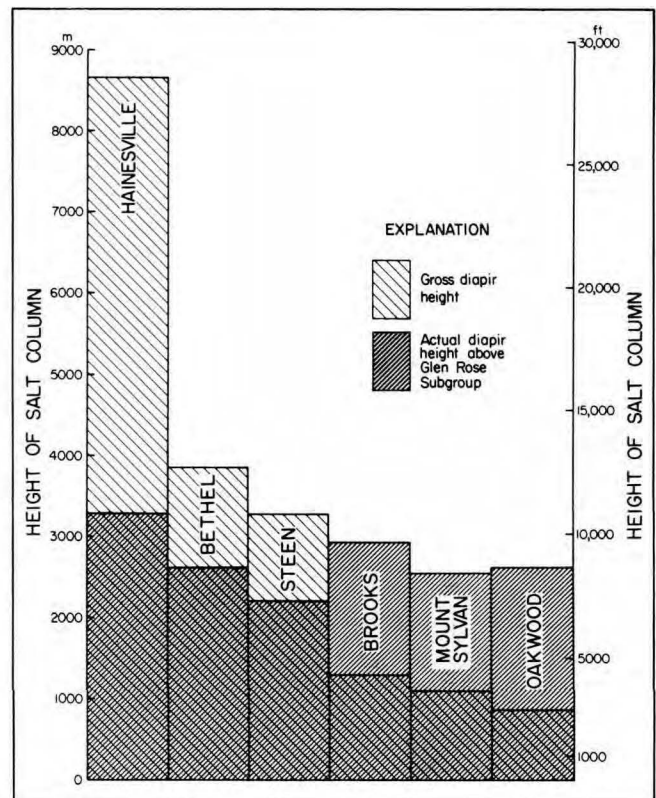
Published rates of dome growth (fig. 57; table 6) vary widely. A comparison of growth rates of salt domes in Gulf Interior Basins shows that maximum

**FIGURE 56. Hypothetical gross and actual heights of some post-Glen Rose diapirs in the East Texas Basin. Hypothetical gross heights were calculated by dividing the volume of the salt-withdrawal basin by the maximum cross-sectional area of the diapir neck. Actual diapir heights above the post-Glen Rose Subgroup are shown for comparison. Hypothetical gross heights exceed actual heights of Hainesville, Bethel, and Steen Domes because crests of these domes have been continually removed by dissolution or extrusion. In the case of Brooks, Mount Sylvan, and Oakwood Domes, the hypothetical gross diapir height is less than the actual height of the salt column above the top of the Glen Rose Subgroup. This is because growth rates during the postdiapir stage were too low to be measured given the contour interval used in this method.**

growth rates range from 12 to 540 m/Ma (40 to 1,770 ft/Ma). Despite this 45-fold spread and despite the variety of techniques used to measure growth rates, the trends are qualitatively similar. Dome growth rates were initially high in the Early Cretaceous or Jurassic (150 to 100 Ma) and generally decline into the Tertiary. The spread in growth rates for the most recent growth episodes is very low (less than twofold) because of an exponential decline in growth rate. Growth rates in the Tertiary are the lowest and range from less than 10 to 20 m/Ma (33 to 66 ft/Ma). The similarity of growth histories for domes in the East Texas and North Louisiana diapir provinces suggests that variations in dome growth were controlled largely by regional processes, including basin evolution, rather than by local processes.


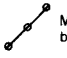

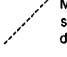
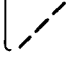
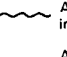
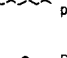

The growth rates calculated in this study provide an excellent means of estimating the strain rate of rock salt undergoing natural, nonorogenic, gravity-driven deformation. The relation between growth rate and strain rate is simple: Growth rate measures the absolute lengthening per unit time (m/Ma), whereas strain rate ( $\dot{\epsilon}$ ) measures the proportional change in length per unit time of 1 s (one second). Appendix 1 outlines methods of converting diapiric growth rate to strain rate.

Converting growth rates to strain rates takes into account the differences in heights of the diapirs;





EXPLANATION

- |            |   |   |   |  |   |
|------------|---|---|---|--|---|
| This study |  | Maximum gross rate of growth of East Texas salt diapirs, based on volume of peripheral sink divided by maximum cross-sectional area of diapir | Netherland, Sewell and Associates, 1976 |  | Maximum net rate of growth of East Texas salt diapirs, based on rate of structural uplift   |
|            |  | Maximum net rate of growth of East Texas salt diapirs, based on maximum rate of sediment accumulation in peripheral sink                      | Kumar, 1977                             |  | Maximum net rate of growth of North Louisiana salt diapirs, based on rate of structural uplift and differential thinning of sediments over diapir crest |
|            |  | Maximum net rate of growth of East Texas salt pillows, based on maximum differential thinning of sediments over pillow crests                 | Trusheim, 1960                          |  | Average rate of growth of North German salt diapirs in diapir stage (method of calculation unknown)   |
|            |   |   | Jaritz, 1980                            |  | Average rate of growth of North German diapirs in postdiapir stage (method of calculation unknown)  |
|            |   |   |   |  | Duration and mid point of analyzed unit   |

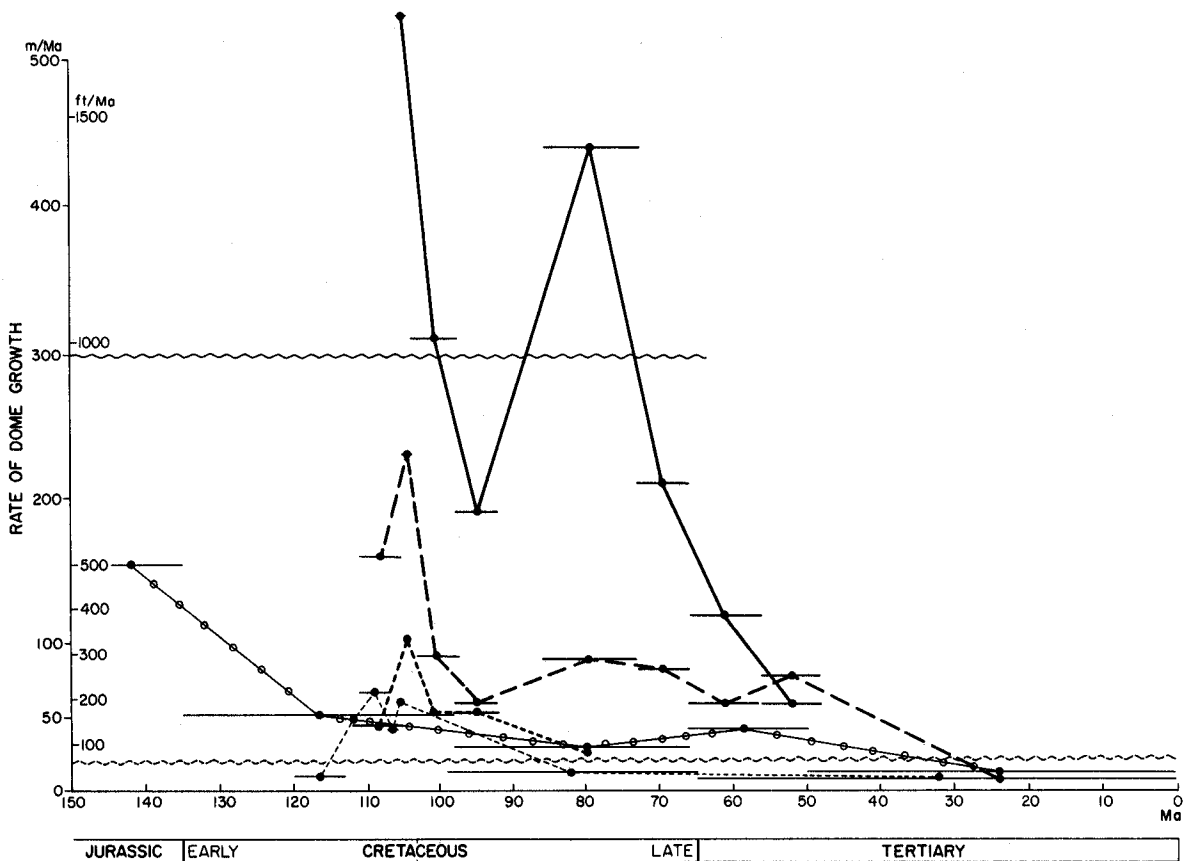


FIGURE 57. Comparison of published net and gross rates and methods of dome growth with those of the present study. The shapes of the growth-rate curves for East Texas diapirs (this study and Netherland, Sewell and Associates, 1976) are similar to those of North Louisiana diapirs (Kumar, 1977), and estimates by different methods yield values within the same order of magnitude. Estimated dome growth rates based on youngest strata decline exponentially and converge to a low value of about 20 m/Ma (66 ft/Ma). A similar terminal growth rate for domes in the North German Zechstein Salt Basin was estimated by Jaritz (1980).

TABLE 6. Comparison of rates of salt-dome growth and methods used to calculate growth rates in this and other studies.

Author	Growth rate ( $\dot{G}$ ) (m/Ma)	Location	Method	Comments
Ewing and Ewing, 1962	1,000	Sigsbee Knolls, Gulf of Mexico	Uplift of dated marker bed	Abyssal-plain seamounts project above flat floor. Pleistocene sediments have been uplifted 150 to 300 m.
Trusheim, 1960	300 (mean)	Zechstein Salt Basin, North Germany	Unknown	Average rates.
Sannemann, 1968	"	"	"	Consistent long-term rate, same for pillows and domes.
Jaritz, 1980	100 to 500 (diapir stage) ~20 (postdiapir stage)	"	"	Long-term growth rates declined from the diapir stage to the postdiapir stage.
Kupfer, 1976	5 to 10	Vacherie Dome, North Louisiana Salt Basin	Volume of salt withdrawn through time	General decrease in dome growth rate through time. Maximum growth in Early Cretaceous is 0.4 km <sup>3</sup> /Ma. Dome growth declined sharply to 0.04 km <sup>3</sup> /Ma in Late Cretaceous.
Kumar, 1977	1 to 42	Various domes, North Louisiana Salt Basin	Stratigraphic thinning and uplift/time	General decrease in dome growth through time. Maximum growth in Early Cretaceous is 42 m/Ma. Maximum growth in Late Cretaceous is 19 m/Ma. Minimum growth rate in Cenozoic is 1 m/Ma.
Netherland, Sewell and Associates, 1976	6 to 44 (range of mean low and mean high values)	Various domes, East Texas Basin	Uplift through time	General decrease in growth rates for individual domes through time. Maximum calculated rate of growth is 54 m/Ma for Mount Sylvan Dome in Early Cretaceous. Minimum calculated rate of growth is 3 m/Ma for Mount Sylvan and Bullard Domes in post-Eocene. Maximum estimated growth rate is 153 m/Ma in Late Jurassic.
This study	13 to 104  26 to 222  10 to 530	Various domes, East Texas Basin  Various domes, East Texas Basin  Various domes, East Texas Basin	Net rate of pillow growth equated with rate of sediment thinning  Net rate of dome growth equated with maximum rate of sedimentation in withdrawal basin  Gross rate of diapir growth calculated by dividing volume of salt moved by maximum cross-sectional area of diapir neck	

obviously a 1-m rise of a 10-m-high diapir is a far larger strain (elongation [e] equals 10 percent) than a 1-m rise of a 1,000-m-high diapir (e equals 0.1 percent), and this is reflected in a higher strain rate in the shorter diapir if both underwent deformation for the same period of time. Another useful attribute of the strain rate is that it enables comparison with all other types of deformation, ranging from meteoritic impacts ( $\dot{\epsilon}$  equals  $10^{+3}/s$ ) to compaction or isostatic rebound ( $\dot{\epsilon}$  equals  $10^{-16}/s$ ) (Price, 1975).

Estimation of the strain rates of natural deformation is still a new science and new techniques and methods of analysis continue to be vigorously pursued. The problem hinges on how to estimate the time during which a measured strain took place. This problem is lessened when dealing with very slow strain rates, because accurate dating is less crucial than in the case of rapid strain rates. All estimates of natural strain rates are made on the basis of several assumptions, so the slow strain rates characteristic of salt diapirs can be obtained to the nearest order of magnitude with a relatively high degree of confidence.

Parameters such as isostatic rebound, displacement rates along the San Andreas Fault, seafloor spreading, and inferred flow rate of the asthenosphere show remarkable agreement, indicating that a representative geologic strain rate is  $10^{-14}/s$  (Heard, 1963, 1976; Carter, 1976). By comparing known finite strains, calculated by strain analysis in orogenic zones, with estimated durations of young orogenies (duration of 5 Ma or less), Pfiffner and Ramsay (1982) bracketed conventional strain rates for orogeny between the limits of  $10^{-13}/s$  and  $10^{-15}/s$ . Diapiric strain rates based on the growth rates in figures 51, 53, and 55 and tables 1, 2, and 3 are shown in table 7. Overall rates are the rates during the entire known history of diapirism; the mean overall rate over the entire 53 Ma is  $6.7 \times 10^{-16}/s$ . The fastest rates are the rates during the stratigraphic period characterized by the most rapid diapirism; the mean "fast" strain rates are  $2.3 \times 10^{-15}/s$  and  $9.8 \times 10^{-16}/s$ , based on gross growth and net growth, respectively, averaged over about 5 Ma. These values accord closely with the lower limit for orogeny of  $10^{-15}/s$  calculated by Pfiffner and

TABLE 7. Overall and fastest bulk-strain rates ( $\dot{\epsilon}_i$  = elongation/s) in East Texas Basin salt diapirs for given durations ( $t_i$ ). These rates are based on net rates ( $\dot{G}_n$ ) and gross rates ( $\dot{G}_g$ ) of growth (given in tables 2 and 3). Domes are listed in order of fastest net growth.

	$t_i$ (Ma)	Overall $\dot{\epsilon}_i$ (based on $\dot{G}_n$ )	$t_i$ (Ma)	Fastest $\dot{\epsilon}_i$ (based on $\dot{G}_n$ )	$t_i$ (Ma)	Fastest $\dot{\epsilon}_i$ (based on $\dot{G}_g$ )
La Rue	56	$1.1 \times 10^{-16}$	7	$1.5 \times 10^{-15}$	----	----
East Tyler	56	$1.1 \times 10^{-15}$	1	$1.5 \times 10^{-15}$	----	----
Boggy Creek	56	$6.8 \times 10^{-16}$	7	$1.4 \times 10^{-15}$	----	----
Brooks	56	$7.4 \times 10^{-16}$	1	$1.3 \times 10^{-15}$	1	$3.7 \times 10^{-15}$
Steen	56	$8.3 \times 10^{-16}$	1	$1.1 \times 10^{-15}$	1	$3.2 \times 10^{-15}$
Brushy Creek	56	$5.9 \times 10^{-16}$	7	$1.1 \times 10^{-15}$	----	----
Butler	56	$5.9 \times 10^{-16}$	1	$1.0 \times 10^{-15}$	----	----
Keechi	56	$6.0 \times 10^{-16}$	1	$9.6 \times 10^{-16}$	----	----
Palestine	56	$5.7 \times 10^{-16}$	1	$9.4 \times 10^{-16}$	----	----
Grand Saline	56	$6.5 \times 10^{-16}$	1	$9.0 \times 10^{-16}$	----	----
Oakwood	56	$5.2 \times 10^{-16}$	7	$8.2 \times 10^{-16}$	----	----
Mount Sylvan	56	$9.7 \times 10^{-16}$	1	$7.9 \times 10^{-16}$	6	$6.2 \times 10^{-16}$
Whitehouse	56	$6.7 \times 10^{-16}$	1	$6.5 \times 10^{-16}$	----	----
Bullard	56	$6.0 \times 10^{-16}$	1	$6.5 \times 10^{-16}$	----	----
Hainesville	30	$6.5 \times 10^{-16}$	13	$6.2 \times 10^{-16}$	13	$3.0 \times 10^{-15}$
Bethel	30	$7.9 \times 10^{-16}$	7	$4.0 \times 10^{-16}$	7	$1.1 \times 10^{-15}$
Mean	53	$6.7 \times 10^{-16}$	4	$9.8 \times 10^{-16}$	6	$2.3 \times 10^{-15}$
Standard deviation	8.9	$2.1 \times 10^{-16}$	3.8	$3.3 \times 10^{-16}$	5.0	$1.4 \times 10^{-15}$

Ramsay (1982). Of course, our estimates refer to a cumulative elongation over millions of years (1 to 17 Ma), as do those of Pfiffner and Ramsay (1982) (1 to 50 Ma). The actual strain rate of the deforming rock salt is likely to be much higher, probably in the range of  $10^{-12}/s$  to  $10^{-14}/s$ , for two reasons, which also apply to other structural settings. First, deformation is likely to be spasmodic rather than steady state, although steady-state growth was assumed in our calculations. Second, deformation is likely to be concentrated in specific parts of the salt stock at any one time; the largest strains and strain rates are in ductile shear zones between more massive tongues of rising rock salt.

## IMPLICATIONS FOR WASTE ISOLATION

This report documents two main aspects of dome growth that affect the evaluation of the suitability of salt domes as repositories of nuclear waste (National Academy of Sciences - National Research Council, 1957, 1970; Kreitler, 1979; ONWM, 1981). First, the geologic history of domes is the basic framework from which past trends of dome growth rates can be deduced; this is one perspective from which the rates of future uplift of an intradomal repository might be evaluated. Second, the structure, porosity, and permeability of the enclosing sediments, which are strongly influenced by syn-depositional topography, both over the domes and in the withdrawal basins, have an important effect on ground-water flow and hydrologic sealing of the dome.

The long-term decline in growth rates of East Texas diapirs is favorable for waste isolation. This decline in growth rates is linked to a cessation of both sediment accumulation and subsidence in the East Texas Basin (Seni and Kreitler, 1981). Gulf Interior Basins in Texas, Louisiana, and Mississippi are currently sites of either sediment bypass or erosion. A change toward conditions of active sedimentation and subsidence, capable of remobilizing diapirs in the East Texas Basin in the next 250,000 yr, is most unlikely. The present tectonic regime is relatively stable and significant amounts of sediment have not accumulated in the basin for the past 50 Ma.

Dome growth rates calculated in this report encompass durations of 1 to 17 Ma. Because the duration of a potential repository is much shorter (10,000 to 250,000 yr), caution must be exercised in applying long-term rates (over periods of 1 to 17 Ma) to much shorter durations. Long-term rates disguise the short-term fluctuation of unsteady dome growth. Thus dome growth over much shorter times may be much greater and more spasmodic. Of the diapirs in

East Texas, Bethel Dome grew the fastest in Wilcox time, when the gross rate of diapir growth was 60 m/Ma. Continuation of these maximum rates would yield a gross rate of diapir growth, independent of dissolution or erosion, of 15 m in 250,000 yr; exponential decline of the more recent growth rates indicates that maximum rates in the future would probably be less.

Other geologic processes affecting diapir stability include properties of the rock salt itself; regional faulting, fracturing, and seismicity; subsurface dissolution by ground water; and rates of erosion and stream incision. Obviously, then, the present study represents only one of several lines of research that must be integrated to reliably predict future stability of salt domes (Jackson and Seni, 1983b).

Erosion of a nonpiercement salt pillow is another postulated mechanism of diapiric growth. In the East Texas Basin, the crests of the shallowest pillows are approximately 3,000 m (10,000 ft) below the surface. Given the present tectonic stability, erosion of approximately 3,000 m (10,000 ft) of overburden in the next 250,000 yr is highly unlikely.

What would happen if erosion breached a shallow diapir rather than a pillow? To what extent erosion and extrusion would motivate renewed dome growth is uncertain, but some rise of salt would be anticipated if the geostatic pressure gradient of the salt is less than that of its overburden (Bishop, 1978). Nevertheless, over the next 250,000 yr, the unroofing of sediments over diapirs in East Texas is improbable on the basis of present rates of denudation and river entrenchment (Collins, 1982).

Variability in depositional facies and textures around diapirs can be viewed as both favorable and unfavorable for isolation of nuclear waste. Diapirs that grew during deposition of the Eocene Wilcox Group are preferentially located in interchannel facies. These facies are characterized by thin, discontinuous sandstone bodies within a mud-rich section. The juxtaposition of diapirs against fine-grained facies is highly favorable because of the potential for retardation of ground-water velocities around the diapir by the fine-grained sheath (Fogg, 1981a; Fogg and others, 1983). However, during deposition of fine-grained facies over the dome, coeval sand-rich channel facies accumulated in rim synclines around the dome. These facies constitute interconnected aquifers around domes and are thus potential pathways of radionuclides leaking from a dome. The nature and distribution of this dome-specific facies variability is difficult to detect, model, and predict. The variability commonly exceeds spacing of available wells. Site characterization for a waste repository must therefore be based on dense well control.

## CONCLUSIONS

As in the Zechstein Salt Basin of North Germany (Trusheim, 1960), the durations of the pillow and diapir stages of salt-dome growth in the East Texas Basin are subequal and range from 10 to 30 Ma. The duration of postdiapir growth is commonly the longest, exceeding 112 Ma in some cases. About  $800 \text{ km}^3$  ( $190 \text{ mi}^3$ ) of salt migrated during Early Cretaceous to Eocene time in the East Texas Basin. Of this, approximately  $380 \text{ km}^3$  ( $90 \text{ mi}^3$ ) was subsequently lost by erosion and dissolution.

Group 1 diapirs, represented by Grand Saline, Butler, Oakwood, Palestine, Keechi, Bullard, and Whitehouse Domes, are the oldest. These domes ceased diapirism before deposition of the Lower Cretaceous Glen Rose Subgroup. They were initiated around the eastern, northwestern, and western periphery of the diapir province because these were the clastic depocenters of the Lower Cretaceous - Jurassic Hosston Formation and Cotton Valley Group.

Group 2 diapirs are La Rue, Boggy Creek, Brushy Creek, Brooks, East Tyler, Steen, and Mount Sylvan Domes. These domes underwent diapirism from 112 to 98 Ma ago, with the sites of maximum diapirism migrating northward along the basin axis. They grew in the area of maximum sediment accumulation during a period of rapid regional subsidence.

Group 3 diapirs are Hainesville and Bethel Domes. These domes underwent diapirism from 86 to 56 Ma ago, a period of low regional sediment accumulation. Local unconformities over Hainesville Dome and the absence of  $165$  to  $203 \text{ km}^3$  ( $40$  to  $49 \text{ mi}^3$ ) of salt from the Hainesville area indicate that erosion of strata above a salt pillow probably triggered diapirism by exposing the pillow. Salt extrusion and subsequent pillow collapse allowed sediments to accumulate rapidly in an enormous secondary peripheral sink surrounding the diapir.

In the East Texas Basin as a whole, peak rates of salt movement were  $39$  to  $65 \text{ km}^3/\text{Ma}$  ( $9$  to  $15 \text{ mi}^3/\text{Ma}$ ) during deposition of the Lower Cretaceous Glen Rose Subgroup and the Paluxy and Walnut Formations. A smaller surge occurred when salt moved at a rate of  $17 \text{ km}^3/\text{Ma}$  ( $4.2 \text{ mi}^3/\text{Ma}$ ) during deposition of the Upper Cretaceous Lower Taylor Formation and Austin Group. Rates of salt movement and dome growth declined exponentially into the Tertiary.

Calculated rates of dome growth vary according to techniques used, but long-term trends are similar. Dome growth rates are highest if calculated by dividing the volume of salt moved by the cross-sectional area of the diapir; this yields gross rates. Net rates of dome growth are equated with the maximum rates of sediment accumulation in peripheral

sinks and with the rates of sediment thinning over the crest of salt pillows. Net growth rates of pillows (which have been affected by dissolution or erosion) are lower if equated with the rate of thinning. Maximum gross rates of dome growth ( $420$  to  $530 \text{ m/Ma}$ , or  $1,380$  to  $1,740 \text{ ft/Ma}$  ago) coincided with maximum regional rates of deposition in the Early Cretaceous from  $112$  to  $104 \text{ Ma}$  ago. Rapid gross rates of dome growth ( $180$  to  $460 \text{ m/Ma}$ , or  $590$  to  $1,510 \text{ ft/Ma}$ ) recurred along the northern and western margins of the East Texas diapir province in the Late Cretaceous from  $86$  to  $56 \text{ Ma}$  ago, resulting in growth of Hainesville and Bethel Domes.

Strain rates during growth of the East Texas salt diapirs, treated as steadily rising homogeneous bodies, averaged  $6.7 \times 10^{-16}/\text{s}$  throughout the diapiric history recorded in strata; strain rates peaked at a mean value of  $2.3 \times 10^{-15}/\text{s}$ . These values are equivalent to the slower orogenic rates estimated in the literature. However, strain rates within the diapirs are likely to have been much higher in rock salt undergoing spasmodic and inhomogeneous strain.

## ACKNOWLEDGMENTS

This research was supported by the U.S. Department of Energy, under Contract Number DE-AC97-80ET46617.

Concepts developed by F. Trusheim provided an indispensable framework for analyzing dome growth by means of thickness variations in surrounding strata. Study of the sedimentary filling of the East Texas Basin was initiated at the Bureau of Economic Geology in 1978. Our report has evolved from preliminary Bureau studies undertaken by E. Guevara, O. Agagu, A. B. Giles, and C. W. Kreitler; we gratefully acknowledge their work and their discussions with us.

We thank L. F. Brown, Jr., W. E. Galloway, N. Tyler, T. E. Ewing, R. T. Budnik, and Malcolm P. R. Light for critically reviewing the manuscript. We also thank E. Bramson, R. J. Burks, R. D. Conti, S. A. Ghazi, S. E. Lovell, B. C. Richter, J. L. Smith, and D. H. Wood for their help in data collection and processing. Michelle C. Gilson edited this publication. Ginger Zeikus and Karen Bonnecarrere typed original manuscripts. Word processing was by Dorothy C. Johnson and Phyllis Hopkins, and typesetting was by Fannie M. Sellingsloh, under the direction of Lucille C. Harrell. John T. Ames, Mark T. Bentley, Margaret L. Evans, Richard P. Flores, Jeffrey Horowitz, and Jamie McClelland drafted figures under the supervision of Dan F. Scranton. Text illustration camerawork was by James A. Morgan. Publication design and assembly were by Margaret L. Evans.

## REFERENCES

- Atwater, G. I., and Forman, M. J., 1959, Nature of growth of southern Louisiana salt domes and its effect on petroleum accumulation: *American Association of Petroleum Geologists Bulletin*, v. 43, no. 11, p. 2592–2622.
- Baldwin, B., Coney, P. J., and Dickinson, W. R., 1974, Dilemma of a Cretaceous time scale and rates of sea floor spreading: *Geology*, v. 2, p. 267–270.
- Barton, D. C., 1933, Mechanics of formation of salt domes with special reference to Gulf Coast salt domes of Texas and Louisiana: *American Association of Petroleum Geologists Bulletin*, v. 17, no. 9, p. 1025–1083.
- Bebout, D. G., Loucks, R. G., and Gregory, A. R., 1978, Frio sandstone reservoirs in the deep subsurface along the Texas Gulf Coast: The University of Texas at Austin, Bureau of Economic Geology Report of Investigations No. 91, 92 p.
- Bishop, R. S., 1978, Mechanism for emplacement of piercement diapirs: *American Association of Petroleum Geologists Bulletin*, v. 62, no. 9, p. 1561–1583.
- Bishop, W. F., 1968, Petrology of Upper Smackover limestone in North Haynesville field, Claiborne Parish, Louisiana: *American Association of Petroleum Geologists Bulletin*, v. 52, no. 1, p. 92–128.
- Boillet, G., 1981, *Geology of the continental margins, translated by A. Scarth*: New York, Longman Inc., 115 p.
- Bornhauser, M., 1958, Gulf Coast tectonics: *American Association of Petroleum Geologists Bulletin*, v. 42, no. 2, p. 339–370.
- \_\_\_\_\_, 1969, *Geology of Day Dome (Madison County, Texas)—a study of salt emplacement*: *American Association of Petroleum Geologists Bulletin*, v. 53, no. 7, p. 1411–1420.
- Bright, T. J., 1977, Coral reefs, nepheloid layers, gas seeps, and brine flows on hard banks in the northwestern Gulf of Mexico, *in Proceedings, Third International Coral Reef Symposium, Miami, Florida*: v. 1, no. 3, p. 39–46.
- Bushaw, D. J., 1968, Environmental synthesis of the East Texas Lower Cretaceous: *Gulf Coast Association of Geological Societies Transactions*, v. 18, p. 416–438.
- Cantrell, R. B., Montgomery, J. C., and Woodward, A. E., 1959, *Heterostegina* reef on Nash and other piercement salt domes in northwestern Brazoria County, Texas: *Gulf Coast Association of Geological Societies Transactions*, v. 9, p. 59–62.
- Carter, N. L., 1976, Steady state flow of rocks: *Reviews of Geophysics and Space Physics*, v. 14, no. 3, p. 301–360.
- Caughy, C. A., 1977, Depositional systems in the Paluxy Formation (Lower Cretaceous), northeast Texas—oil, gas, and groundwater resources: The University of Texas at Austin, Bureau of Economic Geology Geological Circular 77-8, 59 p.
- Collins, E. W., 1982, Surficial evidence of tectonic activity and erosion rates, Palestine, Keechi, and Oakwood salt domes, East Texas: The University of Texas at Austin, Bureau of Economic Geology Geological Circular 82-3, 39 p.
- Crowe, C. T., 1975, The Vacherie salt dome, Louisiana, and its development from a fossil salt high: Louisiana State University, Master's thesis, 172 p.
- DeGolyer, E. L., 1925, Origin of North American salt domes: *American Association of Petroleum Geologists Bulletin*, v. 9, no. 5, p. 831–874.
- Dennis, J. G., Murawski, H., and Weber, K., 1979, *International tectonic lexicon*: Stuttgart, Germany, E. Schweizerbartsche Verlagsbuchhandlung, International Union of Geological Sciences, International Geological Correlation Program, 153 p.
- Dix, O. R., and Jackson, M. P. A., 1981, Statistical analysis of lineaments and their relation to fracturing, faulting, and halokinesis in the East Texas Basin: The University of Texas at Austin, Bureau of Economic Geology Report of Investigations No. 110, 30 p.
- Dixon, J. M., 1975, Finite strain and progressive deformation in models of diapiric structures: *Tectonophysics*, v. 28, p. 89–124.
- Eaton, R. W., 1956, Resume on subsurface geology of northeast Texas with emphasis on salt structures: *Gulf Coast Association of Geological Societies Transactions*, v. 5, p. 79–84.
- Elliot, T. L., 1979, Deposition and diagenesis of carbonate slope deposits, Lower Cretaceous, northeastern Mexico: The University of Texas at Austin, Ph.D. dissertation, 330 p.
- Ewing, M., and Ewing, J., 1962, Rates of salt-dome growth: *American Association of Petroleum Geologists Bulletin*, v. 46, no. 5, p. 708.
- Exploration Techniques, Inc., 1979, Report on gravity modeling for Keechi and Oakwood Domes: Report prepared for Law Engineering Testing Co., Houston, Texas, unpaginated.
- Fisher, W. L., Brown, L. F., Jr., McGowen, J. H., and Groat, C. G., 1973, Environmental geologic atlas of the Texas Coastal Zone—Beaumont - Port Arthur area: The University of Texas at Austin, Bureau of Economic Geology, 93 p.
- Fisher, W. L., and McGowen, J. H., 1967, Depositional systems in the Wilcox Group of Texas and their relationship to occurrence of oil and gas: *Gulf Coast Association of Geological Societies Transactions*, v. 17, p. 105–125.
- Fisher, W. L., McGowen, J. H., Brown, L. F., Jr., and Groat, C. G., 1972, Environmental geologic atlas of the Texas Coastal Zone—Galveston-Houston area: The University of Texas at Austin, Bureau of Economic Geology, 91 p.
- Fogg, G. E., 1981a, Aquifer modeling of the Oakwood Dome area, *in Kreitler, C. W., and others, Geology and geohydrology of the East Texas Basin: a report on the progress of nuclear waste isolation feasibility studies (1980)*: The University of Texas at Austin, Bureau of Economic Geology Geological Circular 81-7, p. 139–149.

- 1981b, Aquifer testing and monitoring around Oakwood salt dome, East Texas, *in* Kreitler, C. W., and others, *Geology and geohydrology of the East Texas Basin: a report on the progress of nuclear waste isolation feasibility studies (1980)*: The University of Texas at Austin, Bureau of Economic Geology Geological Circular 81-7, p. 126–135.
- Fogg, G. E., and Kreitler, C. W., 1981, Ground-water hydrology around salt domes in the East Texas Basin: a practical approach to the contaminant transport problem: *Bulletin of the Association of Engineering Geologists*, v. 23, no. 4, p. 387–411.
- Fogg, G. E., Seni, S. J., and Kreitler, C. W., 1983, Three-dimensional ground-water modeling in depositional systems, Wilcox Group, Oakwood salt dome area, East Texas: The University of Texas at Austin, Bureau of Economic Geology Report of Investigations No. 133, 55 p.
- Folk, R. L., 1980, *Petrology of sedimentary rocks*: Austin, Texas, Hemphill Publishing, 182 p.
- Galloway, W. E., Hobday, D. K., and Magara, K., 1982, Frio Formation of Texas Gulf Coastal Plain: depositional systems, structural framework, and hydrocarbon distribution: *American Association of Petroleum Geologists Bulletin*, v. 66, no. 6, p. 649–688.
- Giles, A. B., and Wood, D. H., 1983, Oakwood salt dome, East Texas: geologic framework, growth history, and hydrocarbon production: The University of Texas at Austin, Bureau of Economic Geology Geological Circular 83-1, 55 p.
- Granata, W. H., 1963, Cretaceous stratigraphy and structural development of the Sabine Uplift area, Texas and Louisiana, *in* Report on selected north Louisiana and south Arkansas oil and gas fields and regional geology: Shreveport Geological Society, Reference Volume V, p. 50–95.
- Gray, D. R., 1979, Geometry of crenulation-folds and their relationship to crenulation cleavage: *Journal of Structural Geology*, v. 1, no. 3, p. 187–205.
- 1981, Cleavage-fold relationships and their implications for transected folds: an example from southwest Virginia, U.S.A.: *Journal of Structural Geology*, v. 3, no. 3, p. 265–277.
- Halbouty, M. T., 1979, *Salt domes—Gulf region, United States and Mexico (2d ed.)*: Houston, Texas, Gulf Publishing Company, 561 p.
- 1980, Methods used, and experience gained, in exploration for new oil and gas fields in highly explored (mature) areas: *American Association of Petroleum Geologists Bulletin*, v. 64, no. 8, p. 1210–1222.
- Halbouty, M. T., and Halbouty, J. J., 1982, Relationships between East Texas Field region and Sabine Uplift in Texas: *American Association of Petroleum Geologists Bulletin*, v. 66, no. 8, p. 1042–1054.
- Halbouty, M. T., and Hardin, G. C., Jr., 1951, Types of hydrocarbon accumulation and geology of South Liberty salt dome, Liberty County, Texas: *American Association of Petroleum Geologists Bulletin*, v. 35, no. 9, p. 1939–1977.
- Heard, H. C., 1963, Effects of large changes in strain rates in the experimental deformation of Yule Marble: *Journal of Geology*, v. 71, p. 162–195.
- 1976, Comparison of the flow properties of rocks at crustal conditions: *Philosophical Transactions of the Royal Society of London, Series A*, v. 283, p. 173–186.
- Hobbs, B. E., Means, W. D., and Williams, P. F., 1976, *An outline of structural geology*: New York, John Wiley, 571 p.
- Hudleston, P. J., 1973, The analysis and interpretation of minor folds developed in the Moine rocks of Monar, Scotland: *Tectonophysics*, v. 17, no. 1, p. 89–132.
- Hughes, D. J., 1968, Salt tectonics as related to several Smackover fields along the northeast rim of the Gulf of Mexico basin: *Gulf Coast Association of Geological Societies Transactions*, v. 18, p. 320–339.
- Jackson, M. P. A., 1982, Fault tectonics of the East Texas Basin: The University of Texas at Austin, Bureau of Economic Geology Geological Circular 82-4, 31 p.
- Jackson, M. P. A., and Harris, D. W., 1981, Seismic stratigraphy and salt mobilization along the northwestern margin of the East Texas Basin, *in* Kreitler, C. W., and others, *Geology and geohydrology of the East Texas Basin: a report of the progress of nuclear waste isolation feasibility studies (1980)*: The University of Texas at Austin, Bureau of Economic Geology Geological Circular 81-7, p. 28–32.
- Jackson, M. P. A., and Seni, S. J., 1982, Geometry and structural evolution of salt diapirs in a marginal rift basin of the Gulf of Mexico (abs.): *Geological Society of America, Abstracts with Programs*, v. 14, no. 7, p. 521.
- 1983a, Geometry and evolution of salt structures in a marginal rift basin of the Gulf of Mexico, East Texas: *Geology*, v. 11, p. 131–135.
- 1983b, Suitability of salt domes in the East Texas Basin for nuclear waste isolation: final summary of geologic and hydrogeologic research (1978-1983): The University of Texas at Austin, Bureau of Economic Geology, report prepared for the U.S. Department of Energy, Office of Nuclear Waste Isolation, 247 p.
- in press, Atlas of salt domes in the East Texas Basin: The University of Texas at Austin, Bureau of Economic Geology Report of Investigations.
- Jackson, M. P. A., Seni, S. J., and McGowen, M. K., 1982, Initiation of salt flow in the East Texas Basin (abs.): *American Association of Petroleum Geologists Bulletin*, v. 66, no. 5, p. 584–585.
- Jaritz, W., 1980, Einige Aspekte der Entwicklungsgeschichte der nordwestdeutschen Salzstöcke: *Zeitschrift Deutsch Geologische Gesellschaft*, v. 131, p. 387–408.
- Johnson, H. A., and Bredeson, D. H., 1971, Structural development of some shallow salt domes in the Louisiana Miocene productive belt: *American Association of Petroleum Geologists Bulletin*, v. 55, no. 2, p. 204–226.
- Kaiser, W. R., 1974, Texas lignite: near-surface and deep-basin resources: The University of Texas at Austin, Bureau of Economic Geology Report of Investigations No. 79, 70 p.

- Kaiser, W. R., Ayers, W. B., Jr., and La Brie, L. W., 1980, Lignite resources in Texas: The University of Texas at Austin, Bureau of Economic Geology Report of Investigations No. 104, 52 p.
- Kaiser, W. R., Johnston, J. E., and Bach, W. N., 1978, Sandbody geometry and the occurrence of lignite in the Eocene of Texas: The University of Texas at Austin, Bureau of Economic Geology Geological Circular 78-4, 19 p.
- Kent, P. E., 1979, The emergent Hormuz salt plugs of southern Iran: *Journal of Petroleum Geology*, v. 2, p. 117-144.
- Kreitler, C. W., 1979, Studies of the suitability of salt domes in East Texas Basin for geologic isolation of nuclear wastes: *Gulf Coast Association of Geological Societies Transactions*, v. 29, p. 157-163.
- Kreitler, C. W., Agagu, O. K., Basciano, J. M., Collins, E. W., Dix, O. R., Dutton, S. P., Fogg, G. E., Giles, A. B., Guevara, E. H., Harris, D. W., Hobday, D. K., McGowen, M. K., Pass, D., and Wood, D. H., 1980, Geology and geohydrology of the East Texas Basin: a report on the progress of nuclear waste isolation feasibility studies (1979): The University of Texas at Austin, Bureau of Economic Geology Geological Circular 80-12, 112 p.
- Kreitler, C. W., Collins, E. W., Davidson, E. D., Jr., Dix, O. R., Donaldson, G. W., Dutton, S. P., Fogg, G. E., Giles, A. B., Harris, D. W., Jackson, M. P. A., Lopez, C. M., McGowen, M. K., Muehlberger, W. R., Pennington, W. D., Seni, S. J., Wood, D. H., and Wuerch, H. V., 1981, Geology and geohydrology of the East Texas Basin: a report on the progress of nuclear waste isolation feasibility studies (1980): The University of Texas at Austin, Bureau of Economic Geology Geological Circular 81-7, 207 p.
- Kreitler, C. W., Guevara, E., Granata, G., and McKalips, D., 1977, Hydrogeology of Gulf Coast aquifers, Houston-Galveston area, Texas: The University of Texas at Austin, Bureau of Economic Geology Geological Circular 77-4, 18 p.
- Kumar, M. B., 1977, Growth rates of salt domes of the North Louisiana Salt Basin, *in* Martinez, J. D., and others, An investigation of the utility of Gulf Coast salt domes for the storage or disposal of radioactive wastes: Baton Rouge, Louisiana, Louisiana State University, Institute for Environmental Studies, p. 225-229.
- Kupfer, D. H., 1970, Mechanism of intrusion of Gulf Coast salt, *in* Kupfer, D. H., ed., *Geology and technology of Gulf Coast salt, a symposium*: Baton Rouge, Louisiana, Louisiana State University, School of Geoscience, p. 25-66.
- \_\_\_\_\_, 1976, Times and rates of salt movement in North Louisiana, *in* Martinez, J. D., and Thomas, R. L., eds., *Proceedings, symposium on salt dome utilization and environmental considerations*: Baton Rouge, Louisiana, Louisiana State University, p. 145-170.
- Lobeck, A. K., 1924, Block diagrams and other methods used in geology and geography: New York, John Wiley, 186 p.
- Loocke, J. E., 1978, Growth history of the Hainesville salt dome, Wood County, Texas: The University of Texas at Austin, Master's thesis, 95 p.
- Magara, K., 1980, Comparison of porosity-depth relationships of shale and sandstone: *Journal of Petroleum Geology*, v. 3, no. 2, p. 175-185.
- Martin, R. G., 1978, Northern and eastern Gulf of Mexico continental margin: stratigraphic and structural framework: *American Association of Petroleum Geologists Studies in Geology* No. 7, p. 21-42.
- McGowen, J. H., Brown, L. F., Jr., Evans, T. J., Fisher, W. L., and Groat, C. G., 1976, Environmental geologic atlas of the Texas Coastal Zone—Bay City - Freeport area: The University of Texas at Austin, Bureau of Economic Geology, 98 p.
- McGowen, J. H., and Morton, R. A., 1979, Sediment distribution, bathymetry, faults, and salt diapirs, submerged lands of Texas: The University of Texas at Austin, Bureau of Economic Geology Special Publication, 31 p.
- McGowen, M. K., and Harris, D. W., 1982, Cotton Valley (Upper Jurassic) and Hosston (Lower Cretaceous) depositional systems and their influence on salt tectonics in the East Texas Basin: Third Annual Research Conference, Gulf Coast Section, Society of Economic Paleontologists and Mineralogists Foundation, Baton Rouge, Louisiana, p. 64-70.
- Nadai, A., 1950, Theory of flow and fracture of solids, vol. 1: New York, McGraw-Hill, 572 p.
- National Academy of Sciences - National Research Council, 1957, The disposal of radioactive waste on land: Washington, D. C., Division of Earth Sciences, Committee on Waste Disposal, Publication 519, 142 p.
- \_\_\_\_\_, 1970, Disposal of solid radioactive waste in bedded salt deposits: Springfield, Virginia, U.S. Government Printing Office, 28 p.
- Netherland, Sewell and Associates, 1976, Geologic study of the interior salt domes of Northeast Texas Salt Dome Basin to investigate their suitability for possible storage of radioactive waste material as of May 1976: report prepared for the Office of Waste Isolation, Energy Research and Development Administration, Union Carbide Corporation, Nuclear Division, 57 p.
- Nettleton, L. L., 1934, Fluid mechanics of salt domes: *American Association of Petroleum Geologists Bulletin*, v. 18, no. 9, p. 1175-1204.
- Nichols, P. H., Peterson, G. E., and Wercestner, C. E., 1968, Summary of subsurface geology of northeast Texas, *in* Beebe, B. W., and Curtis, B. F., eds., *Natural gases of North America: American Association of Petroleum Geologists Memoir* 9, v. 2, p. 982-1004.
- Office of Nuclear Waste Isolation, 1981, National Waste Terminal Storage program criteria for mined geologic disposal of nuclear waste: site performance criteria: Columbus, Ohio, Battelle Memorial Institute, DOE/NWTS-33(2), 13 p.
- \_\_\_\_\_, 1982, Evaluation of area studies of the U.S. Gulf Coast salt dome basins: location recommendation report: Columbus, Ohio, Battelle Memorial Institute, ONWI-109, 95 p.
- O'Neill, C. A., 1973, Evolution of Belle Island salt dome, Louisiana: *Gulf Coast Association of Geological Societies Transactions*, v. 23, p. 115-135.



- Orozco, M., and Galvez, R., 1979, The development of folds in bedded chert and related rocks in the Malaguide Complex, southern Spain: *Tectonophysics*, v. 56, no. 3-4, p. 277-295.
- Parker, T. J., and McDowell, A. N., 1955, Model studies of salt dome tectonics: *American Association of Petroleum Geologists Bulletin*, v. 39, no. 12, p. 2384-2470.
- Pennington, W. D., and Carlsoh, S., in preparation, Summary of observations from the East Texas seismic network (June 1981 - August 1982): The University of Texas at Austin, Bureau of Economic Geology, Department of Geological Sciences, and the Institute for Geophysics, contract report prepared for the U.S. Department of Energy.
- Pfiffner, O. A., and Ramsay, J. G., 1982, Constraints on geological strain rates: arguments from finite strain states of naturally deformed rocks: *Journal of Geophysical Research*, v. 87, no. B1, p. 311-321.
- Powell, C. M., 1974, Timing of slaty cleavage during folding of Precambrian rocks, northwest Tasmania: *Geological Society of America Bulletin*, v. 85, no. 7, p. 1043-1060.
- Price, N. J., 1975, Rates of deformation: *Geological Society of London Journal*, v. 131, p. 553-575.
- Purser, B. H., 1973, Sedimentation around bathymetric highs in the southern Persian Gulf, *in* Purser, B. H., ed., *The Persian Gulf: Holocene carbonate sedimentation and diagenesis in a shallow epicontinental sea*: New York, Springer-Verlag, p. 157-177.
- Ramberg, H., 1981, Gravity, deformation and the Earth's crust in theory, experiments and geological application (2d ed.): London, Academic Press, 452 p.
- Ramsay, J. G., 1967, *Folding and fracturing of rocks*: New York, McGraw-Hill, 568 p.
- Reese, R. J., 1977, Salt kinematics of southern Bienville Parish, Louisiana: Louisiana State University, Master's thesis, 136 p.
- Rezak, R., 1977, West Flower Garden Bank, Gulf of Mexico: *American Association of Petroleum Geologists Studies in Geology* No. 4, p. 27-35.
- Sannemann, D., 1968, Salt-stock families in northwestern Germany, *in* Braunstein, J., and O'Brien, G. D., eds., *Diapirism and diapirs*: *American Association of Petroleum Geologists Memoir* 8, p. 261-270.
- Seni, S. J., 1981, Depositional systems of the Lower Cretaceous Paluxy Formation, East Texas Basin, *in* Kreitler, C. W., and others, *Geology and geohydrology of the East Texas Basin: a report on the progress of nuclear waste isolation feasibility studies (1980)*: The University of Texas at Austin, Bureau of Economic Geology Geological Circular 81-7, p. 53-59.
- Seni, S. J., and Fogg, G. E., 1982, Wilcox Group facies and syndepositional dome growth, southern East Texas Basin: The University of Texas at Austin, Bureau of Economic Geology, report prepared for the U.S. Department of Energy, Office of Nuclear Waste Isolation, 33 p.
- Seni, S. J., and Kreitler, C. W., 1981, Evolution of the East Texas Basin, *in* Kreitler, C. W., and others, *Geology and geohydrology of the East Texas Basin: a report on the progress of nuclear waste isolation feasibility studies (1980)*: The University of Texas at Austin, Bureau of Economic Geology Geological Circular 81-7, p. 12-20.
- Smith, D. A., and Reeve, F. A. E., 1970, Salt piercement in shallow Gulf Coast salt structures: *American Association of Petroleum Geologists Bulletin*, v. 54, no. 7, p. 1271-1289.
- Stude, G. R., 1978, Depositional environments of the Gulf of Mexico South Timbalier Block 54: salt dome and salt dome growth models: *Gulf Coast Association of Geological Societies Transactions*, v. 28, p. 627-646.
- Talbot, C. J., 1977, Inclined and asymmetric upward-moving gravity structures: *Tectonophysics*, v. 42, no. 2-4, p. 159-181.
- Terriere, R. T., 1976, Geology of Fairway Field, East Texas, *in* Braunstein, J., ed., *North American oil and gas fields*: *American Association of Petroleum Geologists Memoir* 24, p. 157-176.
- Trippet, A. R., 1981, Characteristics of diapirs on the outer continental shelf - upper continental slope boundary, northwest Gulf of Mexico: *Gulf Coast Association of Geological Societies Transactions*, v. 31, p. 391-397.
- Trusheim, F., 1960, Mechanism of salt migration in northern Germany: *American Association of Petroleum Geologists Bulletin*, v. 44, no. 9, p. 1519-1540.
- Turk, Kehle and Associates, 1978, Tectonic framework and history, Gulf of Mexico region: Report prepared for Law Engineering Testing Co., Marietta, Georgia, 28 p.
- van Eysinga, F. W. B., 1975, *Geologic time table*: Amsterdam, The Netherlands, Elsevier, 1 p.
- van Hinte, J. E., 1976a, A Jurassic time scale: *American Association of Petroleum Geologists Bulletin*, v. 60, no. 4, p. 489-497.
- \_\_\_\_\_, 1976b, A Cretaceous time scale: *American Association of Petroleum Geologists Bulletin*, v. 60, no. 4, p. 498-516.
- Wood, D. H., and Giles, A. B., 1982, Hydrocarbon accumulation patterns in the East Texas salt dome province: The University of Texas at Austin, Bureau of Economic Geology Geological Circular 82-6, 36 p.
- Wood, D. H., and Guevara, E. H., 1981, Regional structural cross sections and general stratigraphy, East Texas Basin: The University of Texas at Austin, Bureau of Economic Geology Cross Sections, 21 p.
- Woodbury, H. O., Murray, I. B., Jr., and Osborne, R. E., 1980, Diapirs and their relation to hydrocarbon accumulation, *in* Miall, A. D., ed., *Facts and principles of world petroleum occurrence*: Calgary, Canadian Society of Petroleum Geologists, p. 119-142.

## APPENDIX 1

### CALCULATION OF DIAPIRIC STRAIN RATES FROM DIAPIRIC GROWTH RATES

Elongation,  $e$ , is the proportional change in length of a line element:

$$e = \frac{l_i - l_o}{l_o} = \frac{\Delta l_i}{l_o} \quad (1)$$

where  $l_o$  is the original length of the line before a given strain increment,  $l_i$ , is the length after the strain increment, and  $\Delta l_i$  is the change in length.

Strain rate,  $\dot{e}$ , is the elongation per second. Strain may be calculated in two ways (Nadai, 1950, p. 74):

Conventional strain rate:

$$\dot{e}_i = \frac{\Delta l_i}{l_o} \quad (2)$$

Natural strain rate:

$$\dot{e}_i = \frac{\Delta l_i}{l_o + \Delta l_1 + \Delta l_2 \dots + \Delta l_{i-1}} \quad (3)$$

In the present paper,  $\Delta h$  is equivalent to:

$$\Delta h_d = G_g \quad \text{or} \quad \Delta h_d = G_n$$

where  $G_g$  and  $G_n$  are the vertical distances (in m) that a salt diapir rises in duration,  $t_i$  (in Ma), as calculated by the methods of gross growth and net growth, respectively. For comparative purposes these growth values were converted to growth rates,  $\dot{G}_g$  and  $\dot{G}_n$  (in m/Ma):

$$\dot{G} = \frac{G}{t_i} \quad (4)$$

Conventional strain rate can be calculated by rewriting equation 2 as:

$$\dot{e}_i = \frac{G}{h_{do} \times t_i \times 3.16 \times 10^{13}} \quad (5)$$

where  $h_{do}$  is the height of the salt diapir before the strain increment ( $e_i$ );  $t_i$  is the duration in Ma; and  $3.16 \times 10^{13}$  is 1 Ma converted to seconds. Because strain rates are measured in orders of magnitude, approximate estimates of  $h_{do}$ , as calculated by the two methods below, suffice.

#### Method 1: Overall Strain Rates

The mean strain rate throughout recorded diapiric history is referred to as the overall strain rate, symbolized as  $\dot{G}$ . Growth-rate data in this paper show that the growth rate ( $\dot{G}$ ) decreases exponentially with time ( $t$ ) according to the relationship:

$$\dot{G} = a^{-t} \quad (6)$$

where  $a$  is a variable. Accordingly, the current height of the diapir crest ( $h_{di}$ ) above the Louann Salt (or top of pre-Louann basement where salt is absent) is only marginally

greater than the height at the end of the diapiric stage; the current height thus approximates the height at the end of diapirism.

The change in diapir height throughout recorded diapiric history (in m) is calculated by rearranging equation 4:

$$G = \Delta h_d = \bar{G} \times t_i \quad (7)$$

where  $\bar{G}$  is the arithmetic mean of  $n$  individual growth rates calculated from  $n$  isopach units:

$$\bar{G} = \frac{\sum_{i=1}^n \dot{G}_i}{n} \quad (8)$$

Knowing the change in diapir height and the height at the end of diapirism, the original height at the start of recorded diapirism can be calculated:

$$h_{do} = h_{di} - G \quad (9)$$

Equation 5 provides the conventional strain rate:

$$\dot{e}_i = \frac{G}{h_{do} \times t_i \times 3.16 \times 10^{13}}$$

#### Method 2: Fastest Strain Rates

Selecting the highest diapiric growth rate,  $\dot{G}$ , for a single isopach unit, equation 7 is applied to calculate the equivalent growth, or change in diapir height, for that particular stratigraphic unit:

$$G = \dot{G} \times t_i \times 10^3 \quad (10)$$

where  $t_i$  is the duration of the stratigraphic unit.

The original height of the diapir at the start of the particular stratigraphic time interval,  $h_{do}$ , is approximated by the current height of the base of that stratigraphic unit above the Louann Salt (or its basement where salt is absent). This assumes that the crest of the diapir remained near the surface throughout that particular geologic interval. Paleofacies variations given in this paper suggest that this was the case. If the diapir was in fact buried a few hundred feet, this would be offset by the effects of compaction. Thus the current (compacted) height of the base of the stratigraphic unit is a good approximation of the height of the diapir at the start of the time interval under consideration. The base of the stratigraphic unit is measured on the outer edge of the diapiric withdrawal basin to nullify the effects of later subsidence induced by subsequent salt withdrawal.

After  $h_{do}$  is determined, equation 5 can be used to derive strain rates based on both gross growth,  $G_g$ , and net growth,  $G_n$ .

## APPENDIX 2

### LIST OF WELLS BY CROSS SECTIONS

#### Cross Section A-A'

Cross-Section Number	Well Identification Number	Operator	Well Name	County
1	KA-38-25-827	McBee	No. 1 M. Storms	Freestone
2		Letco	TOH-2A	Leon
3	SA-38-29-902	Lake	No. 1 Leon Plantation	Leon

#### Cross Section B-B'

1	AA-38-01-804	Read, John L. & H. L. Gist	No. 1 Derden Heir	Anderson
2	AA-38-01-805	Texas Co.	No. 1 Walton, E. C.	Anderson
3	AA-38-01-841	Texas Co.	No. 2 Cook, Sherwood	Anderson
4	AA-38-01-904	McBee, V. D. et al.	No. 1 Adams Cone, Jr., Gas Unit	Anderson
5	AA-38-02-701	Butler & Douglas	No. 1 Cross, E. M.	Anderson
6	AA-38-02-801	Sunray Mid-Continent Oil Co.	No. 1 Smith, C.	Anderson

#### Cross Section C-C'

1	RA-33-23-502	TXL Co.	No. 1 Liston	Kaufman
2	RA-33-23-601	Humphrey	No. 1 Daves	Kaufman
3	RA-33-23-602	Cable Tool Drilling	No. 1 McDaniel	Kaufman
4	RA-33-24-701	Birdsong	No. 1 Baird	Kaufman
5	YS-33-32-301	Deupree	No. 2 Bruce	Van Zandt
6	YS-34-25-501	Caraway	No. 1 Yates	Van Zandt
7	YS-34-25-302	Superior	No. 1 Porter	Van Zandt
8	YS-34-25-601	Caraway	No. 1 Parker	Van Zandt
9	YS-34-26-801	Caraway	No. 1 Gilmore	Van Zandt
10	YS-34-35-101	Voight	No. 1 Kerr	Van Zandt
11	YS-34-35-201	Powell	No. 1 Edwards	Van Zandt
12	YS-34-36-402	Pan American	No. 1 Hobbs	Van Zandt
13	YS-34-36-501	Byars	No. 1 Jones	Van Zandt
14	YS-34-36-502	Humble	No. 1 Woods	Van Zandt
15	XH-34-36-604	Pace	No. 1 Johnson	Smith
16	XH-34-36-605	Hootkins	No. 1 Talbert	Smith
17	XH-34-36-606	Halstead	No. 1 Talbert	Smith
18	XH-34-36-904	Sun	No. 1 Cade	Smith
19	XH-34-37-702	Huber	No. 1 Tucker	Smith
20	XH-34-37-703	Powell	No. 1 Ferrell	Smith
21	XH-34-37-803	Feldman	No. 1 Verner	Smith
22	XH-34-37-804	Mobley	No. 1 Verner	Smith
23	XH-34-45-301	Standard of Texas	No. 2 Eikner	Smith
24	XH-34-45-302	Standard of Texas	No. 1 Eikner	Smith
25	XH-34-45-303	Standard of Texas	No. 1 Verner	Smith
26	XH-34-45-304	Lyons Petroleum	No. 2 Verner Unit No. 1	Smith
27	XH-34-45-305	Jones-O'Brien	No. 2 City of Tyler	Smith
28	XH-34-45-306	McKnight	No. 1 City of Tyler	Smith
29	XH-34-45-307	Jones-O'Brien	No. 1 Willingham	Smith
30	XH-34-45-308	Jones-O'Brien	No. 1 Cook	Smith
31	XH-34-46-101	McKnight	No. 1 Hey	Smith
32	XH-34-46-601	McKnight	No. 1 Story	Smith
33	XH-34-47-401	Hughey	No. 1 Hudnall & Pirtle	Smith
34	XH-34-47-701	McKellar & Champion	No. 1 Bergfeld	Smith
35	XH-34-47-702	Zephyr	No. 1 Bergfeld	Smith
36	XH-34-47-703	Le Cuno	No. 1 Neill	Smith
37	XH-34-47-801	Goldsmith	No. 1 Bell	Smith
38	XH-34-47-901	Sinclair	No. 2 Connally	Smith
39	XH-34-56-101	Lewis	No. 1 Frazier	Smith
40	XH-34-56-102	Stephens	No. 1 Cook	Smith
41	XH-34-56-201	Stroube	No. 1P Wilson	Smith
42	XH-34-56-501	Woolf & McGee	No. 1 Arnold	Smith

**Cross Section C-C', cont.**

<b>Cross-Section Number</b>	<b>Well Identification Number</b>	<b>Operator</b>	<b>Well Name</b>	<b>County</b>
43	WR-35-49-902	George et al.	No. 1 Talliaferro Heirs	Rusk
44	WR-35-50-703	Trice	No. 1 Harris	Rusk
45	WR-35-58-201	Daniels	No. 1 King	Rusk
46	WR-35-58-301	Trahan	No. 1 Hilburn	Rusk
47	WR-35-58-302	Trahan	No. 1 Anderson	Rusk

**Cross Section D-D'**

1	YS-34-26-801	Caraway	No. 1 Gilmore	Van Zandt
2	YS-34-27-902	Union Oil	No. 10 Maxfield	Van Zandt
3	ZS-34-20-202	Sun Oil	No. 1 Retherford	Wood
4	ZS-34-21-303	Trice & Jackson	No. 1 Pool	Wood
5	ZS-34-31-101	Humble	No. 1 Hawkins	Wood
6	ZS-34-31-201	Humble	No. 15 Hawkins	Wood
7	YK-34-24-901	Sands & Sands	No. 1 McCollum	Upshur

**Cross Section U-U'**

1	XH-34-36-603	Humble	No. 1 F. W. Williams	Smith
2	XH-34-37-101	E. L. Howard	No. 1 C. W. Waters	Smith
3	XH-34-29-701	Ranco Oil Co.	No. 1 R. L. Perry	Smith
4	ZS-34-21-802	Jackson & Deupree	No. 1 York	Wood
5	ZS-34-21-602	British American	No. B-1 Weisenhunt	Wood
6	ZS-34-21-304	Lone Star	No. 1 H. N. Penix	Wood
7	ZS-34-14-701	F. R. Jackson	No. 1 W. J. Bowman	Wood
8	ZS-34-14-502	F. R. Jackson & B. A. Holman	No. 1 Keys	Wood
9	ZS-34-14-501	Mack Hays, Jr.	No. 1 E. M. Ainsworth	Wood
10	ZS-34-14-301	John David Crow et al.	No. 1 G. C. Mann	Wood
11	ZS-34-07-701	Ace Oil Co.	No. 1 J. J. Dickson	Wood

**Cross Section V-V'**

1	XH-34-39-102	Harris R. Fender	No. 1 Brittain Balfour	Smith
2	XH-34-39-403	L. A. Grelling	No. 1 E. S. Atwood	Smith
3	XH-34-39-803	Delta Drilling	No. 1 George Kid	Smith
4	XH-34-47-802	Claud B. Hamill	No. 1 E. H. Barbee	Smith

**Cross Section W-W'**

1	LT-34-52-201	Happy Gist, R. McKellar & Rotary Drilling, Inc.	No. A-1 Sidney Einheber et al.	Henderson
2	LT-34-44-801	Delta Drilling & Atlantic	No. 1 Tom C. Patten	Henderson
3	LT-34-44-301	Clay & Walker	No. 1 Alton Cade et al.	Henderson
4	XH-34-37-804	O. B. Mobley	No. 1 Verner	Smith
5	XH-34-37-501	Harry J. Owens & Victor Witzel	No. 1 J. W. Wilkinson	Smith
6	XH-34-29-803	Dan E. Whelan, Jr.	No. 1 Fannie Smith	Smith
7	XH-34-30-823	Gulf	No. 1 W. G. Atwood	Smith
8	XH-34-30-803	Harris R. Fender	No. 1 Jack B. York	Smith
9	XH-34-30-922	Humble	No. 1 Red Springs Gas Unit	Smith
10	ZS-34-31-102	Humble	No. 1 Little Sandy Hunting & Fishing Club Acct. No. 2	Wood
11	ZS-34-31-101	Humble	No. 1 Hawkins Gas Unit No. 1	Wood

**Cross Section X-X'**

1	XH-34-30-922	Humble	No. 1 Red Springs Gas Unit	Smith
2	XH-34-30-905	Lemon	No. 1 Hubert Lake	Smith
3	XH-34-39-403	L. A. Grelling	No. 1 E. S. Atwood	Smith
4	XH-34-39-803	Delta Drilling	No. 1 George Kid	Smith
5	XH-34-47-802	Claud B. Hamill	No. 1 E. H. Barbee	Smith

**Cross Section Y-Y'**

<b>Cross-Section Number</b>	<b>Well Identification Number</b>	<b>Operator</b>	<b>Well Name</b>	<b>County</b>
1	SA-39-40-703	Sun	No. 1 Diehl	Leon
2	SA-39-40-502	Marino	No. 1 Smith	Leon
3	SA-39-40-503	Lone Star	No. 1 Shows	Leon
4	SA-39-40-603	Phillips	No. 1 Coldiron	Leon
5	SA-39-40-201	P. G. Lake	No. 1 Burroughs	Leon
6	SA-39-40-306	Frankel	No. 1 Cochran	Leon
7	SA-39-40-302	Jordan	No. 1 Van Winkle	Leon
8	SA-39-40-303	Marino	No. 1 Harrington	Leon
9	KA-39-32-901	Roberts et al.	No. 1 Reed et al.	Freestone
10	KA-38-35-402	McBee	No. 1 Settlemyre	Freestone
11	KA-38-25-102	Humble	No. 2C Greer	Freestone
12	KA-38-25-201	Humble	No. 1C Greer	Freestone
13	KA-38-17-804	Humble	No. 1 Butler Gas Unit No. 2	Freestone
14	KA-38-17-805	Le Cuno	No. 1 East Texas National Bank	Freestone
15	KA-38-17-803	Prairie Prod. Co.	No. 1 East Texas National Bank	Freestone
16	KA-38-17-802	Steward	No. 1 Harris	Freestone
17	KA-38-17-801	Gulf	No. 1 Wilson	Freestone
18	KA-38-17-501	Gulf	No. 1 Pearson	Freestone
19	KA-38-17-306	Empire Drilling	No. 1 Marshall	Freestone
20	KA-38-17-305	Continental	No. 1 Hill	Freestone
21	KA-38-17-304	Texaco	No. 1 Hill	Freestone
22	KA-38-17-302	Collins	No. 1 Hill	Freestone
23	KA-38-09-905	Sun	No. 1A Hill	Freestone
24	AA-38-09-904	Continental	No. 1 Cady	Anderson
25	AA-38-10-704	Continental	No. 2 Cady	Anderson
26	AA-38-10-703	Continental	No. 1 F. M. Royall	Anderson
27	AA-38-10-702	Continental	No. 1A Royal National Bank	Anderson
28	AA-38-10-701	Continental	No. 1A Carroll	Anderson
29	AA-38-10-405	Continental	No. 1 Carroll	Anderson
30	AA-38-10-403	Continental	No. 2 Royal National Bank	Anderson
31	AA-38-10-401	Continental	No. 1 Royal National Bank	Anderson
32	AA-38-10-203	Continental	No. 1 DuPuy	Anderson
33	AA-38-10-202	Samedan	No. 1 McKenzie	Anderson
34	AA-38-10-201	Texas Co.	No. 1 Holmes	Anderson
35	AA-38-02-803	May Petroleum	No. 1 Burnett	Anderson
36	AA-38-02-802	Pan American	No. 1 Stafford	Anderson
37	AA-38-02-901	Sanders	No. 1 Adams	Anderson
38	AA-38-02-603	Stanolind	No. 1 Weakley	Anderson
39	AA-38-02-502	Texas Co.	No. 1 Cooper	Anderson
40	AA-38-02-601	Texaco	No. 1 Hanks	Anderson
41	AA-38-03-102	Cities Service	No. 1 Riddles	Anderson
42	AA-34-59-703	Perryman	No. 1 Bailey	Anderson
43	AA-34-59-702	Hughey	No. 1 Larue	Anderson
44	AA-34-59-701	Perryman	No. 1 Anderson County Land & Cattle Co.	Anderson
45	LT-34-59-401	Cities Service	No. 1 Pharris	Henderson
46	LT-34-59-102	Windsor	No. 1 Burkhart	Henderson
47	LT-34-51-801	Murchison	No. 1 Abercrombie	Henderson
48	LT-34-52-401	Fairway	No. 1 Hightower	Henderson
49	LT-34-52-102	British American	No. 1 Anderson County Land & Cattle Co.	Henderson
50	LT-34-44-702	Windsor	No. 1 Jackson	Henderson
51	LT-34-44-701	Windsor	No. 1 Whitehead	Henderson
52	LT-34-44-101	Clay & Walker	No. 1 Cade	Henderson
53	YS-34-36-903	Sinclair	No. 1 Curtis	Van Zandt
54	YS-34-36-902	Basin	No. 1 Stucker	Van Zandt
55	XH-34-37-702	Huber	No. 1 Tucker	Smith
56	XH-34-37-701	Delta	No. 1 Gary	Smith
57	XH-34-37-407	Trantham	No. 1 Buie	Smith
58	XH-34-37-406	Powell	No. 1 Boren	Smith
59	XH-34-37-404	Humble	No. 1 Gary	Smith
60	XH-34-37-403	McKnight	No. 1 Boynton	Smith
61	XH-34-37-104	Marathon Oil	No. 1 Clark	Smith
62	XH-34-37-103	Sinclair	No. 1 Pool	Smith

**Cross Section Y-Y', cont.**

<b>Cross-Section Number</b>	<b>Well Identification Number</b>	<b>Operator</b>	<b>Well Name</b>	<b>County</b>
63	XH-34-37-202	Voight	No. 1 Staples	Smith
64	XH-34-37-201	Phillips	No. 1 Staples	Smith
65	XH-34-29-803	Whelan	No. 1 Smith	Smith
66	XH-34-29-802	Magnolia	No. 1 King	Smith
67	XH-34-29-801	Spence	No. 1 Tomlin	Smith
68	XH-34-29-603	McKnight	No. 1 Balfour	Smith
69	XH-34-29-602	Sun	No. 1 Fleming Oil Unit No. 1	Smith
70	XH-34-29-601	McKnight	No. 1 Wheelis	Smith
71	ZS-34-30-101	F. R. Jackson	No. 1 Harrell	Wood
72	ZS-34-29-301	Bennett	No. 1 MacLin	Wood
73	ZS-34-22-701	Southland	No. 1 Judge	Wood
74	ZS-34-22-406	British American	No. 1 Judge	Wood
75	ZS-34-22-405	Pan American	No. 1 Judge	Wood
76	ZS-34-22-203	General Crude	No. 1 Barrett	Wood
77	ZS-34-22-201	Jackson	No. 1 Jordan	Wood
78	ZS-34-14-601	Belco	No. 1 Windham	Wood
79	ZS-34-15-401	Hootkins	No. 1 Holmberg	Wood
80	ZS-34-15-101	Lodi Drilling	No. 1 McCrary	Wood
81	ZS-34-07-702	Folwell	No. 1 Dickey	Wood
82	ZS-34-07-501	British American	No. 1 Dean	Wood
83	JZ-34-07-201	Stephens	No. 1 Jordan	Franklin
84	JZ-17-63-802	Mobil	No. 1 Lester	Franklin

**Cross Section Z-Z'**

1	LT-34-43-102	Lone Star	No. 1 C. L. B. Palmer	Henderson
2	LT-34-43-801	Lone Star	No. B1 Allyn Estate	Henderson
3	LT-34-43-702	Bruce Smith, Champion, Hamill & Midwest Oil Corp.	No. 1 S. G. Scott et al.	Henderson
4	LT-34-51-201	Bruce Smith & John G. Champion	No. 1 F. F. Alford	Henderson
5	LT-34-50-901	Stanolind	No. 1 Dupree	Henderson
6	LT-34-59-401	Cities Service	No. 1 M. C. Pharris	Henderson
7	AA-38-03-602	British American	No. 1 R. P. Terrel	Anderson
8	AA-38-05-726	Pan American	No. 1 Wm. J. Furnish	Anderson
9	DJ-38-05-802	Humble	No. 13 H. L. Carter	Cherokee
10	DJ-38-06-902	Claud B. Hamill	No. 2 W. W. Glass	Cherokee